ULTRASONIC ASSESSMENT OF EARLY AGE PROPERTY DEVELOPMENT IN HYDRATING CEMENTITIOUS MATERIALS

by

XIAOJUN WANG

A dissertation submitted to the Graduate Faculty in Engineering in partial fulfillment of the requirements for the degree of Doctor of Philosophy, The City University of New York

2010

This manuscript has been read and accepted for the
Graduate Faculty in Engineering in satisfaction of the
dissertation requirement for the degree of Doctor of Philosophy.

Professor Kolluru V. Subramaniam

Date — Chair of Examining Committee

Professor Mumtaz K. Kassir

Date — Executive Officer

Professor Anil K. Agrawal, The City College of New York

Professor Benjamin Liaw, The City College of New York

Professor Hansong Tang, The City College of New York

Professor Huabei Liu, The City College of New York

Professor Feng-Bao Lin, The City College of New York

Supervisory Committee

THE CITY UNIVERSITY OF NEW YORK

Abstract

ULTRASONIC ASSESSMENT OF EARLY AGE PROPERTY DEVELOPMENT IN HYDRATING CEMENTITIOUS MATERIALS

by

Xiaojun Wang

Supervisor: Prof. Kolluru V. Subramaniam

The internal structure (microstructure) of cementitious materials, such as cement paste, mortar and concrete, evolves over time because of cement hydration. The microstructure of the cementitious phase plays a very important role in determining the strength, the mechanical properties and the long-term durability of cementitious materials. Therefore any understanding of the strength gain and the long-term durability of cementitious materials requires a proper assessment of the microstructure of its cementitious phase.

Current methods for evaluating the microstructure of the cement are invasive and primarily laboratory-based. These methods are not conducive for studying the pore structure changes in the first few hours after casting since the changes in microstructure occur on a time scale that is an order of magnitude faster than the time required for sample preparation. The primary objective of the research presented in this thesis is to contribute towards advancing the current state-of-the-art in assessing the microstructure of cementitious systems. An ultrasonic wave reflection technique which allows for real-time assessment of the

porosity and the elastic modulus of cementitious materials is developed. The test procedure for monitoring changes in the amplitude of horizontally polarized ultrasonic shear waves from the surface of hydrating cement paste is presented. A theoretical framework based on a poro-elastic idealization of the hydrating cementitious material is developed for interpreting the ultrasonic reflection data. The poro-elastic representation of hydrating cementitious material is shown to provide simultaneous, realistic estimates of porosity and shear modulus for hydrating cement paste and mortar through setting and early strength gain. The porosity predicted by the poro-elastic representation is identical to the capillary water content within the cement paste predicted by Powers' model. The shear modulus of the poro-elastic skeleton was compares favorably with the value of shear modulus obtained from an independent vibration-based measurement. The relations between porosity and compressive strength developed through experimental techniques and poro-elasticity framework provide an understanding of effects of evolution of porosity on the development of compressive strength for hydrating cement paste and mortar. The ultrasonic measurements and the theoretical framework presented here can be extended monitoring in-situ material property development in hydrating cement-based materials.

Acknowledgements

I would like to express heartfelt gratitude to my advisor, Professor Kolluru V. Subramaniam, for his valuable guidance and continuous support throughout the duration of this study. His physical insight and scientific spirit was indispensable to my work. I would like to sincerely thank him for his patience and encouragement during my work. I would also like to sincerely thank Prof. Feng-Bao Lin for bringing me the opportunity to pursue graduate studies at City College and supervising as my co-advisor. His valuable suggestions and constant assistance during the course of my graduate studies are greatly appreciated.

The help, encouragement and company of many of my colleagues and friends is appreciated. Special thanks are due to Mr. Hadi Kamyab for assistance with experimentation of concrete material and encouragement. I would like to acknowledge Dr. Mingdong Bi, Dr. Fei Zeng, Dr. Zhou Xu, Dr. Zhihua Yi and Mr. Weimin Nian for many helpful discussions, their pleasurable company and support throughout the course of this study. In addition, I would like to thank Miao Feng, Guangyong Liu, Xin Zong, Jianqiu Zhang, Hao Bai, Hongfang Wang, Xiaochen Xu, Yuzhen Han, and Donghui Huang for their friendship and assistance.

I would also like to thank my parents for their confidence on me and moral support they have provided in my study and work.

Finally, I would like to thank my wife Qianmei Hu and my children Yufei Wang and Chloe Hu for always reminding me that there is much more to life than cement.

Table of Contents

List of Figures

List of Tables

Chapter 1 Introduction

1.1 Introduction and Motivation

The internal structure (microstructure)* of concrete evolves over time because of cement hydration. The microstructure of the cementitious phase plays a very important role in determining the strength, the mechanical properties and the long-term durability of concrete. For a given mixture composition, the strength gain and development of elastic material properties of concrete relate directly to the development of microstructure of its cementitious phase [Garboczi and Bentz 1995; Garboczi and Bentz 1996]. In addition, the porosity of the cementitious phase determines the transport properties, shrinkage and creep of concrete and hence its long-term durability [Gardner and Zhao 1993; Grosse et al. 1995; Hoff and Buck 1983; Lange 1989; Mehta 1997; Neville 2000]. Therefore any understanding of the strength gain and the long-term durability of a given concrete mix requires a proper assessment of the microstructure of its cementitious phase.

Current methods for evaluating the microstructure of the cement phase are invasive and primarily laboratory-based [Jennings and Xi 1992; Cook and Kenneth 1993; Daimon et. al. 1971; Diamond and Bonen 1993]. For instance, porosity measurement of the cementitious phase involves sample preparation procedures that disturb or alter the microstructure [Thomas et al. 1999; Jennings et al. 2007]. Also,

*In this thesis, the word "internal structure" has been used interchangeably with "microstructure" to refer to the description of the products of hydration, which are formed at different length scales.

these methods are not conducive to studying the pore structure changes in the first few hours after casting since the changes in microstructure occur on a time scale that is an order of magnitude faster than the time required for sample preparation. Technology to directly infer the microstructure of hardening cementitious phase is needed to extend the fundamental understanding of the strength gain, development of mechanical properties, and durability characteristics of concrete.

The two-fold focus of the work plan outlined in this thesis is (a) to contribute towards advancing the current state-of-the-art in assessing the microstructure of cementitious systems and (b) to develop a fundamental understanding of the property development brought about by changes in the microstructure.

The research presented here deals with the development of a one-sided ultrasonic technique for real-time assessment of the microstructure and porosity of cementitious materials. The work presented here builds on an existing one-sided ultrasonic reflection technique which has been shown to sensitively detect the distinct stages in the development of internal structure of hydrating cementitious matrix. More elaborate experimental test setup is developed. The theoretical framework necessary to interpret the results of the ultrasonic technique and to provide information about the microstructure of the hydrating cement paste in terms of physically-based variables is developed using the poroelastic theory. Poroelastic theory has been used for studying porous media such as rocks, and soils [Stoll and Kan 1981; Chotiros 1995] and offers a natural way for modeling the hydrating cement system. The large quantity of information inherently provided by the presented approach yields substantial insight into the phenomena of hydration and development of

microstructure with time. Fundamental understanding of the relationship between the internal structure variables within the framework of poroelastic theory and macro-properties of cement pastes and mortar (specifically elastic moduli and strength) is developed.

1.2 Objectives and Scope of Work

The objectives of the research presented in this thesis are:

(1) To develop a non-invasive technique for assessing the microstructure and determining the porosity of cementitious systems

(2) To study the evolution of porosity and elastic modulus in hydrating cement paste and mortar

(3) To develop a fundamental understanding of the relationship between the microstructure variables, such as porosity and strength of cementitious material

The goal of the presented research is to contribute to a better understanding of the evolution of microstructure and the influence of the microstructure on the macroscopic properties of a cementitious material.

1.3 Outline of the Dissertation

A brief description of the work presented in different chapters is given below

Chapter 2 gives the review of literature relevant to the presented research, including experimental approaches and theoretical modeling used to study mechanical and microstructural properties of hydrating cement paste and concrete.

Chapter 3 introduces a laboratory-based ultrasonic test system for measuring the acoustic properties of cementitious materials. The experimental setup and the data collection procedures are described. The theoretical framework for relating the measured acoustic properties with the visco-elastic shear moduli of the material is developed and results from cement paste samples are presented.

Chapter 4 focuses on the setting behavior of cement pastes. The response of hydrating cement paste through setting is monitored using rheological measurements and ultrasonic reflection measurements. A poroelastic framework considering a two-phase idealization of hydrating cement paste is presented. Changes in the ultrasonic signal through setting are related with changes in the porosity and stiffness of an equivalent water-filled poroelastic material, which provides identical acoustic impedance. The validity of applying poroelastic idealization to cement paste from immediately after mixing is established.

Chapter 5 presents a theoretical framework based on a poro-elastic idealization of the hydrating cement paste for interpreting the ultrasonic reflection data. The poro-elastic representation of hydrating cement paste is shown to provide simultaneous, realistic estimates of porosity and shear modulus for hydrating cement paste through setting and early strength gain. The porosity predicted by the poro-elastic representation is identical to the capillary porosity predicted by Powers' model. The shear modulus of the poro-elastic skeleton agrees favorably with the value of shear modulus obtained from a vibration-based measurement. The relationship between the porosity and strength in early age cement pastes is shown to be independent of the water-to-cement ratio.

Chapter 6 presents an experimental investigation of the microstructural and mechanical properties of mortar mixtures. Changes in the ultrasonic signal are related to the evolution of porosity and shear modulus obtained from application of poroelastic theory to a two phase idealization of mortar. It is shown that the porosity of mortar obtained from the poroelastic inversion compares favorably with the porosity derived from an application of Power model to hydrating cement paste with identical water-to-cement weight ratio. A unique relations ship between the capillary porosity and compressive strength is shown for hydrating mortars.

Chapter 7 summarizes the findings and presents a discussion of future directions of research which emerge from this study.

Chapter 2 Literature Review

2.1 Introduction

The primary focus of this chapter is to review literature on the relationship between the microstructure and material properties of hydrating cementitious system. The work outlined in the thesis deals with experimental investigation of the setting and hardening process of cementitious system and of cement paste and concrete structure in particular, and is expected to relate the microstructure evolution of the system to the material properties through suitable interpretive material models. A review of the experimental methods applicable for the testing of cementitious system is provided in this chapter. The main emphasis is placed on techniques that closely relate to the subject of this research. A brief review of the theoretical and experimental development of porous medium and the recent applications of Biot's porous elastic theory in acoustics are also provided in this chapter.

2.2 Ultrasonic Wave Reflection Measurements on Cementitious Materials

In 1950s, Mason and Baker [1949] introduced the concept of non-invasive ultrasound viscometer. He measured ultrasonic wave reflections from a liquid–quartz interface and used this data to determine the viscosity response of the fluid. The ultrasonic wave reflection technique was first applied to the area of cementitious materials by Stepisnik et al. [1981]. Valic et al. [2000] showed the ability of the wave

reflection technique to sensitively monitor changes in the hydration behavior of cement paste as it is influenced by different w/c ratios, curing temperatures and material finenesses. The sensitivity of the reflection coefficient to the initial and final setting time of cement paste was examined in the study. The setting times of fast and slow setting cements were tested with the vicat method and it was found that initial and final setting could be related to a certain range of the reflection coefficient. It was stated that after an appropriate calibration, the shear wave reflection coefficient can be used to determine the time of initial and final set.

Chotard et al. [2001] used compression waves to monitor the hydration behavior of cement paste throughout the setting and hardening process. Ultrasonic waves with a frequency of 1 MHz were used in transmission and reflection mode. The cement paste was placed in a PMMA container, which also served as the buffer medium for the wave reflection measurement. Smith et al. [2002] extended the study by examining calcium aluminate cement with three different w/c ratios at various isothermal curing conditions. The measurements were complemented by temperature measurements. It was concluded that the compression wave velocity is closely related to the stiffening process of the paste due to progressive formation of hydrates. Significant changes in the development of the reflection coefficient were found to be related to the time when crystallized hydrates form. Hence it was deduced that the reflection coefficient is linked to morphological changes of the hydrating cement paste, especially to the formation of crystallized hydrates.

Feylessoufi et al. [2001] examined the hydration of Portland cement based powder cement and concrete with ultrasonic measurements in transmission and

reflection mode. Compression and shear waves with a center frequency of 0.5 MHz were used. The ultrasonic measurements were used to determine the reflection coefficient, the phase of the reflected shear waves, and the spectral amplitudes of transmitted compression and shear waves. Based on the investigation, the hydration process was divided into five stages as settling period, aggregation period, a post percolation bond development phase, fully hyperstatic state, and a hyperstatic state with all connected particles.

Subramaniam et al. [2002] investigated the applicability of the wave reflection method to assess the development of the in-situ compressive strength of concrete structures. Three large laboratory-sized concrete slabs were cast with mixtures typically used for pavement and bridge construction. Fly ash, silica fume air entraining agent, and high range water reducer were used as admixtures for the concrete compositions. The measurement of the shear wave reflection coefficient started immediately after casting. A steel plate located on the top surface of the fresh concrete was used as the buffer medium for the reflection measurements. The trends of the compressive strength and the shear wave reflection coefficient for three concrete compositions were normalized and compared to each other over a time range of up to seven days. As seen in Figure 2-1, this comparison showed a very good agreement of the two quantities. The significantly different trends of the strength development of the three concrete mixtures are very well followed by the reflection coefficient.

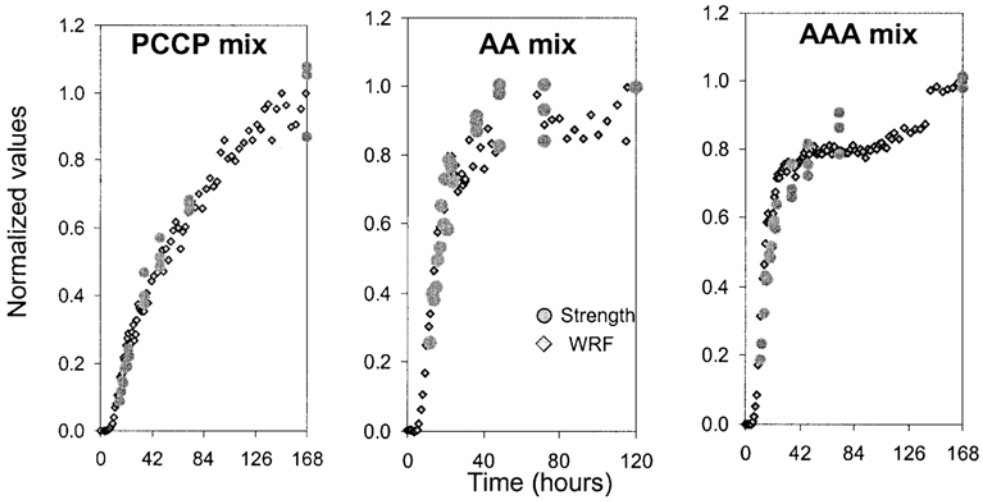

Figure 2-1 Comparison of normalized WRF and strength gain in slabs with different concrete compositions [Subramaniam et al. 2002]

Voigt and Shah [Voigt et al. 2003; Voigt et al. 2004] presented an investigation of the relationship between the reflection loss and basic material parameters of Portland cement mortar. Experiments were conducted on silica mortar with three different w/c ratios cured at isothermal conditions. The wave reflection measurements with shear wave at 2.25MHz were complimented by compression tests, pin penetration, resonant frequency tests, adiabatic calorimetry and thermogravimeter. Due to the determination of the compressive strength at very early ages, an additional feature of the relationship between strength and reflection loss was discovered. The linear trend exhibits a sudden change of its slope at early ages. The time of this slope change is influenced by rate of the strength gain of the tested mortar. The comparison of the dynamic shear moduli as determined from the resonant frequency test and calculated from the wave reflection measurements shows that both quantities have similar features. The authors further presented the relationship between the reflection loss and the degree of hydration, which showed a strong linear trend throughout the

entire monitored time period. From the results of the study the authors concluded that the wave reflection loss measured with shear waves can be directly related to the fundamental material parameters, shear modulus and degree of hydration of the tested mortar mixtures.

2.3 Rheometric Investigation of Cementitious Materials

2.3.1 Introduction

In classical rheology one measures stress at a series of strain rates and plots the results to determine the viscosity. The oscillatory rheometer measures the dynamical modulus of materials to present viscoelastictity. Whether yield stress is a true material property or not is still a controversial issue, however, there is generally an acceptance of its practical usefulness in engineering design and operation of processes where handling and transport of industrial suspensions are involved. The minimum pump pressure required to start a slurry pipeline, the leveling and holding ability of paste, and the entrapment of air in thick pastes are typical problems where the knowledge of the yield stress is essential.

Numerous techniques have been developed for determining the yield stress both directly and indirectly based on the general definition of the yield stress as the stress limit between flow and non-flow conditions. Indirect methods simply involve the extrapolation of shear stress-shear rate data to zero shear rate with or without the help of a rheological model. Direct measurements generally rely on some independent assessment of yield stress as the critical shear stress at which the fluid yields or starts

to flow. The value obtained by the extrapolation of a flow curve is known as "extrapolated" or "apparent" yield stress, whereas yield stress measured directly, usually under a near static condition, is termed "static" or "true" yield value.

2.3.2 Rheological Properties of Cementitious Material

Cement-based materials, such as cement paste, mortar and concrete, usually show plastic flow behavior characterized by yield stress. Tattersall and Banfill [1983] described that the rheological behavior of cement paste, as any flocculated suspension, is very sensitive to its shear history; and when the paste is allowed to flow, the microstructure is broken down and the subsequent yield stress measurements are reduced considerably. The dynamic modulus of cement paste has been determined using the oscillatory shear tests. The in-phase or storage modulus G' reflects the solid-like response of the suspension, and out-of-phase or loss modulus G" reflects the liquid like response. The ratio G"/ G' is equal to the tangent of the phase angle ϕ.

Gregory et al. [1991] used oscillatory shear to study flow behavior of latex polymer modified cement pastes. Experiments were carried out at two frequencies, 0.005Hz and 20 Hz, on the paste made using an ordinary Portland cement with w/c of 0.39. Their results showed that the storage modulus increased with time but the values of storage and loss modulus were similar at these two frequencies.

Measurements conducted by Struble et al.[1993;1995;1998] and Nachbaure et al.[2001] have shown that The changes in dynamic modulus at low strains, in the

linear viscoelastic region, were correlated with changes in vicat needle penetration and heat evolution using isothermal calorimetry. The results showed that after the first few minutes, a more or less exponential increase in G' with hydration was observed with no change in critical strain before and after the initial set. It was also observed that the G" value decreased at later hydration times, adding to the uncertainty regarding the validity of this observation. The results also showed that the liquid to solid ratio has no effect on the general trends of the evolution within the range studied.

Saak et al. [2001] investigated the influence of wall slip on the shear yield stress and modulus of cement paste using a rotational rheometer with smooth walled concentric cylinders and a vane. They directly measured the stress required to initiate measurable flow to determine the yield stress which is considered the best way comparing the empirical and theoretical models that have been used to determine the yield stress based on the data obtained from flow curve measurements. The results of their experiments showed that the concentric cylinders suffer from slip during yield stress measurements due to the formation of a water rich layer at the wall of the cylinders. The use of a vane eliminates slip since shearing occurs within the material. The results of oscillatory tests which were conducted within the determined linear viscoelastic region yield stress determination were in excellent agreement at stresses below the yield point, and the measured complex modulus of cement paste was in the order of 10^5 Pa.

2.4 Modeling the Hydration Process and Cementitious Materials

2.4.1 Modeling of Cement Hydration

Cement hydration is recognized as a complex physico-chemical process and many attempts have been made to describe and quantify the kinetics of hydration. Since the cementitious system is characterized by its microstructural parameters, such as w/c ratio, degree of hydration, or curing history, many of the developed models are provided to explicitly consider the effects of these microstructural parameters. Powers and Brownyard [1958] developed a model to describe the influence of the w/c ratio on the development of the capillary porosity of cement paste. It was pointed out that higher w/c ratio contained much more capillary water than the paste with lower w/c ratio, and the properties of cement paste are much affected by the water content in the paste. Microstructural parameter, called gel-space ratio was first defined by Powers [1958] to describe to what extent the available space is occupied by the gel during the hydration process, where available space is defined as the volume of the gel plus the volume of capillary pores. Powers model, which is governed by physico-chemical parameters of the cement paste, namely degree of hydration, w/c ratio and porosity, has also been developed recently by the researcher to investigate the properties changes in the hydration by relating the microstructural parameters of the cementitious system.

The influence of w/c ratio on cement hydration kinetics was modeled by Bentz [2006] based on simple spatial consideration within Powers model. The models were

presented depending critically on the volume fraction of water-filled and total capillary porosity, and using Powers model these quantities were given as the functions of w/c ratio and degree of hydration of the cement paste. The models for hydration kinetics were built from three level of complexity. It is first assumed that the hydration rate is simply proportional to the volume fraction of this water-filled porosity, then for the next level of complexity, it analyzed as the hydration rate had a first order dependence on both the volume fractions of available water-filled porosity and available unhydrated cement. Finally, for considering the sealed curing conditions, the fraction of unhydrated cement shown in the second model for hydration rate was estimated as the total fraction of unhydrated cement multiplied by the ratio of water-filled to total porosity. The models developed by Bentz [2006] were evaluated in comparison to data sets available from the literature and measured by authors. The most advantage of the provided simply models is that it shows the promise in describing the hydration behavior of cements blended with inert fillers. The models are easily extended to consider the influence of the replacement of a portion of the cement by relatively inert fillers.

2.4.2 Material Models of Cementitious System

Garboczi et al. [1995;1996] presented an investigation of the transport properties of concrete using a multi-scale computer model based on the percolation theory providing an overall picture of the relationships between the microstructure properties. Following the argumentation of Garboczi [1996], cementitious materials are composite materials that exhibit a complex microstructure, which can be described by using a wide range of length scales. Concrete consists of mortar and aggregates with

random features in the order centimeters. Mortar can again be subdivided into cement paste and sand, which results in inhomogeneties of the size of millimeters. Cement paste itself is a heterogeneous material that combines unhydrated cement, CSH, CH and capillary pores. Here, the randomness can be described on the level of micrometers. The CSH as the main phase of the cement paste is a highly heterogeneous material with complexities measured on the nano scale level. Thus, the defined goal of relating properties and microstructure of cement-based materials must be accomplished by spanning a wide range of length scales, covering several orders of magnitude.

Jennings and Johnson [1986] provided a model at the level of single cement particles to represent the microstructure of cement paste. In the model spherical tricalcium C_3S particles are randomly arranged in a three-dimensional space according to the w/c ratio. At each hydration step a certain amount of the particles is converted to CSH causing the formation of hydration shells around the particles. Additionally, calcium hydroxide CH crystals are allowed to nucleate and grow in the pore space. When, due to their growth, spherical particles overlap the overlap volume is redistributed over the particles that are part of the newly formed cluster. Similar to the model of Jennings, the continuum models of cement paste reported by Navi and Pignat [1996] considered spherical particles of tricalcium silicate C_3S placed in a three-dimensional body, where the pore spaces are filled with water. The model was extensively used for studying the connectivity of the capillary pore space and the pore size distribution.

As nanoindentation has provided an unprecedented access to micromechanical properties of the elementary phases of cementitious materials[Velez et al. 2001, Constantinides et al. 2003], it becomes possible to break down the complex microstructure of cementitious materials to the scale where cementitious materials do no more change – in a statistical sense- from on mix proportion to another, within this scale, it becomes possible to employ advanced homogenization techniques of microporomechanics that became recently available[Dormieux et al. 2002], and adapt them to meet the requirements of the multiscale microstructure of cementitious materials, starting at the scale where physical chemistry meets mechanics[Ulm et al. 2004]. A detailed multiscale investigation of cement-based porous materials has been recently reported by Ulm et al. [2003]. The microstructure of cement-based materials was broken down into five elementary levels, as sketched in Figure 2-2 Level '0' is the lowest level of a mechanical representation of the complex microstructure of cement-based material at this scale where the material properties are solely defined by the physical chemistry of the formation process of the material. Then step by step, the proceeded levels were just built on top of the right pre-level. The homogenization has been taken at each level to quantify the effective properties of the complex composite structure. The upscaling schemes finally estimated the stiffness and the poroelastic constants of cement paste and mortar, and results of undrained stiffness of the given cement paste presented closely coincidence with the stiffness value obtained by ultrasound pulse velocity measurements of the cement paste, while the drained stiffness values from multiscale modeling almost coincide with the value from resonance frequency measurement of the cement paste. It pointed out a clear

indication of the predictive capabilities of the homogenization scheme in multiscale modeling for cement paste.

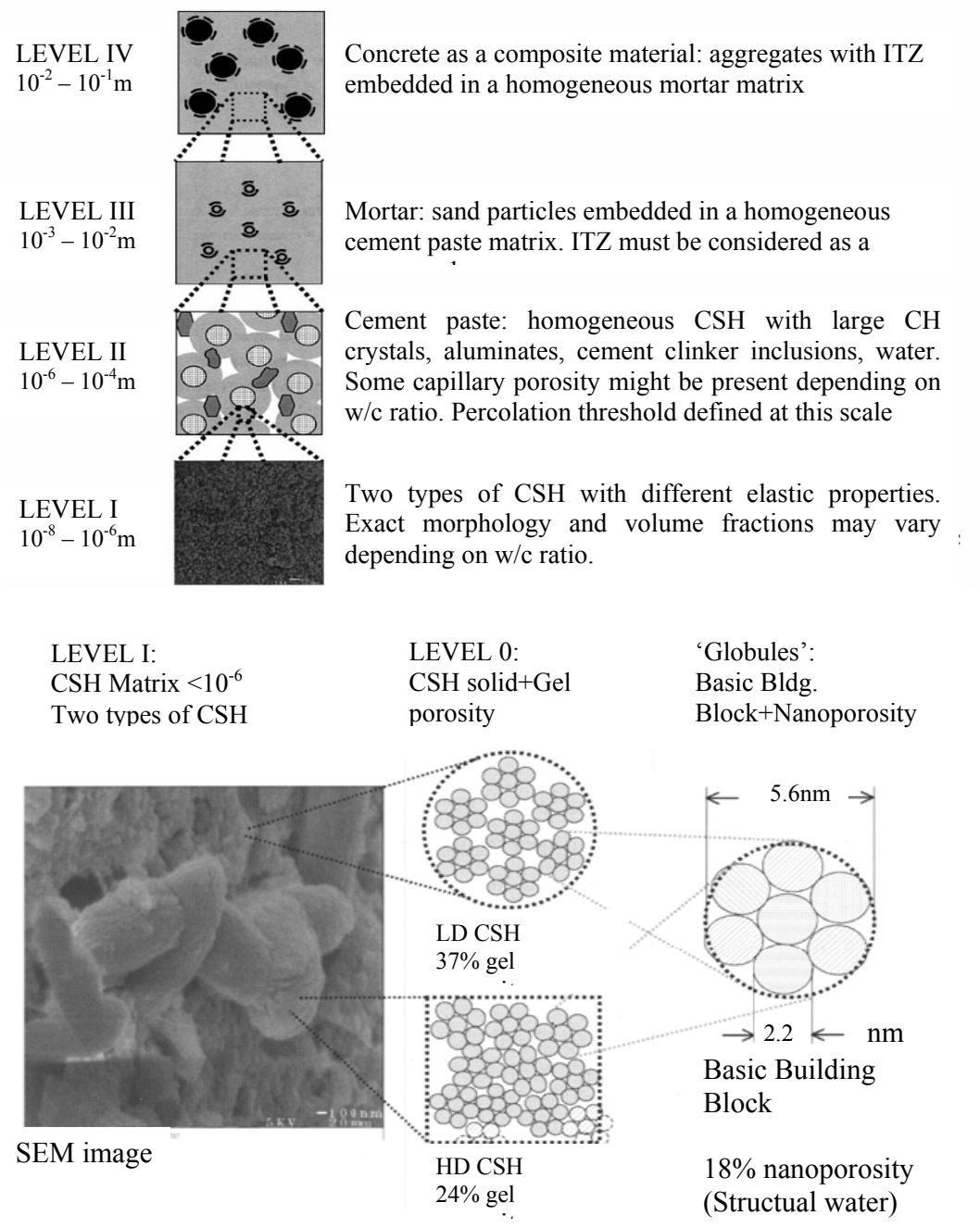

Figure 2-2 Representation of multiscale heterogeneous microstructure of cementitious comoposites [Ulm et al. 2004]

2.5 Acoustics of Porous Media

2.5.1 Introduction

Porous media are aggregates of solid elements, grains, matrix, etc. between which the voids form the pore space itself. These voids within the porous body give rise to wide differences in physical behavior between dense solids and porous substances. The presence of a fluid, even in a very small amount, adds to the overall complexity of the complicated assemblages. Biot [1956;1962] first established a simple and effective two-phase theory for the acoustics of porous media in the mid 1950's. Saturated porous media were considered by taking several general assumptions in Biot's theory. The first assumption states that the wavelength is large in comparison with the dimensions of macroscopic elementary volume. This assumption, which is normally satisfied in geophysical applications, is required for analytical processes based on the continuum mechanics. The second assumption is that the displacements are small for both fluid and solid phases. The third assumption is that the liquid phase is continuous, and the final assumption is that the matrix is elastic and isotropic. Although the development of the theory started with a homogenous and isotropic assumption, anisotropic cases were also examined in a general theoretical manner by Biot and Willis later.

The application of Biot's theory to the wave propagation and reflection in ocean sediments has been widely investigated by a number of researchers. The parameters

used in Biot's theory have also been widely examined experimentally which would contribute to a further understanding of porous media.

2.5.2 Porosity

The ratio of void volume V_p to total volume V_t of the sample is called the porosity. This petrophysical value is usually easy to define and measure. However, the process becomes far more complicated when one attempts to make a geometric description of the pore space. While a few specific cases, such as the pore space existing in the packed spheres of the same diameter, lend themselves easily to quantitative descriptions, most actual pore spaces are too complex to be dealt with in a strictly geometric manner, and only relative descriptions are feasible [Bourbie et al. 1987].

The most common measuring methods on porosity are summarized in the book edited by Bourbie et al. [1987]. Table2-1 shows the main methods for porosity measurement, where the solid volume V_s of porous media is given by

$$V_s = V_t - V_p$$

Table 2-1 Main methods for measuring porosity [Bourbie et al. 1987]

Measured volume	Text reference	Measuring method
Total volume V_t	[1]	Buoyancy in mercury: Mercury, the non-wetting liquid,does not penetrate without pressure into commonly encountered porous media. This method provides a very accurate measurement of the total volume
	[2]	Direct sample measurement of the different lengths: This method is only suitable for test specimens with very regular shapes
Pore Volume V_p	[3]	Setting of wetting fluid by total saturation under vacuum: Pore volume is obtained directly from the difference in dry and saturated weight
Solid volume V_s	[4]	Compressibility of a perfect gas: A plot is made of the pressure vs. volume injected in a container that is first empty and then contains the sample. The difference is used to calculate the volume of solid, whose compressibility is ignored
	[5]	Buoyancy in a wetting fluid totally saturating the porous body: Solid volume is measured directly from the difference between the dry and immersed weight
	[6]	Measurement of solid density: After fine grinding of the porous substance
	[7]	Calculation of the solid density: By quantitative analysis of the constituent minerals

It has also been mentioned in the book that these methods are not equivalent in the actual fact. Techniques [3], [4], and [5] take account only of the pores connected to the exterior, while methods [6] partly and [7] entirely account for all the voids.

The characterization of porosity in cement paste recently has been investigated through indirect measurements. Phuaksuk [2000] has conducted experimental investigation of the early age development of pore structure in hydrating cement paste, and the results clearly established that the pore size is concentrated around its average value. Punurai et al. [2007] examined the capillary porosity and entrained air content in hardened cement paste through a measurement using ultrasonic attenuation method. An ultrasonic attenuation model related to the size and volume fraction of entrained

air voids was proposed in the measurements, and the inversion technique based on Nelder-Mead simplex method was implemented to calculate the volume fraction in hardened cement paste. As shown in Figure 2-3, a simple approach described by Powers model was used to estimate the total capillary porosity in a volume of cement paste with varied water/cement ratios.

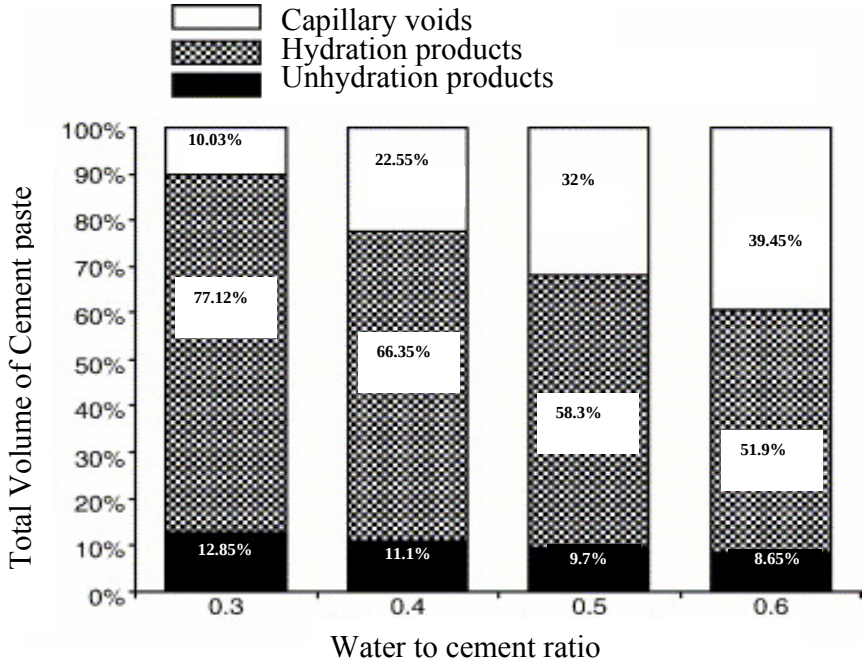

Figure 2-3 Microstructural phase model of hardened cement paste comprising solids, capillary voids and air with varying water/cement ratio with 75% degree of hydration assumed [Punurai et al. 2007]

Their results showed a good agreement with the results obtained by stand petrographic methods and by gravimetric analysis. This indicated that ultrasonic attenuation measurements could be used to quantify the relationship between the increasing porosity (which is related to the increasing w/c ratios) sand ultrasonic wave characteristics.

2.5.3 Wave Propagation and Reflection in Saturated Porous Media

One fundamental feature of Biot's theory of wave propagation in a porous medium is the prediction that there always exists a fast and a slow compressional mode, as well as a shear mode in a fluid-saturated porous solid. However, direct experimental observation of the slow compressional bulk wave at MHz frequencies was not achieved until 1980 by Plona [1980] in a water-saturated porous fused glass bead sample. Since that time, there has been considerable interest in the acoustic theory of porous solid. Reflection and transmission of elastic waves from an interface between fluid and fluid-saturated porous solids is an important problem not only from the viewpoint of applications in ultrasonic nondestructive evaluation (NDE), underwater acoustics, and seismology, but also in the theoretical aspect. However, very few quantitative results on this subject have been published. Most of the results were obtained only for special situations due to the inevitable difficulty in the calculation.

Deresiewicz and Skalak [1963] firstly discussed the boundary conditions of wave propagation and reflection on the surface of discontinuity. A series of conditions have been built with the required continuity across an interface of the total (normal and tangential) traction, of the fluid pressure P (for the case when the two media are in perfect hydraulic contact), of the solid particle velocity v, and of the normal component of the relative fluid velocity. B. Gurevich and M. Schoenberg [1999] derived interface conditions at a boundary between tow porous media directly from Biot's equations of poroelasticity by replacing the discontinuity surface with a thick

transition layer. The interface permeability which was defined by Deresiewicz was addressed with particular interface conditions in the study. The derivation showed that in a certain interface condition, the range of the interface permeability had to be determined to obtain the corresponding boundary equations.

Stoll and Kan [1981] derived reflection coefficients related to displacement potential at a water sediment interface based on Biot's theory. The reflection and refraction of homogeneous plane incidence was discussed, and the velocity and attenuation of the refracted waves were shown to be dependent on the angle of incidence and no critical angle was observed. Numerical examples in the study showed distinct difference in reflection coefficients of the two cases in which a viscoelastic model of sediment was compared to the porous viscoelastic model. It was found that the reflectivity is much more frequency dependent in the porous media. Donald G. Albert [1993] numerically compared the wave propagation characteristics within water-filled and air-filled materials in the 10Hz to 100 kHz band through the use of Biot's theory. The calculations showed that the ratio of fluid to solid motion for the slow compressional wave is around 2 in the water-filled sand, but greater than 300 in the air-filled sand. It was also found when the fluid is water, nearly all of the incident energy is transferred to the reflected wave and to the transmitted fast compressional wave that is traveling mainly in the solid frame, and only slight frequency dependence occurred in the energy transfer. For the case of air filled porous medium, the interaction of the waves with the boundary is strongly dependent

upon the frequency, and most of the incident energy is transferred to the reflected wave and to the transmitted slow compressional wave traveling mainly in the pores.

Water-saturated sand and sediment porous media were investigated by many researchers using Biot's theory. N. Chotiros [1995] reviewed experimental data of various test methods and presented measurements of the speeds and attenuations of both the fast and slow waves. The results were compared with extant Biot model predictions for water-saturated sand, from which it was concluded that certain input parameter values need to be modified. The critical parameters were identified as the grain and frame bulk moduli. In the case of the grain bulk modulus, the value was obtained by direct laboratory measurements. The final result was a set of Blot input parameter values that gave wave speeds and attenuations of both the fast and slow waves in the 10- to 100-kHz band. N .Chotiros [2002] also conducted wave reflection analyses at the water/sediment interface theoretically and experimentally. Based on his results from the testing and the theoretical analysis, the parameters of Biot's model were used to evaluate the dynamic response of sediments.

2.6 Summary

The applications of various nondestructive test methods on concrete have been widely developed recently. For a comprehensive classification of different nondestructive methods that can be applied in laboratories or in the field, a handbook edited by Malhotra and Carino [2004] can be referred to. The International Association for Building Materials and Structures(RILEM)has established a

committee 185-ATC on advanced testing of cement-based materials during setting and hardening. The comprehensive overview about numerical and computer modeling of cement-based materials could be found by Garboczi, Bentz and Ye [Garboczi 1996; Bentz 1997; Ye et al. 2007].

In general, the mechanical properties of early age cement-based materials including elastic modulus, strength are mush more difficult to measure at early ages then later in hydration process, as they are often continuously changing during the course of the physical measurement. Ultrasonic wave reflection measurement gives the advantage of evaluating the materials properties change without disturbing the microstructure of the cement-based materials. It can be used as and indicator of setting, and have also been extended to predict compressive strength gains at early age. Ultrasonic wave reflection measurement could be developed to have more sensitivity on evaluating the change of cement hydration, and reveal more precise microstructure evolution at initial age of hydration. It has to be developed based on improved experimental setup and theoretical analysis. Rheometric investigation provides understanding of the rheologic properties of early age cement-based material, which in common engineering practice reveals the workability and stability of the cement-based material at early age.

Through the classical micro-macro relations of poroelasticity, concrete has been considered as a poromechanics materials, without necessarily distinguishing between nano-, micro- and macro- porosity, and this for both saturated concrete, and

unsaturated cement-based materials[Fauchet 1991; Heukamp 2001]. However, the application using two-phase constrained poromechanics material to investigate concrete faces the difficulties. Concrete has been revealed as highly heterogeneous material[Garboczi 1995], with a heterogeneity which manifests itself at multiple scales, in form of different pore spaces and multiple minerals that build up the solid phase[Bentz 1991]. It was indicated by Ulm et al. [2004] the multi-scale homogenization schemes were suitable to investigate the cement-based materials as a poromechanics material since the solid phase would be homogenized at each scale. Biot's porous theory only deals with two-phase porous media, and it implicitly assumes that the pores in the skeletal frame formed by solid phase are of the same size. A recent experimental investigation of the early age development of pore structure in hydrating cement paste clearly indicated that the pore size is concentrated around its average value [Phuaksuk 2000]. Thus the use of Biot's poro-elastic theory is suitable to study the evolution of porosity of skeletal frame. In addition, it is well documented that the strength of a cementitious materials is dependent on the rate and degree of hydration at any given time. It was shown by Keating et al. [1989] that the change of the porosity increases the connectivity of the solid phase and density and elastic material properties of the pastes at early age. The porosity of cementitious matrix, the density, and the elastic materials properties of the hydration products form the internal system variables (microstructure parameters] of a poroelastic medium. Thus, from a micro to macro- view on the cement-based material, the research study based on the poro-elastic idealization of the microstructure of cementitious materials appears promising.

Chapter 3 Ultrasonic Measurement of Viscoelastic Shear Modulus Development in Hydrating Cement Paste

3.1 Introduction

In cementitious materials, setting, stiffening and subsequent strength gain, are produced by the hydration reaction between cement and water. Initially after mixing, the material is in a fluid state, which allows it to be placed in forms. With time, the cementitious mixture stiffens and becomes less workable. There is a progressive change in the state of the material where the fluid state is transformed into a solid state with continued hydration. This gradual development of rigidity is known as setting. After setting, with time, the solid stiffens and gains strength. The change in the state of the material from a fluid to a solid and the subsequent gain in strength are a result of continuous evolution of the microstructure in the cementitious phase of the material. The microstructure development of the cementitious phase is responsible for the progressive change in the mechanical properties of the material. Monitoring changes in the mechanical properties of the cementitious phase, therefore, provides an insight into the development of the microstructure.

There are very few techniques which are suited for measuring changes in the properties of a cementitious material through setting and early stages of strength gain. Rheological, electrical or ultrasonic techniques have been employed and each has its own limitations and applicability. Low frequency, oscillatory shear measurements

(rheological measurements) indicate that cement paste behaves like a visco-elastic fluid, which can be characterized using loss and storage moduli. With hydration, the increase in the low frequency storage modulus is shown to be significantly higher than the corresponding change in loss modulus, signifying a change in the microstructure to a stiffer and more solid-like state [Struble et al. 2000; Nachbaur et al. 2001; Subramaniam and Wang 2009]. The beginning of setting (or emergence of a solid phase) defines the practical limit of applicability of the oscillatory shear measurements. Electrical measurements indicate a continuous evolution in the resistivity, capacitance and admittance of cement pastes with progressing hydration [McCarter et al. 2003; Christensen et al. 1994; Gu et al. 1993]. While these properties are intimately related to the microstructure of the material, there is no direct relationship with the mechanical properties.

A one-sided experimental technique which monitors horizontally polarized shear (SH) wave reflected at normal incidence from an interface between a buffer material and cementitious material has been applied to monitor the changes in hydrating materials through setting [Valic and Stepisnik 1996 and 2000; Subramaniam and Lee 2003; Subramaniam et al. 2005 and 2007; Sun et al. 2006]. In this technique, changes in the measured phase and amplitude of an ultrasonic pulse reflected from cementitious material were used to determine the evolution of shear modulus with time. The accuracy of the reflection technique depends upon the ability to sensitively detect changes in the characteristics of the ultrasonic wave induced by the reflection, which depends upon the acoustic impedance of the cementitious material. After

mixing and in the early stage of hydration, cementitious materials have very low values of shear modulus and acoustic impedance. Therefore, sensitive measurements of the magnitude and changes in shear modulus from ultrasonic reflection measurements in the first few hours of hydration have remained a challenge. With time, the increase in the shear modulus produces an increase in the acoustic impedance of the material.

One method to improve the accuracy from the ultrasonic reflection measurements, particularly in the early ages, requires using a buffer material with low acoustic impedance. Polymeric materials meet this requirement and PMMA was selected for its chemical inertness to cement. When a buffer material with low acoustic impedance such as poly-methyl methacrylate (PMMA) was used, changes in the shear modulus of the cementitious material were very sensitively detected through the setting process [Subramaniam and Lee 2003]. However, since the high frequency visco-elastic properties of PMMA are not known, the shear modulus of the cementitious materials could not be determined. Only the changes in shear modulus of the cementitious material relative to the shear modulus of PMMA at a given frequency could be measured. It should be noted that PMMA and other polymeric materials which are chemically inert to cement and have low acoustic impedance are also very sensitive to moisture and temperature. There are changes in the acoustic impedance of PMMA with changes in temperature and if it is exposed to water. Both moisture and temperature effects cannot be ignored when dealing with cement pastes since hydration is a water-based, exothermic reaction. In earlier experiments, the

influence of water and temperature changes on PMMA, were carefully calibrated in the laboratory and all measurements were performed under controlled conditions [Subramaniam and Lee 2003]. The temperature and moisture sensitivity make PMMA an unsuitable material for practical applications.

After a review of the available materials, fused quartz was found to be a suitable material which provides chemical inertness with cement paste and moisture insensitivity. Fused quartz however has relatively high acoustic impedance compared to cementitious materials in the early ages, which may not provide sufficient sensitivity in measurements to delineate early age changes in cement paste. Reflection of SH waves using fused quartz buffer plates has been applied for monitoring other aging visco-elastic materials such as curing epoxy systems [Alig et al. 1997; Shah and Balasubramaniam 2000]. It has also been shown that one-sided reflection measurements have several sources of inaccuracies which potentially limit the accuracy of the technique. For instance, at normal incidence, changes in the amplitude of the ultrasonic wave were shown to be very small for low viscosity liquids resulting in a large uncertainty in the measured viscosity [Dixon and Lanyon 2005]. Sources of error in phase measurements which have been shown to have a significant effect on the material property determination are associated with (a) temporal resolution and (b) temperature variations. Accurate measurements of phase changes for ultrasonic waves in the Mega-Hertz range requires a minimum digitization rate of 1ns; No shift was observed using an oscilloscope with a 10 ns data acquisition rate, suggesting the need for higher resolution digitizers and/or lower

probing frequencies. In the laboratory, temperature changes of a one degree of the elastic substrate were found to have a significant effect on the phase and arrival-time measurements. Introducing the sample on the elastic substrate has been shown to produce temperature changes which can effect the measured phase. To overcome the problem of accurate phase measurements, corrections were made by simultaneously running two probes, one with the sample and second without (blind probe) and subtracting the results [Alig et al. 1997]. A calibration to correct for the influence of temperature effect was also developed by Dixon and Lanyon [2005]. In reflection measurements, using higher frequencies has been shown to provide better accuracy in amplitude measurements. The accuracy in phase measurements is however lower with higher frequencies. To overcome the problem of accurate phase measurement from reflected waves in normal incidence measurements, an interferometer-like arrangement has been explored [Shah and Balasubramaniam 2000].

Sources of inherent measurement errors and inaccuracies in one-sided reflection measurements from cement paste using fused-quartz buffer material are presented in this paper. From an analytical evaluation, considering reflection of a shear wave with fused-quartz as the buffer material, oblique incidence is shown to provide higher sensitivity to low impedance materials than normal incidence. It is shown that monitoring reflected waves at oblique incidence allows for sensitively monitoring changes in the stiffness of the material in the early stage of hydration (through setting). Reflection measurements obtained from hydrating cement pastes are

presented and changes in the elastic and viscous components of shear modulus are related with physical changes in the cementitious material.

3.2 Theoretical Background

Prior to performing an inversion to determine the shear modulus of the cement paste in contact with fused-quartz using the reflection data, it is instructive to study the response of reflected waves at the interface between the two materials (Figure 3-1). While fused-quartz is an elastic material, cement paste can be treated as a visco-elastic material. From a stress-based formulation for one-dimensional wave propagation, the reflection coefficient for an SH wave at the interface between materials 1(Elastic medium) and 2(Visco-elastic material) can be derived applying conditions of stress and velocity continuity across the interface as [Achenbach 1973]

$$re^{j\Phi} = \frac{Z_2 \cos\theta_2 - Z_1 \cos\theta_1}{Z_2 \cos\theta_2 + Z_1 \cos\theta_1} \tag{3-1}$$

where Z_i is the acoustic impedance of material *i*, *r* and Φ are the changes in the amplitude and phase of the stress-wave upon reflection, θ_1 is the incident angle, θ_2 is the angle of the refracted wave.

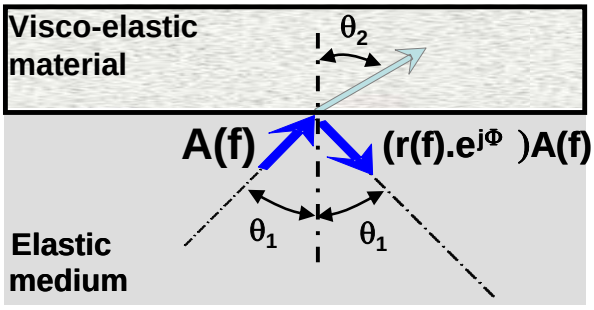

Figure 3-1 Schematic representation of reflection at an interface

The acoustic impedance can be related to the shear modulus of the material as

$$\boldsymbol{Z_i} = \sqrt{\rho_i \boldsymbol{G_i}} \tag{3-2}$$

where ρ_i and G_i are the density and shear modulus of the material i respectively. The frequency dependent dynamic shear modulus of visco-elastic material is a complex quantity and could be written as

$$G^*(\omega) = G'(\omega) + jG''(\omega) \tag{3-3}$$

where G', the real part of the complex shear modulus, is called the storage modulus and describes the elastic portion of the material behavior; G'', the imaginary part, is the loss modulus and represents the viscous behavior, ω is the circular frequency ($\omega = 2\pi f$); f is the frequency; and $j = \sqrt{-1}$. The complex shear modulus can be written in another form as

$$\boldsymbol{G}^*(\omega) = \boldsymbol{G}(\omega)\boldsymbol{e}^{j\phi(\omega)} \tag{3-4}$$

where $G(\omega)$ is the frequency dependent dynamic shear modulus of the material and $\varphi(\omega)$ is the phase angle. Further, G and φ can be related to G' and G'' as

$$G(\omega) = |G^*(\omega)| = \sqrt{G'^2 + G''^2} \tag{3-5}$$

$$\phi = \tan^{-1}\left(\frac{\boldsymbol{G}''}{\boldsymbol{G}'}\right) \tag{3-6}$$

The acoustic impedance of visco-elastic material can be written as

$$\boldsymbol{Z}^* = \sqrt{\rho(\boldsymbol{G}' + \boldsymbol{jG}'')} = \sqrt{\rho \boldsymbol{G}}\,\boldsymbol{e}^{j\frac{\phi}{2}} \tag{3-7}$$

The acoustic impedance of visco-elastic material has a real part describing the mechanical resistance and an imaginary part representing the mechanical reactance.

$$\boldsymbol{Z}^* = \boldsymbol{R} + \boldsymbol{jQ} \quad \text{or} \quad Z^* = \left|Z^*\right| e^{j\chi} \tag{3-8}$$

where $\chi = \tan^{-1}\left(\frac{\boldsymbol{Q}}{\boldsymbol{R}}\right) = \frac{\phi}{2}$ and $\left|\boldsymbol{Z}^*\right| = \sqrt{\boldsymbol{R}^2 + \boldsymbol{Q}^2} = \sqrt{\rho \boldsymbol{G}}$.

Stress-based reflection coefficient for SH waves traveling in an elastic medium at the interface with a visco-elastic material can therefore be written as

$$r(f)e^{j\Phi(f)} = \frac{Z_2^* \cos\theta_2 - Z_1 \cos\theta_1}{Z_2^* \cos\theta_2 + Z_1 \cos\theta_1} \qquad \text{or} \qquad re^{j\Phi} = r(\cos\Phi + j\sin\Phi) \quad (3\text{-}9)$$

where Z_2^* is the complex impedance of the viscous medium, Z_1 is the impedance of the elastic solid, θ_1 is the incident angle, θ_2 is the angle of the refracted wave, *r(f)* and Φ(*f*) are frequency dependent reflection amplitude and phase coefficients. θ_1 and θ_2 are related by Snell's law.

$$\frac{\sin\theta_1}{\boldsymbol{v}_1} = \frac{\sin\theta_2}{\boldsymbol{v}_2} \quad (3\text{-}10)$$

where v_1 and v_2 are the shear wave velocities in medium 1 and 2, respectively. The wave reflection at such an interface introduces a phase shift and an amplitude change between the incidence and the reflection waves.

Inversion of visco-elastic properties based on reflection coefficient

The frequency dependent storage modulus *G'(f)* and the loss modulus *G''(f)*, can be calculated from the measured *r(f)* and Φ(*f*) using Equation (3-8) and (3-9) as

$$\boldsymbol{G}' = \frac{\boldsymbol{R}^2 - \boldsymbol{Q}^2}{\rho_2} = \boldsymbol{Z}_1^{\,2} \frac{(1-\boldsymbol{r}^2)^2 - 4\boldsymbol{r}^2 \sin^2\Phi}{\rho(1+\boldsymbol{r}^2 - 2\boldsymbol{r}\cos\Phi)^2} \frac{\cos^2\theta_1}{\cos^2\theta_2} \quad (3\text{-}11)$$

$$\boldsymbol{G}'' = \frac{2\boldsymbol{RQ}}{\rho_2} = \boldsymbol{Z}_1^{\,2} \frac{(1-\boldsymbol{r}^2)4\boldsymbol{r}\ \sin\Phi}{\rho(1+\boldsymbol{r}^2 - 2\boldsymbol{r}\cos\Phi)^2} \frac{\cos^2\theta_1}{\cos^2\theta_2} \quad (3\text{-}12)$$

where

$$R = Z_1 \frac{1 - r^2}{1 + r^2 - 2r\cos\Phi} \frac{\cos\theta_1}{\cos\theta_2} \tag{3-13}$$

$$\boldsymbol{Q} = \boldsymbol{Z}_1 \frac{2\boldsymbol{r}\sin\Phi}{1 + \boldsymbol{r}^2 - 2\boldsymbol{r}\cos\Phi} \frac{\cos\theta_1}{\cos\theta_2} \tag{3-14}$$

The frequency dependence has been dropped from the terms in Equations (3-11) to (3-14) for convenience of writing. Therefore both the elastic and viscous components of shear modulus can be determined from the measured amplitude and phase changes of the reflected signal.

Consideration for low impedance materials

The successful use of the inversion formula to determine the G' and G" of the cementitious material, requires that the measured r and Φ be higher than the resolution of the system. The role of the different parameters can be evaluated by considering that r and Φ depend upon the ratio of acoustic impedances, $\left(\left| \boldsymbol{Z}_2^* \right| / \boldsymbol{Z}_1 \right)$ and the incident and refracted angles

$$re^{j\Phi} = \frac{\left(\left| Z_2^* \right| / Z_1 \right) e^{j\chi} \frac{\cos\theta_2}{\cos\theta_1} - 1}{\left(\left| Z_2^* \right| / Z_1 \right) e^{j\chi} \frac{\cos\theta_2}{\cos\theta_1} + 1} \tag{3-15}$$

Considering cement paste in contact with fused-quartz, $v_2 << v_1$ (in the early stages of hydration, when the cement paste is a fluid, its shear wave velocity is negligible

compared to the shear wave velocity of fused-quartz). Therefore, the reflection can be approximated as

$$re^{j\Phi} = \frac{\frac{\left(\left|Z_2^*\right|/Z_1\right)e^{j\chi}}{\cos\theta_1} - 1}{\frac{\left(\left|Z_2^*\right|/Z_1\right)e^{j\chi}}{\cos\theta_1} + 1} \tag{3-16}$$

Also, for cement paste in the fluid state, $\left|Z_2^*\right|$ is significantly smaller than Z_1. This implies the imaginary part of $\left(\left|Z_2^*\right|/Z_1\right)e^{j\chi}$ would be significantly smaller than 1.0. Therefore the phase change in the signal, Φ, would depend upon θ_1 If θ_1 is zero (normal incidence), Φ approaches 180 degrees. Also, changes in Φ associated with small changes in $\left(\left|Z_2^*\right|/Z_1\right)$ would be of a very small magnitude and experimentally difficult to detect. The measured Φ can be increased by increasing θ_1, which would result in a larger magnitude of the imaginary component relative of $\left(\left|Z_2^*\right|/Z_1\right)e^{j\chi}$ and hence a larger Φ. Therefore, oblique incidence would provide a larger Φ, which imposes lesser restrictions on the resolution required for measurements. This is also illustrated in Table 3-1, where the percentage change in the measured Φ is computed for a 10% change in the value of $|Z_2^*|/Z_1$ for different values of χ at incident angles equal to 0 degrees (normal incidence) and 60 degrees.

Table 3-1 Percentage change in the measured at 0 and 60 degree angles of incidence for a 10% change in $|Z_2^*|/Z_1|$.

$\|Z_2^*\|/Z_1$	χ (deg)	% change in Φ at Incident Angle (θ_1) 0	60
0.001	10	0.001	0.002
0.01	10	0.011	0.022
0.01	30	0.032	0.064
0.1	10	0.115	0.250
0.1	30	0.335	0.731

3.3 Experimental Setup and Test Procedure

A schematic diagram of the experimental setup for oblique ultrasonic wave reflection measurement is shown in Figure 3-2. The experimental system includes temperature sensors, a function generator, an oscilloscope, a temperature controlled chamber, a computer and a test probe. The test probe comprises of ultrasonic transducers attached to a buffer plate made of fused quartz, which is in contact with the hardening cement paste. The properties of fused-quartz are given in Table 3-2. A matched pair of commercially available broad-band, direct-contact, ultrasonic shear transducers (PanametricsTM, V153) with a nominal center frequency of 1 MHz was mounted on the opposite oblique surfaces of the plate as shown in the figure. In the figure, labels T and R identify the transmitting and receiving transducers, respectively. These two transducers were aligned precisely at the center of the surfaces of the sending and receiving ends of the expected wave path along the plate. The transducers were bonded to the fused-quartz using a thin layer of solid couplant (the couplant after solidification bonds the transducer to the quartz). While attaching the transducers, the axes of the transducers were aligned to generate a horizontally

polarized shear wave (SH) in the fused quartz. A function generator (Agilent 33250A) was used to send a 1 MHz, 10-cycle, tone burst with pulse repetition period equal to 200 ms. Simultaneously, a trigger pulse was sent to the oscilloscope to initialize data capture. The reflected signal detected by transducer was digitized by the oscilloscope (TektronicsTM, TDS 3054B). The data was then transferred to the computer via GPIB for storage and processing. The oscilloscope had a digitization rate of 5 GS/s which provides a temporal resolution of 0.2 ns. 100 waveforms were averaged to minimize the influence of random noise in the signal. An averaged waveform was acquired every 10 minutes allowing sufficient time to take the average and minimize the volume of data collected over typical monitoring period. Each acquired waveform comprised of 8500 points of data. Temperature data was collected from the top and bottom surfaces of the fused quartz buffer plate, and from inside the material being monitored. A data logger connected to the computer was used to collect temperature data from three thermo-couples, at the same time the reflection data collection was triggered. The data acquisition and storage was automated using a program developed using LabViewTM, which allows for controlling the oscilloscope and data retrieval over the GPIB interface.

Table 3-2 Properties of the substrate

Substrate	Density ρ_1 (kg/m^3)	Shear Modulus G_1 (GPa)	Shear impedance Z_1 (kg/ms)	Shear velocity $\boldsymbol{v}_1$ (m/s)
Fused Quartz	2.2x10^3	31.0	8.26x10^6	3.75x10^3

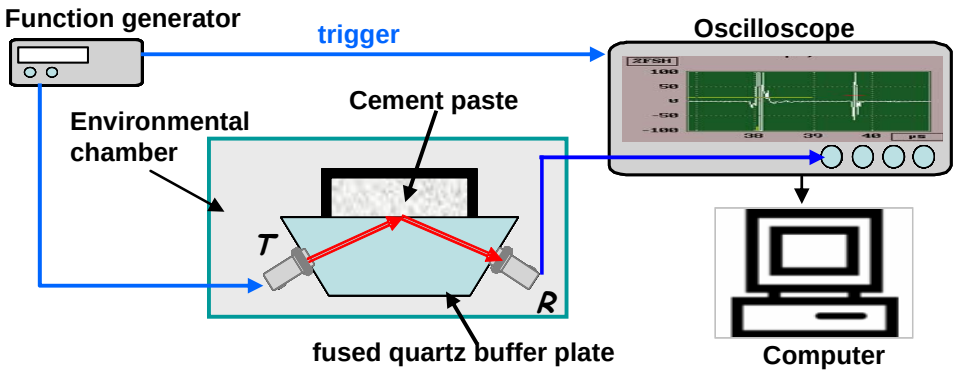

Figure 3-2 Schematic diagram of oblique ultrasonic wave reflection experimental setup

The test procedure comprised of collecting reflected signals at the fused-quartz/air interface prior to placing the test material on the fused quartz. The signal received after reflection at the fused-quartz/air interface was used as a reference for evaluating changes in the reflected signal with any other test material. The procedure for determining the amplitude and phase change after reflection at the fused-quartz/test-sample interface is schematically illustrated in Figure 3-3. The change in the amplitude of the wave at frequency f, is given by the reflection factor $r(f)$. $r(f)$ was obtained using the self-compensating technique, which involves processing data in the frequency domain [Achenbach et l992; Subramaniam and Lee 2003]. Using the reflected signal from the fused-quartz/air interface as the reference, r(f) at the test material/quartz interface can be determined by normalizing the reflected magnitude from the test sample/fused-quartz interface with the reflected amplitude from the air/quartz interface. In the frequency domain, the stress wave signals received after a single reflection at the air/quartz and sample/quartz interfaces can be represented as

$$F^{air/quartz}(f) = s(f)d_1(f)d_2(f) \tag{3-17}$$

$$F^{sample/quartz}(f) = s(f)r(f)d_1(f)d_2(f) \tag{3-18}$$

where $F(f)$ is the magnitude of FFT of the reflected time domain signal as received by the transducer, $d_1(f)$ represents the signal losses in the couplant, $d_2(f)$ is the material signal loss along the signal path in the elastic fused quartz, $s(f)$ is the input source function, and $r(f)$ is the reflection coefficient at the bi-material interface. Therefore, the reflection coefficient can be determined by normalizing the magnitude of reflected wave recorded at the sample/quartz interface with respect to the amplitude of reflected wave recorded at the air/quartz interface as shown below

$$r(f) = F^{sample/quartz}(f) / F^{air/quartz}(f) \tag{3-19a}$$

The reflection coefficient, $r(f)$, determined by Equation (3-19a) defines the ratio of the amplitudes of the reflected and incident waves at the interface and is free from the influence of signal losses due to material and other geometric effects. Since all measurements were performed at 1 MHz, the amplitude reflection co-efficient at 1 MHz, r(1) was determined as

$$r(1) = F^{sample/quartz}(1) / F^{air/quartz}(1) \tag{3-19b}$$

where $F(1)$ is the magnitude of FFT of the reflected time domain signal at 1 MHz as received by the transducer.

The phase change introduced after reflection at the test material/fused-quartz interface was obtained from the temporal shift in the signal, measured in the time

domain, considering the reflected signal from the air/fused-quartz interface as a reference. The temporal shift is related to a phase change in the reflected signals as

$$\Delta t = \frac{\Phi_r^{\,sample/quartz} - \Phi_r^{\,air/quartz}}{\omega} \tag{3-20}$$

where, Δt is the measured temporal shift in the signal from the sample/quartz interface when compared with the air/quartz interface, $\Phi_r^{\,sample/quartz}$ is the phase of reflected signal from test-material/ quartz interface and $\Phi_r^{\,air/quartz}$ is the phase of the reflected signal from air/quartz interface. Since $\Phi_r^{\,air/quartz}$ is known and is equal to π, the value of $\Phi_r^{\,sample/quartz}$ can be determined from Equation (3-20) if the temporal shift in the signal is known.

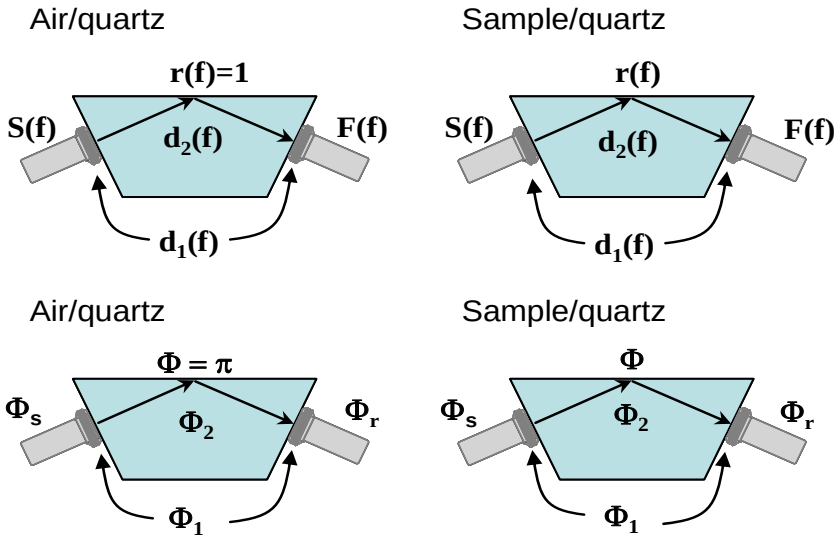

Figure 3-3 Schematic representations of reflections at fused-quartz/ air and fused-quartz/sample interfaces showing changes in amplitude (a and b) and phase (c and d) along the wave path.

As shown in Figure 3-3, the phase of recorded reflected waves can be represented as

$$\Phi_r^{air/quartz} = \Phi_s + \Phi_1 + \Phi_2 + \pi \tag{3-21a}$$

$$\Phi_r^{sample/quartz} = \Phi_s + \Phi_1 + \Phi_2 + \Phi \tag{3-21b}$$

where Φ_s is the phase angle of the incident wave, Φ_1 and Φ_2 are the phase changes introduced during transmission through the couplant and fused quartz and refers to the measured phase change at 1 MHz from the temporal measurements. From Equations (3-20 to 3-21), the phase change in the reflected wave from the sample/quartz interface can be derived as:

$$\Phi = \pi - \omega\Delta t \tag{3-22}$$

To calculate the temporal shift, the zero crossing reference point, the point where the signal crosses the horizontal axis, was used to measure the position of the reflected waves. Since the digitization step was 2ns, the zero crossing was determined by linear interpolation between points located on either side of zero vertical scale. The average of zero crossing reference points from four consecutive clear sine waveforms located in the middle of the signal was taken in order to minimize the random errors. Thus the temporal delay associated with the reflected signal was obtained as

$$\Delta \boldsymbol{t} = \frac{\Sigma(\boldsymbol{t_n}^{\boldsymbol{sample/quartz}} - \boldsymbol{t_n}^{\boldsymbol{air/quartz}})}{\boldsymbol{n}} \tag{3-23}$$

where $\boldsymbol{t_n}^{\boldsymbol{sample/quartz}}$ and $t_n^{air/quartz}$ are the n-th corresponding zero crossing reference points of the reflected waves from the sample/quartz and air/quartz interfaces, respectively.

3.3.1 Verification and Calibration of System

Sources of random and systematic errors in the measured phase and amplitude were determined and the linearity of the system was established prior to initiating measurements. Since the phase change in the reflected signal is calculated from the temporal shift in the signal, the temporal resolution of the discrete signal in the time domain determines the accuracy of the zero crossing reference point. Once the center frequency of transducers is defined, the resolution for the phase measurement relating to the temporal delay can be defined as follows:

$$\varepsilon_p = 2\pi f \Delta t_a \tag{3-24}$$

where f is the center frequency of transducers and Δt_a is the data acquisition rate. Considering the 2 ns temporal resolution, the possible error in the measured phase angle is in the range of ($\pm$ 0.72^o). A higher data acquisition rate would yield a higher resolution of phase measurement. However, limitation of the highest data acquisition rate provided by the oscilloscope used in the experimental setup restricts the accuracy in the measurement. The resolution error can however be improved by continuous averaging waveforms for every acquisition, which provides a higher effective sampling rate. The waveforms were zero-padded to a length of 16384 points, which provided a frequency resolution of 30 kHz. Typical variations in amplitude (of FFT at 1 MHz) and phase obtained from several averaged signals acquired from the fused-quartz/air interface for the 50 degree angle of incidence and 23^{o}C at 10 minute intervals are shown in Figure 3-4. The influence of both systematic errors associated with the finite temporal resolution and the inherent noise in the measurements, contribute to the range of values obtained from one measurement. A measure of the

magnitude of the variation can be obtained from the standard deviations of the values, which can be related to the error in the measured phase and amplitude, and were found to be equal to 0.024^{o} and 0.059, respectively. It should be noted that while increasing the temporal resolution would decrease the systematic source of error, the random noise would still be fixed fraction of the lowest resolution.

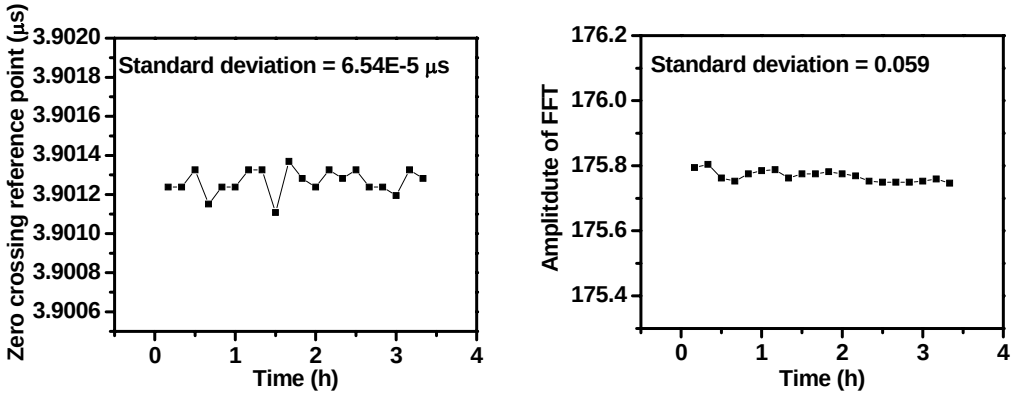

Figure 3-4 Variation of zero crossing point and amplitude changes of reflected signals

The linearity of the system and self-calibrating procedure were verified from reflection measurements at the fused-quartz/air interface using well defined inputs provided by a function generator. In the first set of tests, incident signals of three different amplitudes, 1 V, 3 V, and 5 V, and the same incident phase angle were applied to the transmitting transducer. The changes in the amplitude of the received signal (amplitude of FFT at 1 MHz) for the three different inputs are plotted as a function of the applied signal amplitude as shown in Figure 3-5. The linearity of the system in amplitude is verified by the high 0.99999 coefficient of regression for a linear fit to the data. To evaluate the phase, an incident signal with amplitude 5 V and

four different phase angles, 0^o, 30^o, 60^o, and 90^o, were applied to the transmitting transducer. The linear fit between the applied phase angle and the obtained phase of the reflection with a coefficient of regression equal to -0.99999 verified the linearity in phase measurements.

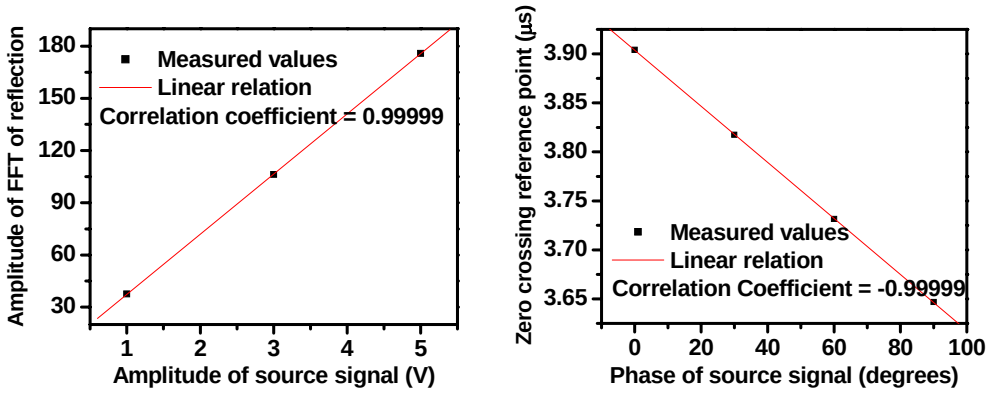

Figure 3-5 Calibration curves for the effects of varying the amplitude and phase of the incident wave on the reflected signals.

3.3.2 Temperature Calibration

Changes in the signal transmission on account of temperature sensitivities of the couplant used to attach the transducers, the transducers and the buffer material were investigated using a temperature controlled chamber. The reflection at the interface between the air and fused quartz was recorded as the temperature was increased in steps of 1^oC from 23^oC to 29^oC and then decreased back to 23^oC. The ratio of the signal amplitudes at 1 MHz, $\Delta r(1)$, at different temperatures was determined, considering 23^oC to be the reference. Similarly the change in phase at 1 MHz, $\Delta\Phi(1)$, with temperature was determined from the measured temporal shifts

using 23°C as the reference. The changes in the signal amplitude and phase at the air/fused quartz interface due to the temperature changes are shown in Figure 3-6 and can be written as:

$$\Delta \boldsymbol{r}(1) = 1 + \boldsymbol{C}_{T1}\boldsymbol{T} = 1 + 0.01\boldsymbol{T} \tag{3-25}$$

$$\Delta\Phi(1) = 180 - \boldsymbol{C}_{T2}\boldsymbol{T} = 180 - 1.5\boldsymbol{T} \tag{3-26}$$

where T is the change in temperature in deg C and the unit for the phase shift is degrees; $\boldsymbol{C}_{T1}$ and $\boldsymbol{C}_{T2}$ are coefficients obtained through the experimental calibration.

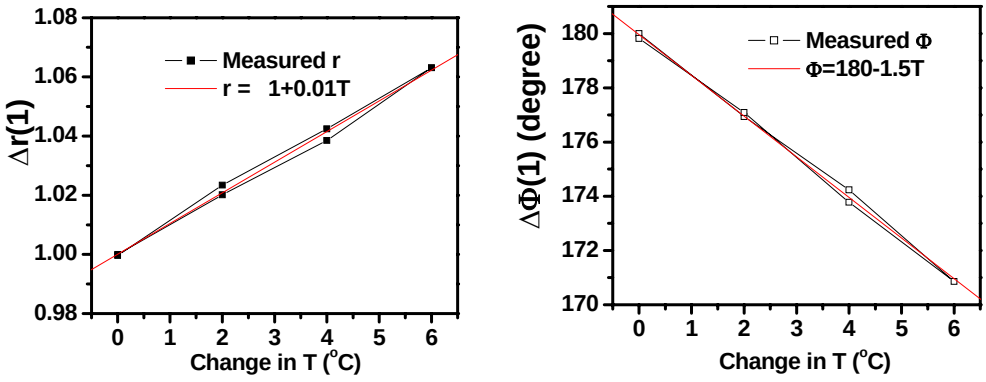

Figure 3-6 Temperature effects on amplitude and phase reflection coefficients.

Since hydration of cement is associated with a temperature rise, careful consideration must be given to determining r(1) and Φ (1) (measured at 1 MHZ) from the signals recorded at different temperatures. If we consider T_1 as the reference temperature and $T_2(t)$ the temperature produced during the hydration reaction, the frequency domain representation of the signals obtained from the fused-quartz/air interface can be written as $\boldsymbol{F}_1^{air/quartz}$ and $\boldsymbol{F}_2^{air/quartz}$ for signals obtained at T_1 and $T_2(t)$, respectively. Similarly, the representation in the frequency domain for reflected signals from the cementitious material/fused quartz interface at T_1 and $T_2(t)$ can be

written as $\boldsymbol{F}_1^{cem-mat/quartz}$ and $\boldsymbol{F}_2^{cem-mat/quartz}$ respectively. $\boldsymbol{F}_1^{air/quartz}$ is obtained before casting the samples, and $\boldsymbol{F}_2^{cem-mat/quartz}$ is recorded after casting the samples and the temperature shifts from $\boldsymbol{T}_1$ to $\boldsymbol{T}_2$(t). From Equation (3-19), the reflection coefficient at $\boldsymbol{T}_2$ is given as

$$\boldsymbol{r}(1) = \boldsymbol{F}_2^{cem-mat/quartz}(1) / \boldsymbol{F}_2^{air/quartz}(1) \tag{3-27}$$

From the temperature effect relation in Equation (3-25),

$$\boldsymbol{F}_2^{air/quartz}(1) / \boldsymbol{F}_1^{air/quartz}(1) = 1 + \boldsymbol{C}_{T1}\left[\boldsymbol{T}_2(\boldsymbol{t}) - \boldsymbol{T}_1\right] \tag{3-28}$$

Therefore

$$\boldsymbol{r}(1) = \frac{1}{1 + \boldsymbol{C}_{T1}\left[\boldsymbol{T}_2(\boldsymbol{t}) - \boldsymbol{T}_1\right]} \frac{\boldsymbol{F}_2^{cem-mat/quartz}(1)}{\boldsymbol{F}_1^{air/quartz}(1)} \tag{3-29}$$

Similarly, we can get the following expression for the phase (phase change produced by reflection):

$$\Phi = \Phi_2^{cem-mat/quartz}(1) - \Phi_1^{air/quartz}(1) - \boldsymbol{C}_{T2}\left[\boldsymbol{T}_2(\boldsymbol{t}) - \boldsymbol{T}_1\right] + 180 \tag{3-30}$$

It should be noted that the temperature correction only applies when the temperature is uniform across the entire wedge.

3.3.3 Viscosity Measurement of Standard Liquid

A liquid with well defined viscosity was added to the surface of the fused quartz buffer plate, 15 minutes after collecting data on the reflection from fused-quartz/air interface. A liquid with nominal viscosity 1 Pas (1000 cps) and density equal to 889 kg/m^3 was used (NIST traceable viscosity standard). A low-viscosity liquid was chosen for evaluation for two reasons: (a) to test the sensitivity of measurements to detect changes produced by a liquid of low acoustic impedance; and (b) it has been

shown that the dynamic viscosity from ultrasonic measurements for low viscosity liquids corresponds well with the actual viscosity measured with other techniques. For highly viscous liquids there is significant difference in the dynamic viscosity obtained using ultrasonic waves and the viscosity obtained from standard rheological measurements [Shah and Balasubramanian 2000].

Typical variations in the amplitude and phase of the reflected signals before and after placing the liquid on the fused-quartz plate for normal and 50^{o} angles of incidence are shown in Figures 3-7 and 3-8, respectively. The results show that for normal incidence measurement, changes in both the amplitude and the phase are comparable to the level of noise in the measurement. This is particularly noticeable for phase measurements, where the change in phase is indistinguishable from the noise. It can be seen that the changes in the amplitude and phase of the signal upon adding the liquid to the surface of the fused quartz plate is significantly higher than the inherent noise in the measurement for the case of oblique incidence This confirms that the measurement at oblique incidence provides higher sensitivity to changes in impedance of the material in contact with the fused-quartz. Some drift evident in the measured amplitude and phase of the signals is associated with minor temperature fluctuations associated with stabilization of the temperature inside the chamber.

The results from the measurements from the 1 Pa s liquid at 23^{o}C are tabulated in Table 3-3. The exact viscosity of the liquid at 23^{o}C specified is equal to 0.965 Pa s. The values of Φ and r given in the table correspond to averaged value obtained from

three repeated measurements using different samples of the liquid for each measurement. The reflection coefficient r was calculated from the measured decrease in the amplitude of FFT following the procedure outline before. The corresponding error in each measured quantity corresponds with the range in the multiple measurements. The average value and the range of viscosity calculated from the measured values of r and Φ from the normal, and 50 degree oblique incidence are shown in the last three columns of the table. The viscosity of the liquid was obtained using the relationship for dynamic shear modulus $G''=\eta\,\omega$ [Shah and Balasubramanian 2000]. It can be seen that differences in the viscosity of tested samples for normal and oblique incidence experimental results are significant. The range of viscosity values obtained from the oblique incidence is significantly smaller than the magnitude of the value. There is also a closer agreement between the values of viscosity determined from the ultrasonic measurement and the actual value. The value obtained from normal incidence, however does not agree with the other values. The range of measured viscosity is also significant when compared to the measured value.

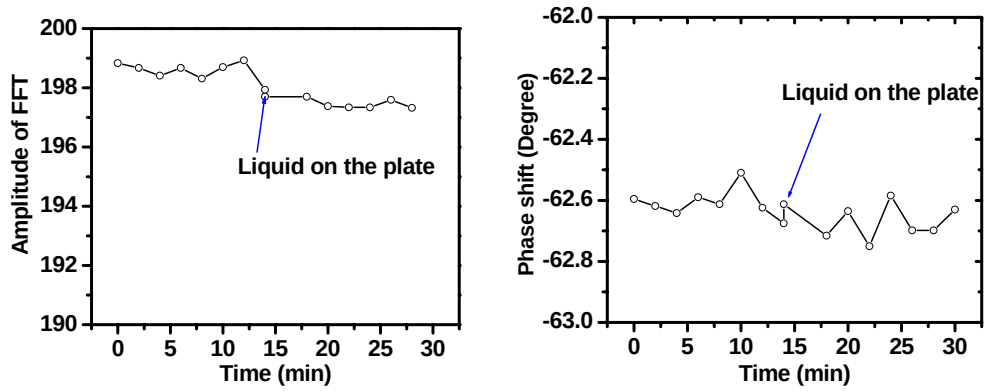

Figure 3-7 (a) Amplitude of FFT and (b) Phase change from temporal shift of the reflected signal collected from normal incidence measurement.

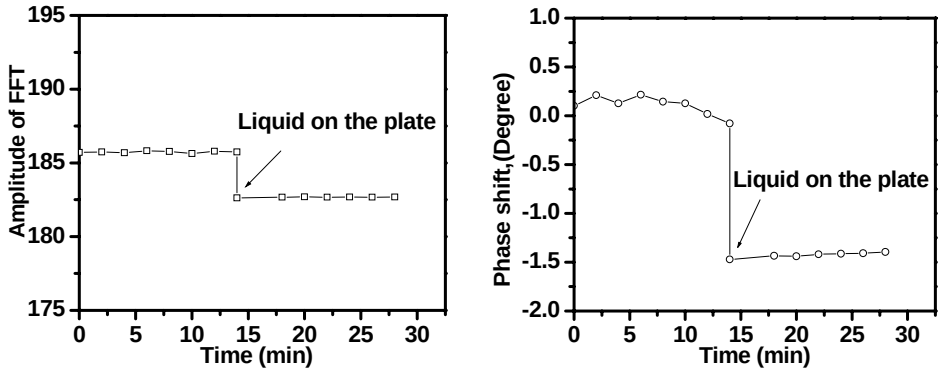

Figure 3-8 (a) Amplitude of FFT and (b) Phase change from temporal shift of the reflected signal collected from an oblique incidence measurement.

Table 3-3 Comparison between normal and oblique incidence for standard liquid of viscosity 0.965 Pa s (at 23°C)

Density (kg/m^3)	Measured Phase (deg)		Measured Amplitude (r)		Measured Viscosity(Pa s)	
	Normal	Oblique 50°	Normal	Oblique 50°	Normal	Oblique 50°
889	179.95 ±0.06	178.47 ±0.03	0.994 ±0.001	0.983 ±0.001	0.039 ±0.033	1.123 ±0.023

The advantages of employing oblique incidence to measure changes in phase and amplitude corresponding to a given change in the impedance ratio of the materials in contact with fused quartz (air initially and standard fluid) are obvious from the larger change in the measured quantities for a given change in the impedance ratio. This implies that oblique incidence would provide a higher sensitivity1 in the measured phase and amplitude changes for a given change in the impedance ratio. Conversely, for normal incidence, small variations in the measured amplitude would lead to a large variation in the measured viscosity. Further, considering the viscosity of the

[1] Sensitivity refers to the change in the measured quantity for a unit change in the material property

liquid, the expected values of r(1) and Φ(1) may be below the limits of experimental detection.

The higher sensitivity of the measurements at oblique incidence when compared to normal incidence results in better signal-to-noise ratio in measurements. This is particularly important for low impedance materials when the ratio of acoustic impedances is low. For cement paste, since the acoustic impedance ratio in the early stages of hydration starts from a low value, higher sensitivity in this range of impedance ratio would result in more reliable experimental outcomes from oblique incidence. The viscosity of cement paste (for range of water to cement ratio between 0.3 and 0.5) measured using low-amplitude rheological measurements is typically in the range of 10^{-2} to 1.0 Pas [Saak 1999; Domone 2003]. The results from the standard liquid clearly demonstrate that using normal incidence, for viscosity below 1.0 Pas, the measured phase change would lead to significant experimental errors with very high uncertainty in measured viscosity at a temporal resolution equal to 2 ns. This implies that the viscous component of shear modulus, G", cannot be accurately measured using normal incidence unless the temporal resolution is significantly higher than 1 ns. Accurate phase measurement at normal incidence for low viscosity liquids requires a specialized setup such as an interferometric arrangement [Shah and Balasubramanian 2000]. Oblique incidence measurement provides sufficient sensitivity, with a higher accuracy in the measured values and can be used directly.

3.4 Experimental Results from Hydrating Cement Pastes

A temperature controlled chamber, which was maintained at 25^{o}C was used for performing measurements on hydrating cement pastes. The test probe comprising of the fused quartz buffer plate and the transducer were placed inside the chamber two hours before initiating data collection. Data was collected from the fused-quartz/air interface before placing the cement paste on the buffer plate. After mixing, the cement paste samples were placed in the chamber for 1 hour before placing the cement paste on the buffer plate to ensure the temperature of the paste attained 25^{o}C. To reduce the influence of minor temperature fluctuations associated with stabilization of the temperature inside the chamber, ultrasonic date collection was initiated 1 hour after placing the cement paste on the fused quartz. All measurements were performed using SH shear waves at 50 degree angle of incidence. During measurements, the cement samples were kept sealed to prevent moisture loss.

Cement paste samples were mixed using a paddle mixer following a procedure suggested by Williams et al. [Williams et al. 1999], which is similar to ASTM C-305. Cement and water were initially mixed at 140 rpm for 30 s, followed by a pause for 1 minute before mixing for another 2.5 minutes at 285 rpm. Cement paste adhering to the sides of the mixing bowl was scraped and the entire mixture was mixed for another 2.5 minutes following a 1 minute pause. Cement paste samples with three different water-to-cement ratios (w/c) equal to 0.4, 0.5 and 0.6, were evaluated in the test program.

Typical time domain signals captured after one reflection at the cement paste/fused-Quartz interface and its corresponding representation in the frequency domain are shown in Figures 3-9 and 3-10, respectively. The signals are shown at distinct time periods after the first contact of cement with water. Decrease in the amplitude of the signal and phase shifts can be observed for ultrasonic waves recorded at successive times from the cement paste interface. In the time domain, the shape of the signal and the frequency content of the reflected waves (the relative magnitudes of the different frequencies) are relatively unaltered. Initially, in the first few hours (up to 4 hours after mixing cement and water), there is a very small change in reflected waveforms. However, there is a significant change in the reflected waveforms after the first few hours, which is discernable in both the time and the frequency domains.

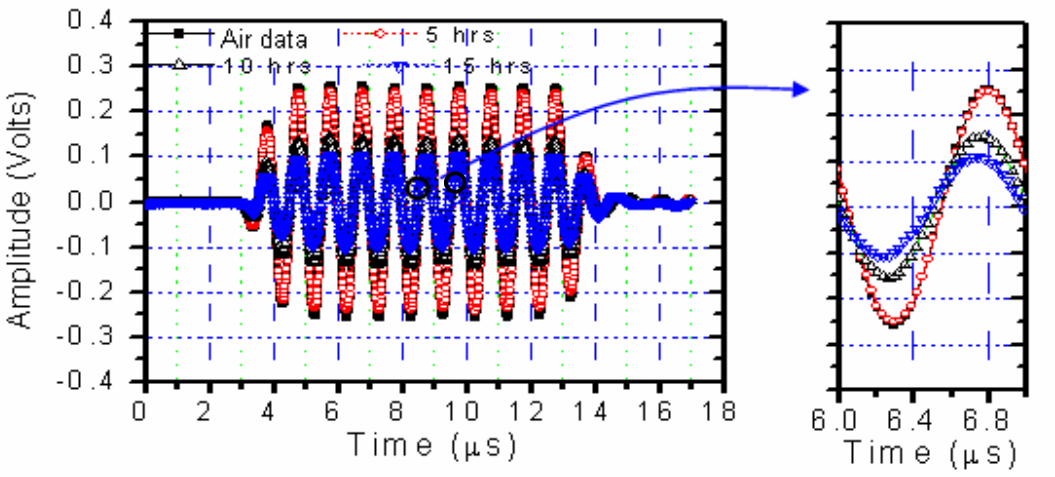

Figure 3-9 Time domain waveforms of the stress waves recorded after reflection at the fused quartz/paste interface for the mixture with w/c = 0.4 at different times.

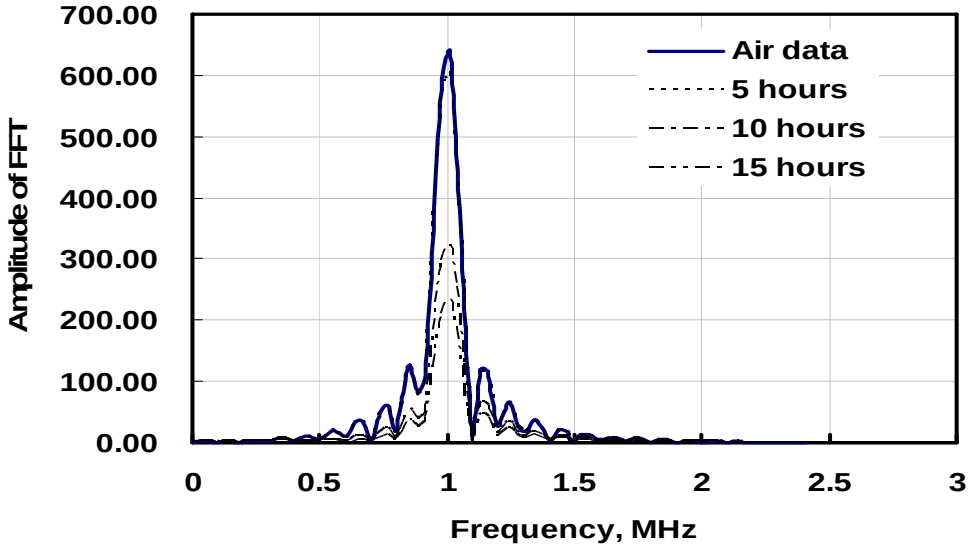

Figure 3-10 Amplitude of FFT of the stress waves recorded after reflection at the fused quartz/paste interface for the mixture of w/c equals to 0.4

For each w/c ratio, three replicates were tested. r(1) and Φ(1) for three different w/c ratios as a function of elapsed time after mixing cement and water are shown in Figure 3-11, 3-12 and 3-13, respectively. The temperature changes recorded from the cement paste are also shown for reference. From the temperature measurements it was found that the rate of temperature change produced by the hydration reaction was slow enough to produce a nearly uniform temperature across the wedge during heating and cooling. The temperature difference between the top and bottom surface of the fused-quartz wedge was less than 0.5 deg C at all times. Temperature correction was applied to r(1) and Φ(1) using the temperature of the cement paste. It is apparent that the measurements on the cement paste samples show good repeatability in both amplitude and phase. Further the general trends in r(1) and Φ(1) with time are similar for all three cement mixtures. There is initially a very gradual decrease in r(1) and Φ(1) in the first few hours after mixing, which is followed by a

period of very rapid decrease in both quantities. There is evidence of a slight slow down in the decrease of r(1), which occurs between 8-12 hours. This is more noticeable as the w/c ratio is increased. Changes in the measured r(1) and Φ(1) correlate well with the distinct stages in the hydration reaction determined from the measured temperature changes. Changes in temperature are indicative of the rate of reaction, r(1) and Φ(1) represent changes in the cementitious material due to hydration. There is a gradual decrease in r(1) and Φ(1) during the dormant period when there is no temperature change. The rise in temperature following the dormant period, which is associated with the accelerating stage of the hydration reaction, produces a rapid change in the material properties. This is reflected in the rapid decrease in measured r(1) and Φ(1)The onset of the deceleration stage, which is indicated by a decrease in the temperature, is indicated by a noticeable decrease in the gradient of r(1) and Φ(1) with time.

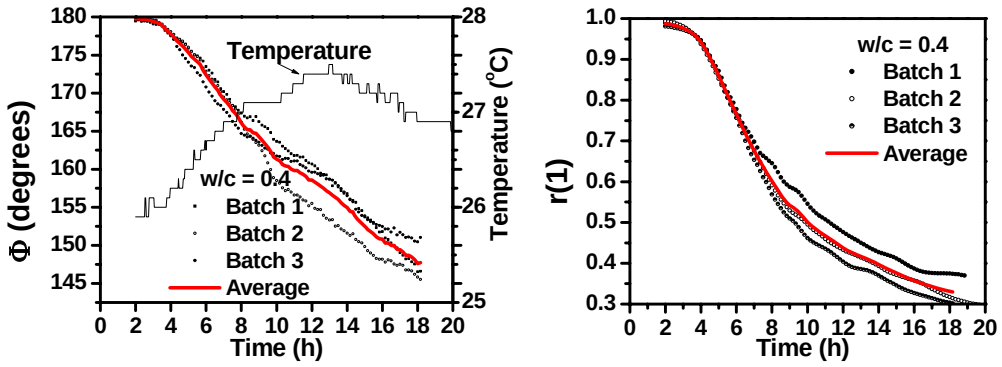

Figure 3-11 Measured amplitude and phase reflection coefficients as a function of elapsed time for w/c equals to 0.4

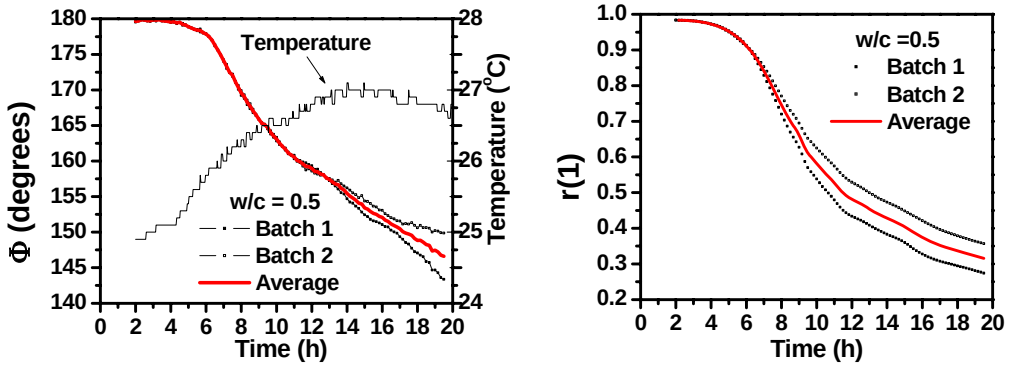

Figure 3-12 Measured amplitude and phase reflection coefficients as a function of elapsed time for w/c equals to 0.5

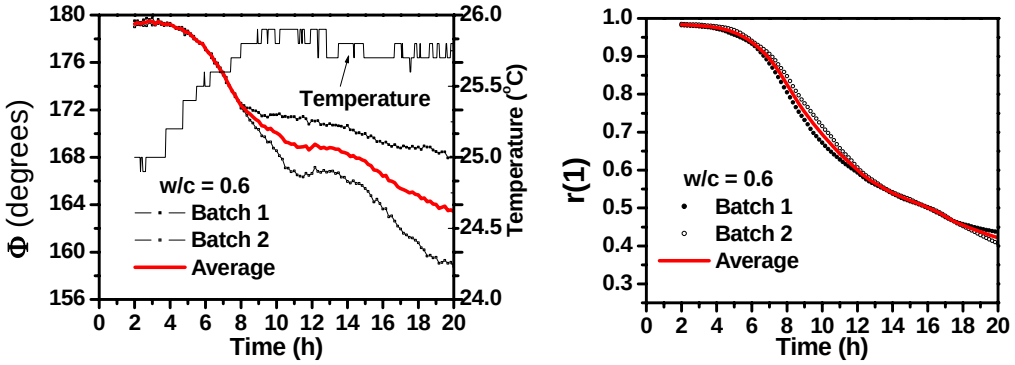

Figure 3-13 Measured amplitude and phase reflection coefficients as a function of elapsed time for w/c equals to 0.6

An idealized representation for interpreting the observed changes in r(1) in terms of physical changes in the state of the material had previously been developed [Subramaniam et al. 2002, 2005] and is shown in Figure 3-14. Point A signals the end of the dormant period and the beginning of the acceleration stage of hydration reaction, which is water-based reaction. The region between points A and B corresponds physically with the transition from the fluid paste to a solid form by the products of the hydration reaction. Further decrease in the amplitude factor after B is

due to the continuing hydration process that results in the strength gain of the solid. The point B signals a change in the rate controlling step in the hydration reaction, from a water-based dissolution and precipitation to diffusion control.

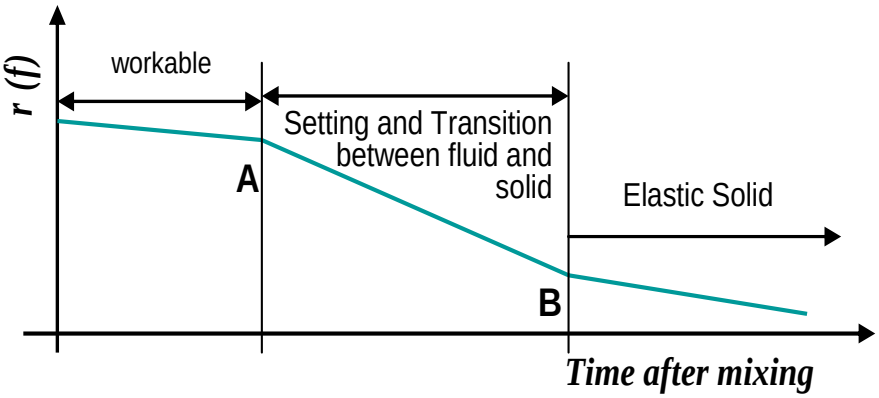

Figure 3-14 Schematic representation of hydration process monitored by the ultrasonic wave reflection method

A comparison of the amplitude reflection factors for all three w/c ratios is shown in Figure 3-15 with the corresponding schematic representations of each cement paste. The higher reactivity of lower w/c cement pastes is indicated by the larger relative decrease in the magnitude of r(1) at any time. This is consistent with the rate of hydration indicated by the temperature measurements. Further, the stages of hydration indicating the transitions between the different stages are distinctly identifiable in all three cases. The times for initiation and the end of the fluid-to-solid transition are increased as the ratio of w/c increases.

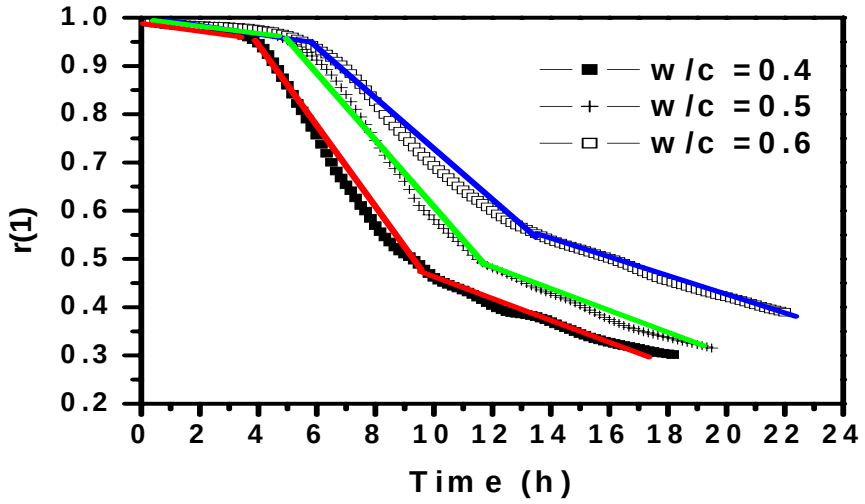

Figure 3-15 A comparison of amplitude coefficients as a function of the elapsed time for w/c equal to 0.4, 0.5 and 0.6 respectively

3.5 Analysis and Discussion

During hydration, the strains associated with volumetric changes produced by thermal and shrinkage phenomena are of the order of 10^{-4} – 10^{-3} mm/mm and the mass change in sealed specimens is less than 1% [Lura and Jensen 2007; Lura 2003]. These changes will therefore result in a negligible change in the density of the cementitious material with time. Therefore, $\rho_{\text{fused-quartz}}/\rho_{\text{paste}}$ can be treated as a constant and the observed changes in the reflected ultrasonic signals are produced by change in the shear modulus of cement paste. The density of each cement paste sample was determined at the end of the test when it was in a hardened state and was found to be 1.98, 1.87 and 1.77 g/cm^3 for samples with w/c = 0.4, 0.5 and 0.6, respectively. The values of the storage modulus G', the loss modulus G″ and the phase ϕ of the complex modulus G* for cement paste were calculated from the experimentally measured r(1) and $\Phi(1)$ and are shown in Figure 3-16, 3-17 and 3-18

for w/c = 0.4, 0.5 and 0.6, respectively. The increase in the shear modulus and measured changes in temperature are also plotted for comparison. It can be seen that there is continuous evolution of both storage and loss moduli with time resulting in four orders of magnitude increase in the magnitudes of both G' and G" up to 20 hours. Within the first few hours after mixing, there is a very rapid, almost exponential increase in both G' and G" with time which eventually leads to a period of steady, almost linear increase. The phase angle, ϕ(depends on the ratio of G" to G') shows an increase in the first few hours followed by a decrease. In a period lasting between 5 to 8 hours after mixing, depending upon the w/c ratio of the cement paste, the phase angle increases up to values greater than 70^{o}. It is interesting to note that the end of the rapid increase in phase approximately corresponds in time with the end of the exponential increase in G* (the inflection point in the G* response). This suggests that during this period, there is a larger increase in the viscous component of shear modulus, and it contributes more significantly to the increase in the shear modulus. In the period following this initial rise, there is a rapid decrease in the phase angle which lasts up to 10 to 14 hours depending on the w/c ratio. After this period, there is a steady almost linear decrease in phase with time, suggesting larger relative increase in the elastic component.

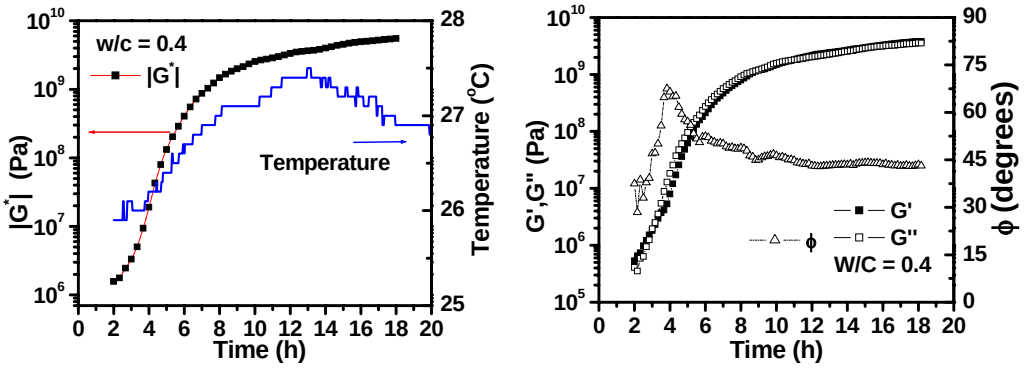

Figure 3-16 (a) G″, G′ and phase of shear modulus ϕ as a function of elapsed time at 1MHz for w/c equal to 0.4; (b) |G*| at 1 MHz and temperature as function of elapsed time for w/c equals to 0.4

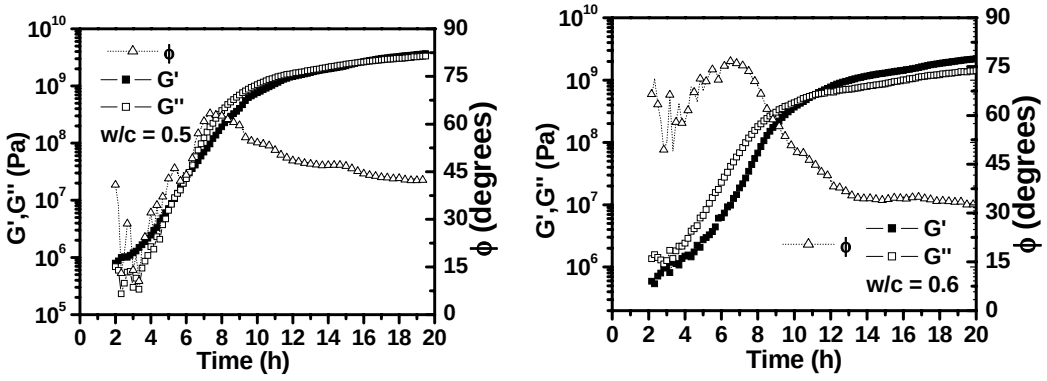

Figure 3-17 (a) G″, G′ and phase of shear modulus ϕ as a function of elapsed time at 1MHz for w/c equal to 0.5; (b) |G*| at 1 MHz and temperature as function of elapsed time for w/c equals to 0.5

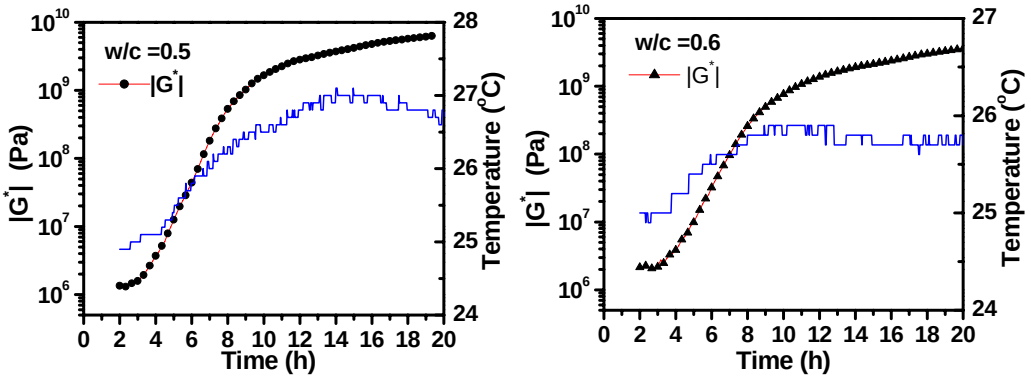

Figure 3-18 (a) G″, G′ and phase of shear modulus ϕ as a function of elapsed time at 1MHz for w/c equals to 0.6; (b) |G*| at 1 MHz and temperature as function of elapsed time for w/c equals to 0.6

The frequency of the ultrasonic wave determines the length-scale of the material microstructure accessed by the waves. The measurements from cement paste correspond with changes on a length scale comparable to the wavelength of the ultrasonic waves. For the measurements reported in this paper, the wavelength of the shear wave varies from 10^{-6} to 10^{-3} m as the cement paste gains in stiffness. Therefore, while the frequency remains the same, reflected shear waves contain information about different length scales at different times. To provide a basis for comparing length scales, the size of cement grains are typically in the order of 10^{-5}-10^{-6} m. The pore structure in hardening cement paste, through and following setting, evolves with time and contains pores ranging from 10^{-9} to 10^{-4} m. The wavelengths of the ultrasonic waves therefore overlap with the length scales associated with the microstructure of cement paste. Conventional rheological measurements, on the other hand, are performed at frequencies in the range of 0.1-10 Hz, and access information at a significantly larger length scale than the microstructure. The shear modulus from the rheological measurements is typically in the range 10^{3} – 10^{5} Pa. The rheological

measurements therefore obtain material response which is a composite average over length scales which are significantly larger the microstructure. This can potentially contribute to the large frequency dependence in the measured shear modulus since the values obtained from the ultrasonic measurements are in the range of $10^6 – 10^9$ Pa.

By reconciling the information available from the change in shear modulus, G* and the relative magnitudes of G' and G", an understanding of the changes in the material during setting can now be developed. Using the measured temperature to provide a reference for the different stages of hydration reaction, it is clear that following the dormant stage there is a very rapid, almost exponential increase in the shear modulus during the early part of the acceleration stage of the hydration reaction. For w/c = 0.4 and 0.5, close to the end of the dormant period and in the early part of the acceleration stage, G' determined from the ultrasonic measurements has a larger magnitude than G". This is in agreement with the observations from the rheological measurements [Nachbaur et al. 2001]. The setting of cement paste as indicated by penetration measurements is known to occur within the acceleration stage [Valic et al. 1999; Subramaniam et al. 2005]. It is now known that from measured changes at the length scale accessed by the 1 MHz wave, during setting, the cement paste initially becomes more viscous followed by larger increase in the elastic stiffness. This correlates well with observed physical changes in the materials. The increase in the viscous component correlates with the decrease in the workability of cement paste, which is known to occur in the initial part of the accelerating stage. The increase in

the elastic stiffness would correspond to final setting when the cement paste is able to retain the shape of an imprint.

During the acceleration stage of the hydration reaction, the rate of increase in G* is roughly coincident with the rate of reaction indicated by the measured temperature change. The early part of the acceleration stage is associated with active dissolution and precipitation in fluid medium, which contribute to the exponential increase in both G' and G". The slower rate of the increase in G* following the initial exponential increase, signals the emergence of a solid skeleton from within the fluid medium, which initiates a change in the rate controlling mechanism, from a water-based to a diffusion control process. Following the peak temperature, which corresponds with the end of the acceleration stage of hydration, there is a steady linear increase in G* with time, while there is decrease in the rate of reaction. This suggests that within the solid, the relationship between the reaction rate and the increase in modulus is more complex.

In a previous investigation, the viscosity of cement pastes obtained from normal incidence measurements, have been reported [Sun et al. 2006]. The viscosity of the cement paste samples in the first few minutes after mixing, obtained at 2.25 MHz, were reported to be in the range of 0.2-0.35 Pas. Considering the change in impedance relative to air (used as reference) measuring changes in the phase of reflected waves at normal incidence at 2.25 MHz, would require an effective sampling rate significantly higher than 1 ns. In addition, the measurements did not

include corrections for temperature effects and losses along the signal path. Thus the measured values of viscosity could potentially contain a significant influence of temperature effect. The recorded phase change may be a result of temperature effects.

3.6 Conclusions

An ultrasonic wave reflection technique for continuous monitoring of cementitious materials through setting is reported in this paper. Calibration of experimental errors of the testing system and the temperature compensation were described. The measured amplitude and phase of the waves reflected at the cement paste/fused-quartz interface were used to determine the changes in storage and loss moduli of cement paste. The ultrasonic measurements at oblique incidence are shown to be sensitive to changes in visco-elastic properties from a very early age. Based on the results presented in this paper, the following conclusions can be drawn:

(a) Normal incidence does not provide sufficient sensitivity for measurement of phase and amplitude changes in the case of low viscosity liquids when using the pulsed ultrasonic wave reflection technique of the kind used in this study.

(b) Using an oblique incidence in the measurement will contribute to achieve higher sensitivity for monitoring the changes in the early age than applying the normal incidence considering the same substrate.

(c) There is a continuous change in the stress waves reflected at the interface of fused quartz and hydrating cementitious materials with each water/cement ratio equals to 0.4, 0.5 and 0.6, respectively. Changes in the stiffness of cement paste produce a decrease in the amplitude and phase coefficients of the

reflected waves at 1 MHz. For each batch of the cement paste of a given material composition, the response of the reflection coefficients are consistent with the rate of reaction indicated by the temperature measurements.

(d) The observed change in the reflected waveforms with time can be interpreted in terms of a continuous change in the visco-elastic material properties, the storage modulus G' and the loss modulus G'', with time after casting.

(e) The early changes in the material properties of the cementitious material can be attributed to a relatively larger increase in the viscous component of the shear modulus, which produces a loss of workability. This is followed by a period where the elastic component increases at a faster pace resulting in emergence of a solid structure capable of retaining the shape of an imprint.

Chapter 4 Microstructure Evolution in Hydrating Cement Paste through Setting using Ultrasonic and Rheological Measurements

4.1 Introduction

Accurate determination of the changes in the microstructure through setting, which result in an increased capacity of the hydrating cement paste to resist applied shear stress has remained a major experimental challenge. Conventional methods for probing the microstructure are not conducive to studying changes in microstructure in the first few hours after casting since sample preparation procedures either alter or disturb the microstructure [Thomas et al. 1999] and the changes in microstructure occur on a time scale that is an order of magnitude faster than the time required for sample preparation. Limited studies on direct observation of evolution of the solid phase from within the fluid medium and changes in the microstructure of hardening solid phase of the cementitious material using X-ray techniques [Juenger et al. 2003 and Chotard et al. 2003] and small angle neutron scattering (SANS) have been reported recently [Thomas et al. 2007]. These methods, which provide information about the evolution of microstructure in cement paste however, do not simultaneously provide information about the mechanical properties of the material. Mechanical and vibration-based techniques which provide reliable measures of elastic mechanical properties on the other hand do not provide information about the microstructure and are not applicable during setting. In the absence of a direct measurement of microstructural variables the current understanding of the microstructure changes

during setting of cement pastes has been developed by application of computer-based models which simulate the development of microstructure [Bentz et al.1999; Ye etal. 2003].

Setting behavior is usually investigated using penetration tests (vicat or pin penetration), which provide a measure of resistance to penetration. The approximate time for the emergence of a solid skeleton is identified from the resistance to penetration of an indenter. Such a measurement does not allow for evaluating the properties of the skeleton since no data pertaining to deformation of the material is collected. Immediately following the emergence of a connected network of hydration products from within the fluid medium, the resulting solid is very weak and obtaining reliable values from penetration measurements is not possible due to limitations of force detecting capabilities. Probing cement paste using ultrasonic waves offers the advantage reliable low-stress measurement, which does not perturb the microstructure. Further, propagation of an ultrasonic wave through a material depends upon its mechanical properties, which in turn can be related to its microstructure [Keating et al.1989 and D'angelo et al.1995].

The primary focus of the research presented in this chapter is to assess changes in the microstructure of a hydrating cement paste through the early stages of hydration and through the setting process. Two different measurements were concurrently performed on cement paste samples after mixing. The rheological response of cement paste was examined up to the initiation of setting using low amplitude oscillatory

shear and yield stress measurements. Changes in an ultrasonic wave produced by a reflection off of the hydrating cement paste were also monitored. Such measurements have previously been used for studying the evolution of strength and visco-elastic properties of hydrating cementitious materials [Subramaniam 2002; Subramaniam 2005 and Voigt et al. 2003]. More elaborate experimental test setup than used previously is presented. The theoretical framework necessary to interpret the results of the ultrasonic technique and provide information about the microstructure of the hydrating cement paste in terms of physically-based variables is developed using the poro-elastic theory. Poroelastic theory has been used for studying porous media such as rocks, and soils [Subramaniam 2005; Johnson and Plona 1982; Johnson and Sen 1981; Stoll and Tan 1981; Chotiros 1995; Yamamoto and Turgut 1988 and Bourby et al. 1987] and offers a natural way for modeling the hydrating cement system [D'Angelo 1995]. An understanding of the microstructure evolution through setting is obtained by combining the information obtained from the ultrasonic measurements with the observed changes in the rheological behavior.

4.2 Background

Setting and increase in elastic stiffness in a hydrating cement paste is a very complex multi-scale phenomenon involving changes in state and in the internal structure with time (see Taylor 1985 and Pratt and Jennings 1981 for comprehensive reviews) The change in state can be visualized as a transformation of cement paste from a material in which bulk flow is produced at relatively low applied shear stress to a solid where significantly high stresses are required to produce small strain. The

fluid state may be characterized as a suspension of cement grains in water with an internal structure comprised of arrangements of grains. At large strains, there is a reorganization of the internal structure which results in a different arrangement of grains. The bulk properties of the material are however not affected by this rearrangement. The solid state is characterized by the existence of a long-range order in the microstructure due to the presence of bonds between the individual cement grains. In a solid, irreversible changes associated with complete disruption of the microstructure resulting from breaking of bonds are produced at large strains.

Our current understanding of changes in the microstructure during setting obtained from the computer simulation models[Bentz et al.1999; Ye et al. 2003] indicates that initially, a weak skeleton emerges from within the fluid medium when the products of hydration link up to provide a continuous network of solid within the fluid filled space. The emergence of a continuous solid phase within the fluid medium has been identified as the percolation threshold [Bentz et al.1999; Ye et al. 2003]. Following percolation threshold, setting behavior is initiated in the cement paste. Through setting, as the products of hydration form within the fluid-filled spaces of cement paste, a network of pores and a pore structure develops.

Idealization of the Cement Paste

The poroelastic framework proposed by Biot provides realistic representation of for developing constitutive relations for hydrating cement paste [Biot 1956a; Biot 1956b and Biot 1962]. According to Biot's theory, the volume fraction of the fluid

within a unit volume of the material is referred to as the porosity. It is implicitly assumed that the walls of the pores are impervious and the pore size is concentrated around its average value. The pore structure is assumed to be comprised of inter-connected void space, which allows bulk motion of the fluid relative to the solid. The porous solid and the solid-fluid system are assumed to be statically isotropic. The propagation of waves in the fluid-saturated poro-elastic medium depend upon the internal system variables which are the effective elastic properties of the porous solid, the porosity, and the parameters related to the pore structure, which influence the bulk flow of the fluid in the porous solid.

Considering a fluid-saturated porous solid, a pair of coupled displacement equations of motion governing both rotational and dilatational motions is obtained by combining the Biot's constitutive relationship and Darcy's law for flow through a porous medium [Biot 1962]

$$\mu_b \nabla^2 \vec{\boldsymbol{u}} + (\boldsymbol{H} - 2\mu_b)\nabla(\nabla \cdot \vec{\boldsymbol{u}}) - \boldsymbol{C}\nabla(\nabla \cdot \vec{\boldsymbol{w}}) = \rho_b \ddot{\vec{\boldsymbol{u}}} - \rho_f \ddot{\vec{\boldsymbol{w}}} \tag{4-1a}$$

$$C\nabla(\nabla \cdot \vec{u}) - M\nabla(\nabla \cdot \vec{w}) = \rho_f \ddot{\vec{u}} - m' \ddot{\vec{w}} - \eta/\kappa \dot{w} \tag{4-1b}$$

where the average displacement of solid skeletal frame and the fluid are denoted by $\vec{u} = \vec{u}(x,t)$ and $\vec{U} = \vec{U}(x,t)$, respectively, $\vec{w}(x,t) = \beta(\vec{u} - \vec{U})$ is the relative displacement of fluid and skeletal frame, β is the void volume fraction of the fluid or porosity (assumed to be isotropic), $\rho_b = (1-\beta)\rho_s + \beta\rho_f$ is the total mass density, ρ_s is the solid mass density, ρ_f is fluid mass density, η is the fluid viscosity, and κ is the coefficient of permeability of the porous frame, $\boldsymbol{m}' = \boldsymbol{c_T}\rho_f / \beta$, $\boldsymbol{c_T}$ is the

tortuosity coefficient (dimensionless parameter), which is a experimentally determined, μ_b is the shear modulus of the skeletal frame (under drained conditions). In Equation(s) (4-1) H, C and M represent operators that characterize the response of the composite, and are given as [Stoll and Kan 1981]

$$H = \frac{(K_s - K_b)^2}{D - K_b} + K_b + \frac{4\mu_b}{3} \tag{4-2a}$$

$$M = \frac{K_s^{\,2}}{D - K_b} \tag{4-2b}$$

$$\boldsymbol{C} = \frac{\boldsymbol{K_s}(\boldsymbol{K_s} - \boldsymbol{K_b})}{\boldsymbol{D_e} - \boldsymbol{K_b}} \tag{4-2c}$$

where K_b is the bulk modulus of the skeletal frame (under drained conditions), $\boldsymbol{D_e} = \boldsymbol{K_s}(1 + \beta \frac{\boldsymbol{K_s}}{\boldsymbol{K_f} - 1})$, K_s is the bulk modulus of the material of the skeletal frame and K_f is the bulk modulus of the pore fluid. The solutions of Equation(s) (4-1) for a specific set of boundary and initial conditions yield expressions for displacements and stresses in a poroelastic medium due to wave propagation. Solutions for these equations have been worked out by several researchers [Johnson and Plona 1982, Zimmerman and Stern 1994].

In order to employ Biot's porous model, thirteen material constants are required, and independent experimental measurements would be necessary to obtain these parameters. However, as presented by Berryman [1980], the analysis can be simplified considering inter-relations between some of the material parameters. In

Berryman's approach, the tortuosity of porous media is estimated theoretically and is given as

$$\boldsymbol{c_T} = 1 - \boldsymbol{s_e}(1 - 1/\beta) \tag{4-3}$$

In general, the value of r must be calculated from a microscopic model of the frame moving in the fluid. It was found that the value of s_e equal to ½, which is the exact value for the case of spheres in a fluid medium provided a reasonable estimate for a porous medium with constant porosity within the range $\beta<0.4$. The relationship between permeability, pore size and porosity, given by the Kozeny-Carman relation, was found to be suitable for most porous media and is given as

$$\kappa(1-\beta)^2/\beta^3 = \kappa_0(1-\beta_0)^2/\beta_0^3 = \boldsymbol{const}. \tag{4-4a}$$

and similarly

$$\boldsymbol{a_p}^2/\kappa = \boldsymbol{a_{po}}^2/\kappa_o = \boldsymbol{const}. \tag{4-4b}$$

where a_p is the pore diameter.

The predicted wave propagation using Berryman's simplifications were comparable to the experimental results obtained by Plona [1980], on fine grained sands and sintered porous glass. It was shown that the assumptions provided in Equations 4-3 and 4-4, provide a reliable way for evaluating parameters, which leads to an accurate description of elastic wave propagation in fluid-saturated porous media. The results were also found to be insensitive to the exact relationships between

porosity of the solid and properties which influence bulk flow of the fluid such as permeability and tortuosity. From their experiments on model systems considering glass beads, it was shown that the differences between the response of a free arrangement of glass beads and fused beads could clearly be identified using ultrasonic waves. In the free arrangement of glass beads there was no bonding between the individual beads. The fused system was obtained by applying pressure and heat to the free arrangement resulting in a structure where the glass beads were fused at the points of contact. While there was a negligible difference in the porosity, there was considerable difference in the elastic stiffness of the porous solid for the two systems [Johnson and Plona 1982].

4.3 Experimental Test Program

Cement paste samples were mixed using a paddle mixer following a procedure suggested by Williams et al. [1999], which is similar to ASTM C-305[ASTM C305]. Cement and water were initially mixed at 140 rpm for 30 seconds, followed by a pause for 1 minute before mixing for another 2.5 minutes at 285 rpm. Cement paste adhering to the sides of the mixing bowl was scraped and the entire mixture was mixed for another 2.5 minutes following a 1 minute pause. In the test program cement pastes with w/c ratios equal to 0.4, 0.5 and 0.6 were evaluated. These w/c ratios were selected to minimize the influence of chemical shrinkage (if any), during the setting process.

The experimental program comprised of rheological and ultrasonic measurements. Changes in the elastic response and flow behavior of the cement paste sample were evaluated as a function of age using rheological measurements. In addition, changes in the ultrasonic waves, reflected from the hydrating cement paste, were monitored. The evolution of the rheological behavior of cement paste, up to the initiation and early stages of the setting behavior are related to the changes in the microstructure inferred from the ultrasonic measurements. In addition, setting time measurements were also performed using the conventional Vicat needle penetration to provide a reference. The time zero for all measurements from each procedure corresponds to the time when water was added to the cement powder.

4.3.1 Rheological Measurements

All rheological measurements were performed using a stress-controlled rheometer with a 14 mm vane tool. A vane tool was chosen for the rheological measurements to minimize the influence of wall slip, which is a problem in high w/c ratio cement pastes [Nachbaur et.al 2001; Saak et.al. 2001]. The vane tool also offers the advantage that artefacts resulting from large particles are avoided and therefore it has been used for yield stress determination of concentrated suspensions, emulsions and cement paste [Mezger 2006; Saak 1999]. It has been shown that the storage modulus of cement paste is independent of the measuring tool and the vane tool was shown to produce comparable value of storage modulus when compared to other test geometries such as the parallel plate and coaxial cylinder.

The diameter and depth of the cup were equal to 28 mm and 60 mm, respectively. The cup was filled with cement paste in three layers. After each layer the cup was vibrated for 10 seconds. After filling the last layer, the excess cement paste was struck off and the top surface of the cement paste was finished while vibrating. The cup was placed in the rheometer and the vane was inserted to the prescribed depth. Three different measurements were performed for each w/c ratio tested and each test procedure is described in detail below.

4.3.2 Stress Sweep Measurements

Stress sweep measurements were performed to determine the yield stress and to establish the linear visco-elastic domain (LVD) of the cement paste. The sample was subjected to an increasing applied stress at a constant rate. It has previously been shown that initially up to a critical value of stress; there is a linear relationship between applied stress and strain. With increasing stress past the critical stress, the response becomes nonlinear eventually producing flow once the yield stress is exceeded. At low applied stress within the LVD, there is little or no change in structure of the material. There is a gradual breakdown of the structure past the LVD. At higher stresses, the structure of the sample is irreversibly destroyed and the material starts to flow as its yield value is exceeded. The material circumscribed by the vane starts moving as a solid cylindrical body [Saak 1999].

Stress sweep measurements were performed at regular intervals up to 5 hours of age or when the capacity of the machine was reached, whichever occurred earlier.

Since the structure of the sample is destroyed during the test, each test was performed on a fresh sample. The vane was introduced into the cement paste immediately after placing the sample in the cup, which was then left inside the test machine until the prescribed time.

4.3.3 Low-amplitude Oscillatory Shear Measurements

The value of applied torque was chosen to be within the linear viscoelastic domain (LVD) of the material. The applied torque for the oscillatory shear measurement was significantly lower than the corresponding torque at the end of the LVD. The measured torque at the end of the LVD, where the measured viscoelastic properties of cement paste start decreasing with applied strain was determined from the stress-sweep measurements. In the test, the vane tool was introduced in the sample immediately after preparing the sample and repeated measurements were made on the same sample.

4.3.4 Step Stress Measurement

A limited number of constant stress measurements were performed on cement paste samples to determine the response of the material to constant applied stress. In this test the cement paste was subjected to stress of a constant magnitude and the resulting strain was monitored. The applied stress was instantaneously increased to the prescribed magnitude and held constant. For each w/c ratio, tests were conducted at two different magnitudes of applied stress, corresponding to values above and below the yield stress of the material. All tests were performed at 1 hour after mixing.

4.3.5 Oblique Ultrasonic Measurements

A schematic diagram of the experimental setup for oblique ultrasonic wave reflection measurement is shown in Figure 4-1. The experimental system included a function generator, an oscilloscope, a computer and the test probe. The test probe comprises of ultrasonic transducer(s) attached to a buffer plate made of fused quartz, which is in contact with the hardening cement paste. Multiple pairs of transducers were mounted on precisely machined faces at matched angles with respect to the vertical to collect reflection data at different angles of incidence. Wave reflection at the fused-quartz/cement paste interface was monitored at 0, 50 and 60 degree angle of incidence.

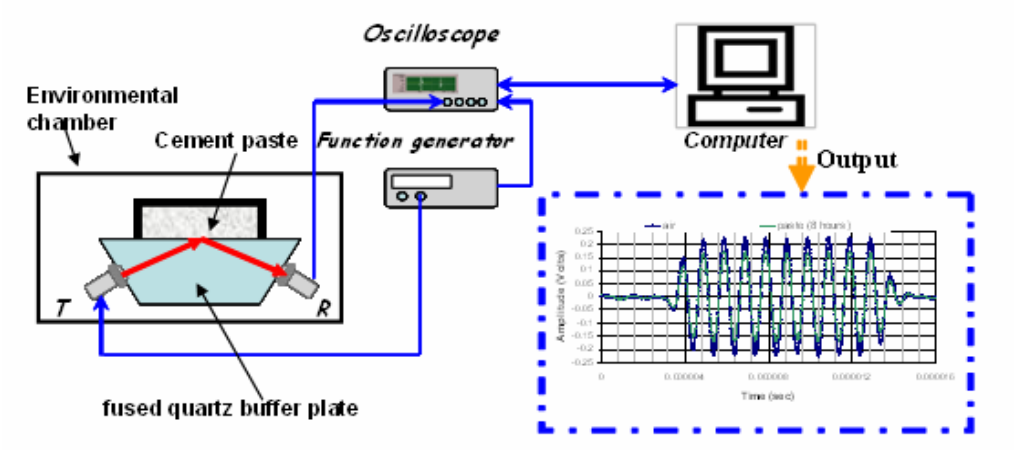

Figure 4-1Schematic diagram of test setup for ultrasonic measurement.

At each angle of incidence, a matched pair of direct contact, ultrasonic shear-wave transducers with a nominal center frequency of 1 MHz, labeled T for transmitting and R for receiving was mounted on the opposite angled surfaces of the

buffer plate. The two transducers were aligned precisely at the center of the angled surfaces. While attaching the transducers, the axes of the transducers were aligned to generate a horizontally polarized shear (SH) wave in the fused quartz. A source signal comprising of 1 MHz, 10-cycle, tone burst with pulse repetition period equal to 200 ms was sent by the function generator to the transducer T. Simultaneously, a trigger pulse was sent to the oscilloscope to initialize data capture. The reflected signal detected by transducer R was digitized by the oscilloscope. The data was then transferred to the computer over a GPIB interface for storage and processing. The data acquisition and transfer are controlled by the computer. The oscilloscope had a digitization rate of 500 MS/s which provides a temporal resolution of 2 ns. In each acquisition, 100 waveforms were averaged by the oscilloscope in order to minimize the influence of random noise in the signal. At any given time only one transmitting transducer was active. An averaged waveform was acquired every 30 minutes allowing sufficient time to take the average and minimize the volume of data collected over typical monitoring period. The buffer plate and cement paste were placed inside an environmental chamber, which was maintained at 24 deg C throughout the duration of the test.

Prior to placing the cement paste sample in the sample holder (attached to the top face of the fused-quartz buffer plate), ultrasonic signals were collected with an empty sample holder The reflected signals collected from the fused-quart/air interface were used as reference signals for evaluating the changes in the signal introduced by the cement paste. Immediately after mixing, the cement paste was placed in the sample

holder and vibrated for 10 seconds before initiation data collection. Data processing of the ultrasonic signals comprised of obtaining the amplitude change of the incident wave upon reflection at the fused-quartz/cement paste interface. The change in the amplitude of the wave is given by the amplitude reflection factor, $r(f)$. $r(f)$ was obtained using the self-compensating technique, which involves processing data in the frequency domain [Achenbach 1992]. In the frequency domain, the stress wave signals received after a single reflection at the air/quartz and sample/quartz interfaces can be represented as:

$$F^{air/quartz}(f) = s(f)d_1(f)d_2(f) \tag{4-5a}$$

$$F^{sample/quartz}(f) = s(f)r(f)d_1(f)d_2(f) \tag{4-5b}$$

where $F(f)$ is the magnitude of FFT of the captured reflected time domain signal, $d_1(f)$ is the geometric and material signal losses in the couplant, $d_2(f)$ is the material signal losses along the signal path in the elastic fused quartz, $s(f)$ is the input source function, and $r(f)$ is the amplitude reflection coefficient at the bi-material interface. Using the reflected signal from the fused-quartz/air interface as the reference, *r(f)* at the cement paste/quartz interface can be determined by normalizing the reflected magnitude off the mortar-fused quartz interface with the reflected amplitude off the air-quartz interface [Subramaniam and Lee 2003].

$$r(f) = F^{sample/quartz}(f) / F^{air/quartz}(f) \tag{4-6}$$

The time domain signals were transformed to frequency domain using the FFT algorithm and the amplitude reflection factor at 1 MHz, r(1), was determined as the ratio of the respective magnitudes of the FFT of the ultrasonic signals from the quartz/cement paste to the quartz/air interface at that frequency.

4.4 Results from Rheological Measurements

A typical result from an oscillatory stress sweep for cement paste with w/c = 0.4 is shown in Figure 4-2. The variation of the elastic component of the shear modulus (G') is plotted as function of the applied shear stress. Nominally similar results were obtained from all w/c ratio tested. From the measured response, a relatively constant value of G' is obtained when the applied shear stress is within the LVD. This is followed by a gradual breakdown of the structure when the magnitude of the applied stress is increased. With increasing stress there, is a decrease in the elastic modulus and eventually, the structure cannot resist the applied stress and it begins to yield. From Figure 4-2 changes in the cement paste microstructure produced by hydration are evident in the increase in the elastic modulus and yield stress with time.

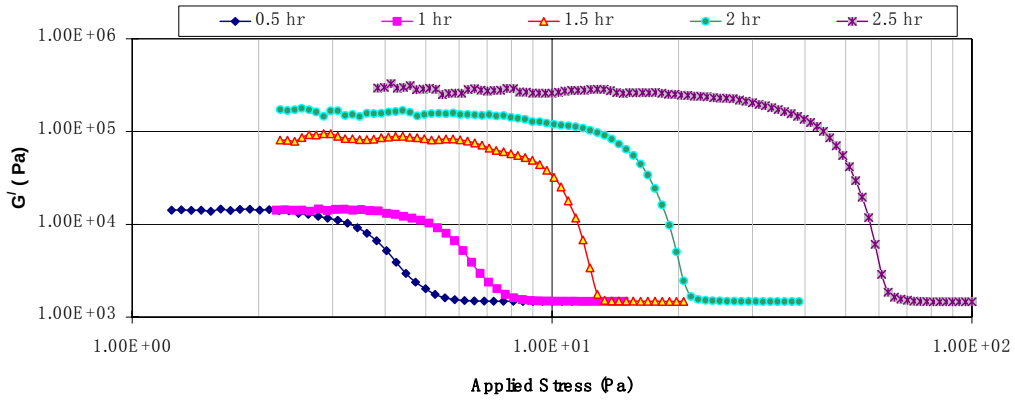

Figure 4-2 Results of stress sweep tests on cement paste with w/c = 0.4

The increase in the shear modulus obtained from oscillatory shear measurements with time for cement pastes with the different w/c ratio are shown in Figure 4-3 (a). The corresponding increase in the yield stress obtained from stress sweep measurements are plotted in the Figure 4-3(b) for comparison. The yield stress was determined from the measured stress amplitude sweep of the sample, as the value of the applied stress when the curve starts to deviate more than 10% from the low-stress asymptote [Mezger 2006]. It can be seen that there are similarities between the measured increases in the shear modulus and the yield stress of the material with time. For w/c = 0.5 and 0.6, initially, in the first few hours, there is no significant change in the shear modulus. In this period, there is a very gradual increase, almost linear in the yield stress with time. There is a very rapid, almost exponential increase in both quantities which follows this initial period. In the case of w/c = 0.4, the initial period of inactivity is very short; there is an almost continuous increase in the elastic modulus and yield stress after mixing. In general, cement paste with a lower w/c ratio achieves a fixed value of shear modulus and yield stress earlier in time.

The penetration depths obtained from the Vicat penetration needle test are also shown in Figure 4-3(c) to provide a comparison. The time for initial setting determined as per the guidelines of ASTM C-191 for w/c = 0.4, 0.5 and 0.6 are 186, 253 and 327 minutes, respectively. By comparing the yield stress measurements with the penetration measurements it is immediately obvious that the penetration measurements are not sensitive to the early changes in the microstructure. Changes in the material are more readily evident in the rheological yield stress measurements.

While there is an order of magnitude increase in the yield stress, there is no measureable change in the penetration. Discernable changes in the penetration occur significantly later in time than the observed changes in yield stress and shear modulus.

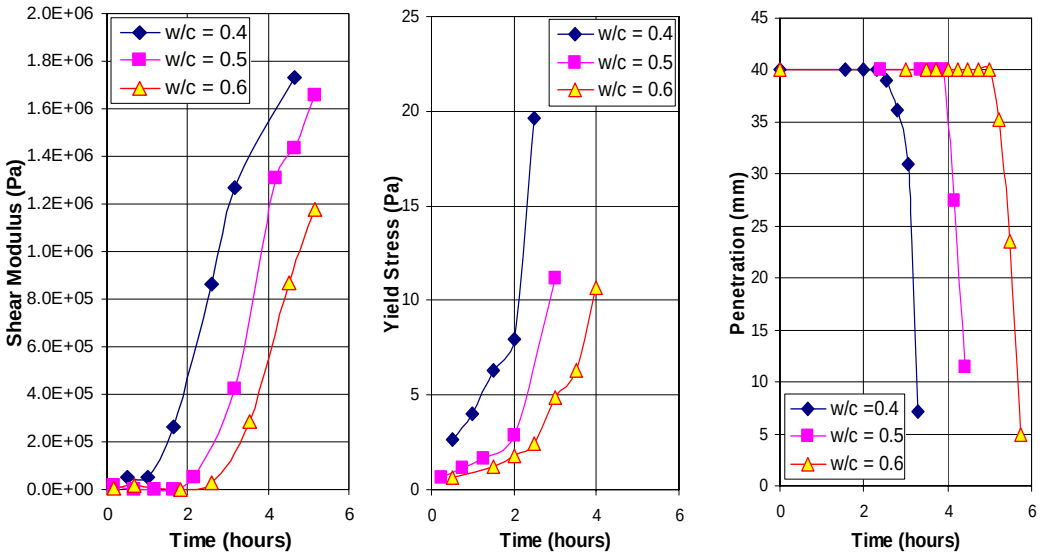

(a) (b) (c)

Figure 4-3 Increase in yield stress and shear modulus with time

In materials which have a finite yield stress, a stress larger than the yield stress is required to initiate flow [Mezger 2006]. Immediately after mixing, the yield stress of cement paste can be attributed to resistance to flow offered by the internal structure comprising of agglomerates of cement grains and weak inter-particle forces (if any). When the material goes through setting, there is a decrease in the ability to flow under applied stress. Therefore, the increase in the yield stress is a very good indicator of the setting behavior. Assuming the changes in the arrangements of cement particles (if any) with time are negligible, the increase in yield stress is produced by the products of hydration. It can be reasoned that the sharp rise in the yield stress is

associated with the emergence of a continuously connected solid network of cement grains; once a continuously connected network of solid grains emerges, small increases in the volume of hydration products within the paste would translate to a significantly higher stress required to produce movement of one cement grains relative to the one another. The sharp increase in yield stress can therefore be associated with the initiation of setting behavior within the cement paste. The experimental trends from the rheological measurements suggest that cement pastes with lower w/c set faster than the cement pastes with higher w/c ratio. Measurements indicate that for w/c =0.5 and 0.6 the yield stress increases after a period when there is a very low rate of change. For w/c =0.4, however, there appears to be a continuous increase in yield stress after mixing. This suggests that for w/c = 0.5 and higher, a connected network of grains emerges later time in time when there is sufficient increase in solid fraction. For w/c =0.4 on the other hand, the initial state of agglomeration of grains requires a smaller increase in solid fraction to produce a continuously connected solid network.

Typical response from a step stress measurement for cement paste with w/c = 0.6 is shown in Figure 4-4. Nominally similar responses were obtained from all w/c ratio tested. Constant stress measurements were performed one hour after mixing by prescribing constant torque corresponding to half and 1.2 times the yield stress of the material. At the stress greater than yield stress, the measured rotation appears to reach a steady state, where there is a linear increase in rotation with time. The steady increase in rotation for a constant applied stress is indicative of steady state fluid flow.

There is a fundamental difference in the response of cement to constant applied stress of magnitude smaller than the yield stress. The rate of increase in rotation decreases steadily and the rotation approaches an asymptotic value.

The observed rotational response in the step-stress measurement can now be interpreted considering the response of a visco-elastic material subjected constant stress. The steady increase in rotation for a constant applied stress obtained past yield is consistent with the viscous fluid flow under constant stress. In this case, the slope of the constant increase in rotational displacement is related to the viscosity of the liquid. The displacement of the material approaching an asymptotic constant value is consistent with the response obtained from a visco-elastic solid subjected to constant stress.

The results from the response of the material under constant applied stress suggest that even at an early age, before setting, there is a long range order in the material, which is capable of transmitting low magnitudes of shear stress. While the individual grains of cement may not be bonded to each other, the agglomerates of particles and the inter-particle forces present an internal structure within the material which allows for a build up of a three-dimensional network of forces to enable the material to resist applied shear. In the low deformation range, a stable solid-like response is obtained from this network at low deformations. Therefore, for low levels of applied stress, the cement paste can be treated as composed of a solid frame with weakly connected cement grains.

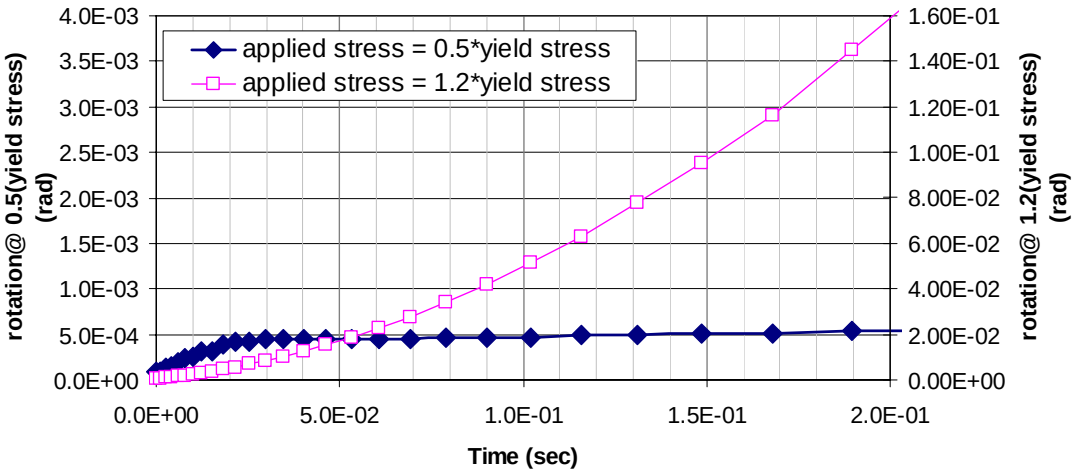

Figure 4-4 Step stress response of cement paste with w/c = 0.6 at two different magnitudes of applied stress

4.5 Analysis of Ultrasonic Data

Changes in r(1) and temperature for cement pastes with the different w/c ratios are shown in Figure 4-5. In all cases, the temperature of the paste initially decreases to 24 deg C in the first few hours. The period when there is no perceptible change in the measured temperature may be identified with the dormant period in cement hydration. The increase in temperature after the dormant period signals the beginning of the acceleration stage. Immediately after mixing, the measured r(1) for the three angles of incidence are close to 1.0, suggesting that a significant portion of the incident wave energy is reflected at the quartz-cement paste interface. The general trends in measured changes in r(1) are similar at all incident angles. It can be seen that measurements are a higher angle of incidence give smaller values of r(1) and register larger changes with time. The value of r(1) obtained from normal incident measurement shows the smallest change with time when compared to the

corresponding changes from the measurements at oblique incidence. It can be seen that for w/c = 0.4 there is an almost continuous decrease in r(1) after mixing for all angles of incidence. For the case of w/c = 0.6 on the other hand there is no perceivable change in r(1) up to 2 hours. There is an increase in the rate of change of r(1) with time. Starting from a gradual rate of change there is an accelerated change at later times. It can also be seen that while the measured response from all w/c ratios are nominally similar, there is larger decrease in r(1) with time for smaller w/c ratio. It is interesting to note that there is a marked decrease in r(1) before the end of the dormant period indicated by the temperature measurements. It should be mentioned that the accuracy in temperature measurements was on the order of +0.5 deg C which may not be sufficient for discerning small temperature changes in this period..

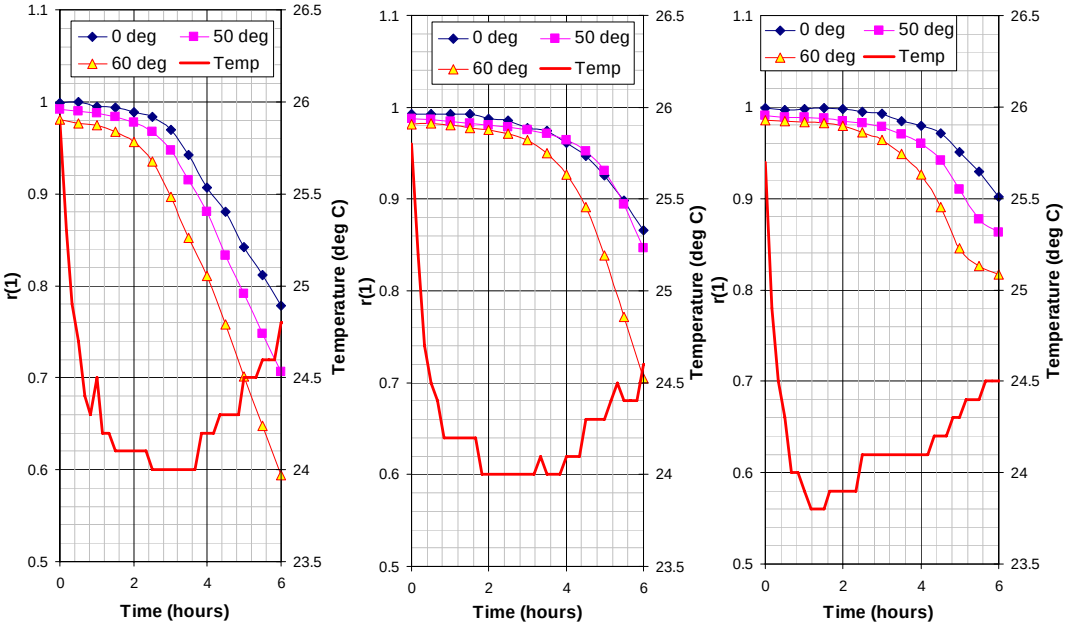

Figure 4-5 Amplitude reflection factor, r(1), at different angles of incidence for w/c = 0.4, w/c= 0.5 and w/c = 0.6

The measured changes in the r(1) at the fused-quartz/cement paste interface can now be interpreted in terms of the expected result from the reflection of an SH wave at the interface between an elastic and a poro-elastic material. In the poro-elastic idealization, the hydrating cement paste is assumed to be comprised of water filled porous skeleton. The material of the skeleton is assumed to be homogenous and isotropic. Reflection of a planar wave, initially traveling in an elastic medium, incident on an interface with poroelastic material would produce changes in both amplitude and phase of the wave. For a poro-elastic material with known properties (internal system variables are known), the exact magnitude of r(f) after reflection can be obtained considering dynamic equilibrium and displacement continuity at the interface [Stoll and Kan 1981]. The conditions for dynamic equilibrium and the form of the expressions for r(f) are summarized in Appendix A.

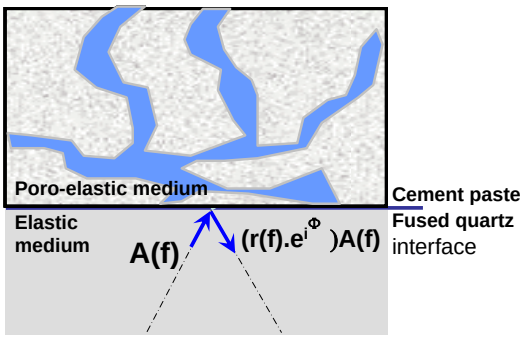

Figure 4-6 Schematic representation of ultrasonic wave reflection at the interface between elastic and poro-elastic materials.

For an SH wave traveling in an elastic material, incident at the interface with the poro-elastic material, changes in the amplitude and phase of the wave following reflection from the poro-elastic material can be symbolically expressed as

$$R_s = r(f)e^{i\Phi} = R_s(\rho_e, E_e, \upsilon_e, \rho_s, \rho_f, K_f, \mu_b, \beta, \eta, a_p, c_T, \kappa, \delta_\mu) \quad (4\text{-}7)$$

Where ρ_e, E_e and υ_e are the density, the Young's modulus and the Poisson's ratio of the fused quartz. μ_b is the shear modulus of the skeletal frame (under drained conditions) which is a real value to present the properties under the static conditions. For the porous medium, the dynamic shear modulus of the skeletal frame is given by a complex number

$$\mu_b^* = \mu_b(1 + \delta_\mu \boldsymbol{j}) \tag{4-7a}$$

where the loss factor δ_μ, was introduced by Stoll to consider the energy loss due to the friction among the phases of porous media. δ_μ is usually a small number in the range of 0.11 – 0.17[Stoll and Kan 1981; Yamamoto et.al. 1988]. In Equation 4-7, the internal system variables of the fluid filled porous medium are shown in grey. The information about the poro-elastic material is contained in the reflection coefficient *r(f)*. Considering the relationships between tortuosity, permeability, pore size and porosity, in Equations 4-3 and 4-4, the number of independent system variables in the expression of *r(f)* can be decreased

$$R_s = r(f)e^{i\Phi} = R_s(\rho_e, E_e, \upsilon_e, \rho_s, \rho_f, K_f, \mu_b, \beta, \eta, \delta_\mu) \tag{4-8}$$

Determination of r(f) as described by Equation(4-8), requires the input of several internal system variables of the porous medium. When applied to the case of hydrating cement paste, some simplifications can be introduced to the expression for R_s, assuming the hydrating cement paste is a water-filled porous skeleton made up of cement grains and products of hydration. The bulk properties of water are readily available as $K_f = 2.0 \times 10^9$ Pa, and the viscosity $\eta = 1.0 \times 10^{-3}$ Kg/ms. Further, changes in density of the hydrating cement paste with age (on account of chemical shrinkage)

can be considered to produce insignificant changes in the bulk density of the material. Thus considering the hydrating cement material to be composed of two components, the porous skeleton and water, a simple relation can be obtained considering composite theory

$$\rho_b = (1-\beta)\rho_s + \beta\rho_f \tag{4-9}$$

where, ρ_b is the density of the cement paste. ρ_b can be considered to be constant through the hydration process. The ρ_b of cement paste samples with w/c = 0.4, 0.5 and 0.6 were determined at three days of age and were found to be 1.98, 1.87 and 1.77 g/cm^3, respectively. Using this value, the ρ_s, which represents the effective density of the solid material, can be obtained using Equation (4-9), further reducing the number of internal variables in the expressions for *r(f)* .

$$R_s = R_s(\rho_e, E_e, \upsilon_e, \mu_b, \beta, \delta_\mu) \tag{4-10}$$

Since the material properties of fused quarts are readily available, the reflection at the fused quartz/cement paste interface can be expressed in terms of the two key internal system variables, porosity and shear modulus of the skeleton, as

$$R_s = R_s(\mu_b, \beta, \delta_\mu) \tag{4-11}$$

In the simplified form, changes in the amplitude of the incident SH wave depend upon three key internal variables of the poro-elastic medium. These internal system variables which describe the poro-elastic material are functions of age (time after mixing). Since the obtaining analytical expressions for the inversion of the internal variables form the expression for R_s is intractable, numerical inversion was performed to optimize the material constants such that the theoretical prediction is close to the experimental response. The experimental data used in the optimization comprised of

the r(1) at three different angles of incidence. The Generalized Reduced Gradient nonlinear optimization scheme was used to minimize an objective function given as

$$F(c_i) = \sqrt{\frac{\sum_{n=1}^{3}\left(\left|R_s^{\exp}(\theta_n, c_i)\right| - \left|R_s^{theo}(\theta_n, c_i)\right|\right)^2}{3}} \tag{4-12}$$

where θ_n is the discrete incident angle at which experimental values are obtained, and c_i are the internal system variables of the poroelastic solid. For the numerical inversion, the starting guess of porosity for the first measurement after mixing was obtained using the relation

$$\beta_o = \frac{\rho_c\left(w/c\right)}{1+\rho_c\left(w/c\right)} \tag{4-13}$$

where ρ_c, the specific gravity of cement was assumed to be 3.2. The starting guess for μ_b was taken as 10^5 Pa. The range for δ_μ was initially prescribed to be within 0.01 – 0.3. It was found that within the prescribed range, there was no influence of δ_μ on the final values of μ_b and β. The solution obtained at a given time was then used as the starting guess for the next time.

The shear modulus and porosity of the cement paste obtained from the numerical inversion of the test data are shown in Figure 4-7 The initial values of shear modulus and porosity obtained immediately after mixing were ($8.56\text{x}10^5$ Pa, 0.555), ($3.59\text{x}10^5$ Pa, 0.611) and ($1.58\text{x}10^5$ Pa, 0.653) for cement pastes with w/c = 0.4, 0.5 and 0.6, respectively. The trends in the shear modulus increase obtained from the ultrasonic measurements are qualitatively similar to those obtained from the oscillatory shear rheological measurements. There appears to be an exponential

increase in shear modulus following a period when there is no noticeable change. Consistent with established results a higher rate of modulus increase is obtained for a lower w/c ratio. Cement paste with w/c=0.4 exhibits the most rapid increase in modulus, while cement paste with w/c=0.6 exhibits an extended period when there is no noticeable change followed by a slower rate of increase. The rate porosity change are also significantly higher for cement paste with w/c = 0.4 when compared to the other two w/c ratios. In the cement paste with w/c = 0.4 there appears to be an almost continuous change in porosity after mixing. Cement paste with w/c = 0.6, on the other hand, exhibits an insignificant change in porosity up to 4 hours, following which there is a rapid decrease.

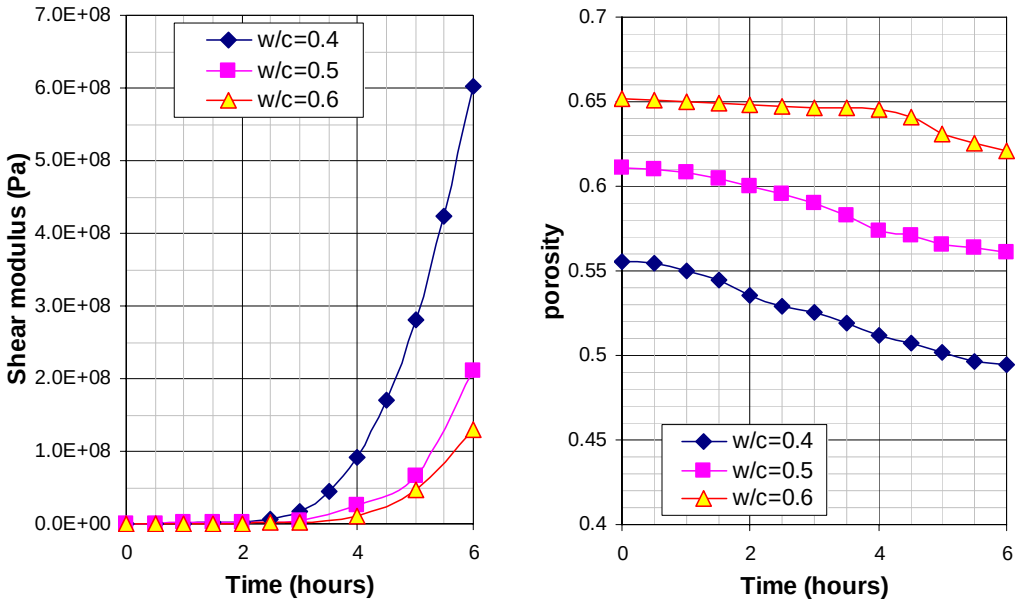

Figure 4-7 Shear modulus and porosity of cement paste obtained from inversion of ultrasonic data

The porosity obtained from the ultrasonic data corresponds to relative proportion of the water filled space within a solid skeleton. The measured decrease in porosity is

therefore equal to the increase in the solid fraction within the cement paste. The increases in the solid fraction with time are shown in Figure 4-8. It can be seen that for w/c = 0.4, there is an almost continuous increase in the solid fraction with time. Cement paste with w/c = 0.6 on the other hand exhibits a prolonged period with relatively little change in the microstructure. After 2 hours, both w/c = 0.4 and 0.5 exhibit an almost linear increase in solid fraction with time. It is interesting to note that while the increase in the solid fraction for both w/c=0.4 and 0.5 is linear with time; correspondingly, there is an exponential change in the elastic modulus. Comparing the relative changes in the shear modulus and porosity obtained from the ultrasonic data, it is interesting to note that there is a three order of magnitude increase in the shear modulus corresponding to relatively small change in the porosity. There is hence a very non-linear relationship between the decrease in porosity and increase in modulus. After 2 hours, the rates of increase in the solid fraction for w/c = 0.4 and 0.5 are comparable. w/c = 0.4, however, exhibits a significantly higher rate of increase of elastic modulus. This suggests that for a lower w/c ratio, because of the initial closer spacing of cement grains a smaller volume of hydration products produce a higher change in the shear modulus.

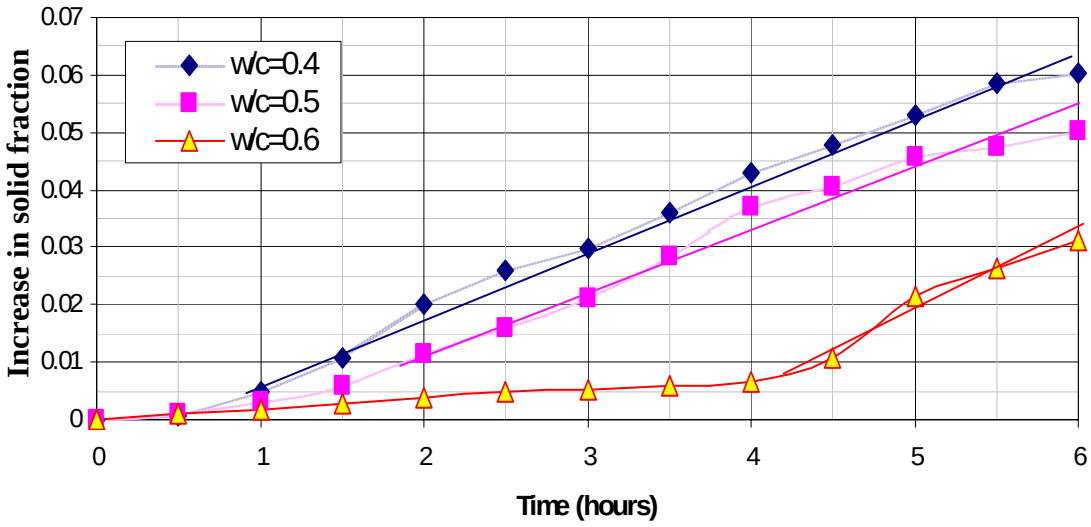

Figure 4-8 Increase in solid fraction within the cement paste as a function of time.

4.6 Discussion

In the previous sections, the development of microstructure was evaluated in terms of internal system variables of a poro-elastic material, which provides identical acoustic properties as the hydrating cement paste. The application of the poro-elastic idealization for interpreting response of the material to the low-amplitude shear stress produced by an ultrasonic wave is supported by the evidence of the solid-like response obtained in the step-stress rheological measurements. Ultrasonic waves used in this study assess changes in the microstructure at a length scale corresponding to the wavelength. Considering the range of shear moduli and densities of cement paste with the different w/c ratios, the wavelength within the period of observation ranges from 10^{-5} m, initially, to 10^{-4} m at 6 hours. Ultrasonic measurements therefore provide indication of changes at these small length scales. The increase in the solid fraction

indicates that there is an almost continuous change in microstructure after mixing at this small length scale.

A comparison between the shear moduli obtained from the rheological and ultrasonic measurements is shown in Figure 4-9. The shear modulus obtained from the ultrasonic measurements is a few orders of magnitude higher than the corresponding value from rheological measurement. This is consistent with established findings in materials which exhibit frequency dependent moduli, where the dynamic properties determined at higher frequencies are higher than those obtained at lower frequencies. It should also be noted that the shear modulus obtained from the rheological measurements relates to the bulk of the material while the ultrasonic measurements provide a measure of the stiffness of the solid skeleton. The results from the different w/c ratios however suggest that there is unique relationship between the low and high frequency shear moduli.

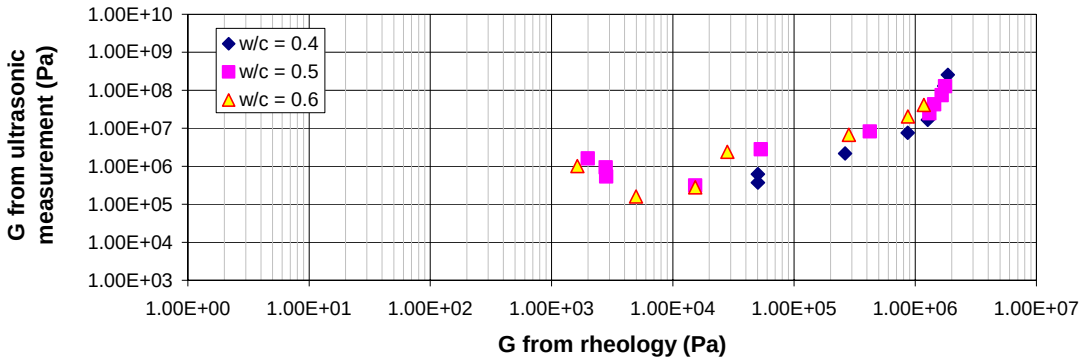

Figure 4-9 Comparison between shear moduli from rheological and ultrasonic measurements

The results from the two measurement techniques can now be compiled to develop an understanding of the changes in the microstructure which produce setting in cement pastes. The increase in the shear modulus of the solid obtained from the ultrasonic measurements is compared with the increase in yield stress from rheological measurements in Figure 4-10. It can be seen that there is a high level of correspondence between the two quantities. The sharp rise in the yield, which signals the emergence of a fully connected solid network within the cement paste, coincides in time with the observed sharp increase in shear modulus with time. The high level of correspondence between the two measurements suggests that the emergence of a continuously connected solid coincides with significant increases in the shear modulus of the skeleton. Therefore, if yield stress is taken as an indicator of setting in cement paste, the rapid increase in the rapid rise in shear modulus obtained from ultrasonic measurements can be used to determine the point in time when a continuously connected solid emerges within the cement paste.

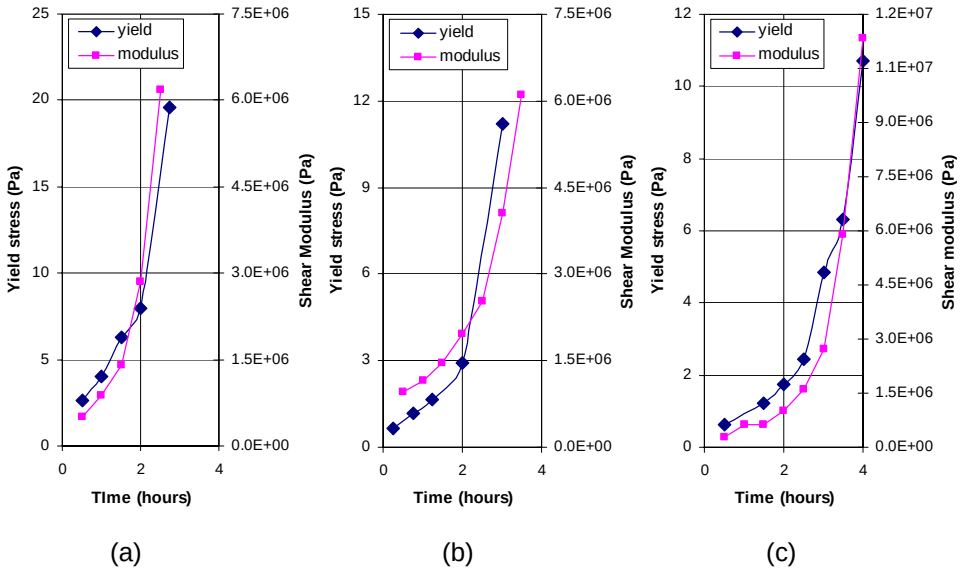

Figure 4-10 Comparison between the yield stress and shear modulus increases for different w/c ratios: (a) w/c = 0.4; (b) w/c = 0.5; and (c) w/c = 0.6.

Relating the changes in the shear modulus and yield stress obtained from rheological measurements with the changes in porosity from the ultrasonic data, it can be seen that there is a larger change in elastic modulus than yield stress for a given decrease in porosity. Changes in porosity are produced when the water is replaced with products of hydration. The formation of hydration products produces a larger relative increase in elastic modulus than yield stress. Measurements for elastic modulus are associated with infinitesimal relative motions between the individual grains and do not disturb the arrangement of grains. Yield stress, the stress required to initiate flow, on the other hand, depends upon the effort for individual grains to move relative to the other grains and on the capacity of the bond between the individual grains. Yield stress is therefore related to the stress required to produce large relative movements between the grains. In the early stages if hydration, the formation of the hydration products and their placement contribute to a larger relative increase in inter-particle elastic interaction between cement grains than the force required to produce a large separation between the grains.

4.7 Conclusions

Combining the information obtained from ultrasonic and rheological measurements allows for relating changes in the microstructure with the mechanical properties of hydrating cement paste through setting. Specifically,

1. Low amplitude stress measurements indicate that even for a high w/c ratio, there is sufficient long-range order within the material that it provides a solid-like response to applied shear stress.
2. After mixing, there is a continuous evolution of microstructure at the length scales corresponding to the wavelength of the ultrasonic wave. For all w/c ratios tested, there is a continuous increase in the solid fraction associated with the products of hydration after mixing. There is a slower rate of increase in the solid fraction for a higher w/c ratio.
3. A decrease in porosity (an increase in solidity) produced by the products of hydration results in an increase in shear modulus and yield stress. There is a larger relative increase in modulus than yield stress for a given decrease in porosity.
4. Both rheological and ultrasonic measurements indicate changes in the material behavior which are not detected by the penetration measurements. Setting behavior indicated by a sharp rise in the yield stress occurs at a time when the penetration measurements indicate no change in the material response.
5. Setting behavior within cement paste, associated with a sharp increase in the yield stress of the material is indicative of the formation of a continuously connected solid network.
6. The sharp increase in the yield stress is coincident with a sharp increase in the shear modulus of the solid obtained from the ultrasonic measurements.

Chapter 5 Ultrasonic Monitoring of the Capillary Porosity and Elastic Properties in Hydrating Cement Paste

5.1 Introduction

In the first few hours after mixing cement and water there are significant changes in the microstructure, which influence property development in the material. Determination of the changes in the microstructure and elastic properties of hydrating cement through setting, and early strength gain of the material has remained a major experimental challenge. Applying conventional methods for studying changes in microstructure in the first few hours after casting are challenging because (a) sample preparation procedures either alter or disturb the microstructure [Thomas et al. 1999; Jennings et al. 2007] and (b) changes in microstructure in the hydrating system occur on a time scale that is an order of magnitude faster than the time required for sample preparation [Juenger et al 2003].

Porosity of cement paste is one of the most important microstructural features, which manifests at different length scales. The capillary porosity is associated with the larger length scale, while the gel pores are finer. The volume of porosity has been measured using gas sorption, solvent exchange and thermogravimetric methods [Parrott 1983]. From the measurements of the evaporable and non-evaporable water contents in the cement paste, the degree of hydration and porosity are estimated using relations which are based on known reaction stoichiometry and volumetric

proportions of the reaction products [Hansen 1986; Powers and Brownyard 1947; Powers 1958]. The sample preparation required for any of these techniques involves drying and does not permit real-time estimation of porosity changes. Recently, techniques based on small angle scattering (SAS) have been applied to study the development of porosity. Small angle neutron scattering (SANS) and small angle X-ray scattering (SAXS) allow for porosity measurements at the nano-scale and can be used on wet samples without the need for drying. The interpretation of the microstructure of a complex system such as cement paste from the SAS data requires the use of microstructure models for obtaining the relevant quantitative parameters [Jennings et al. 2008].

Different aspects of the pore structure development have been assessed by assimilating information from different techniques. For instance, early age evolution of porosity and changes in the density of the hydration products, have been estimated from the measurement of chemical shrinkage, isothermal calorimetry and imaging [Fernandez 2008]. The evolution of the pore connectivity was inferred from electrical measurements by relating the measured bulk electrical conductivity to the pore solution conductivity and porosity, which was obtained from weight loss measurements [Sant et al.2006]. It is shown that there are significant changes in the pore connectivity within the first 24 hours, which is prominent for low water-to-cement ratios. Experimental investigation of pore structure of hydrating cement paste using scanning electron microscopy and low temperature calorimetry revealed significant changes in the capillary pore system within the first few days of

hydration, while the gel pores system is shown to develop later [Bentz and Stutzman 2006]. Changes in the pore structure have been shown to have a significant influence on the mechanical properties. The capillary porosity in particular is associated with changes in the mechanical properties, while the finer gel pores influence properties such as shrinkage and creep [Jennings et al. 2007]. Currently a tool for simultaneously monitoring the evolution of porosity and elastic properties of cement paste, which provides non-invasive, real-time assessment, is not available.

The development of microstructure in hydrating cement pastes, especially in the early ages has been simulated using computer models, which indicate that initially starting from a weak skeleton composed of loosely connected cement grains within the fluid medium, the products of hydration link up to provide a continuous network of hydration products within the fluid filled space [Bentz and Garboczi 1991; Ye et al. 2003]. The emergence of a continuous solid phase within the fluid medium has been identified as the percolation threshold [Bentz and Garboczi 1991; Chotard et al. 2003; Jennings et al. 2007]. Following the percolation threshold, setting behavior is initiated in the cement paste. Through setting, as the products of hydration form within the fluid-filled spaces of cement paste, a network of pores and a pore structure develops. Successful implementation of the computer models requires calibration of semi-empirical parameters for any given cement.

An ultrasonic technique and data interpretation for continuous simultaneous monitoring of changes in the porosity and elastic material properties in hydrating

cement paste are presented in this Chapter. The primary focus of the research presented here is to assess changes in the microstructure associated with porosity of a hydrating cement paste through the setting process from ultrasonic measurements. The ultrasonic reflection method comprises measuring the changes in the amplitude of a horizontally polarized shear wave (SH waves) at the interface between a buffer plate and the hydrating cement paste. Reflected shear waves have previously been used for studying the setting behavior and evolution of visco-elastic material properties of hydrating cement paste [Subramaniam et al. 2005; Voigt and Shah 2004; Wang et al. 2009]. Changes in reflected waves also provide a favorable prediction for strength gain in concrete [Akkaya et al. 2003]. An improved test system, with the capability of collecting wave reflection measurements at multiple angles of incidence, is presented. The measured wave response is related to the changes in the microstructure of hydrating cement paste using a poro-elastic representation of cement paste. A poroelastic equivalent material for hydrating cement paste is derived by matching the measured reflections response with changes in the poro-elastic parameters. The results of the study show that the porosity of the equivalent poro-elastic material compares favorably with the capillary porosity obtained from thermo-gravimetric measurements by the application of Power's model [Powers and Brownyard 1947; Powers 1958]. In addition, the shear modulus of the hydrating cement material obtained from the poro-elastic equivalent is shown to compare favorably with the value obtained from a vibration based measurement. The method presented here allows for real-time assessment of capillary porosity and shear modulus in hydrating cement paste.

5.2 Background

The microstructure of hydrating cement can be idealized as a water-filled porous skeleton with evolving porosity and skeleton properties. Previous experimental investigation had revealed that even initially after mixing, cement paste has sufficient structural integrity within the arrangement of cement grains to transmit low magnitude shear stress through the material [Subramaniam and Wang 2010]. At low amplitude shear stress, the freshly mixed cement paste behaves as a weak porous skeleton composed of grains of cement. With time, the cement grains form a three dimensional network where all grains are continuously connected to the adjacent grains with products of hydration [Bentz and Garboczi 1991; Ye et al. 2003, Subramaniam and Wang 2010]. On a representative scale, the solid skeleton of cement paste consists of unhydrated cement and the hydration products.

The poro-elastic representation of the microstructure of hydrated cement paste has been found suitable for the microstructure of cement paste at different length scales [Pichler et al. 2007; Ulm et al. 2004; Bernard et al. 2003; Lin and Meyer 2008]. The mechanical properties at a given length scale have been derived from the properties of components at a lower length scale using homogenization techniques [Ulm et. al 2004]. Using a poro-elastic representation for microstructure of hardened cement paste, the volumetric changes associated with shrinkage have been predicted [Pichler et al. 2007; Bernard et al. 2003; Lin and Meyer 2008]. The poro-elastic theory developed by Biot has also been updated to account for partial saturation of the medium to account for drying [Coussy 2004].

In this chapter, the poro-elastic representation developed by Biot is used to interpret the wave propagation in hydrating cement paste [Biot 1956a and b; Biot 1962]. According to Biot's theory, the volume fraction of the fluid within a unit volume of the material is referred to as the porosity. It is implicitly assumed that the pore size is concentrated around its average value. The pore structure is assumed to be composed of inter-connected void space, which allows relative motion between the fluid of known viscosity and the solid. The porous solid and the solid-fluid system are assumed to be statistically isotropic [Biot 1956a]. The propagation of waves in the fluid-saturated poro-elastic medium depends upon the internal system variables which are the effective elastic properties of the porous solid, the porosity, and the parameters related to the pore structure, which influence the relative local movement between the fluid and the solid [Biot 1956a and b; Stoll and Kan 1981].

Considering Biot's poroelastc idealization for hydrating cement paste, the solid skeleton at any given time is assumed to be composed of the products of hydration and the unhydrated cement. The porosity would be three dimensional water-filled pore space within the skeleton. The disconnected pore space, if any, forms a part of the solid skeleton and it influences the effective materials properties of the skeleton. The fraction of total volume occupied by water within connected pores is the porosity, ϕ, which is assumed to be isotropic on a representative length scale.

The basic equations for wave propagation in a poroelastic medium are presented in Appendix A. The solutions for these equations have been worked out by several

researchers [Stoll and Kan 1981, Albert 1993, Zimmerman and Stern 1994]. Three distinct modes of wave propagation including two compression waves and a single shear wave have been shown for a fluid-filled porous medium [Johnson and Plona 1982]. For the case of the compression wave, the solution for reflection at the interface between a fluid/elastic material and a porous medium has been determined previously [Stoll and Kan 1981; Chotiros 2002]. Using a similar procedure, the reflection co-efficient, $r^*(f)$, for a horizontally polarized shear wave reflected at the interface between an elastic material and a porous medium, with consideration of a specific set of boundary conditions [Deresiewicz 1963; Gurevich and Schoenberg 1999], can be derived as (see derivation in Appendix A)

$$\boldsymbol{r}^*(\boldsymbol{f}) = \frac{\mu_b^* \boldsymbol{k}_{sh}^* \cos(\alpha^*) - \mu_1 \boldsymbol{k}_1 \cos(\theta)}{\mu_b^* \boldsymbol{k}_{sh}^* \cos(\alpha^*) + \mu_1 \boldsymbol{k}_1 \cos(\theta)} \tag{5-1}$$

where μ_b^* is the complex dynamic bulk shear modulus of the solid skeletal frame of the porous medium, μ_1 is the shear modulus of elastic material, k_{sh}^* (complex) and k_1 are the wave numbers in the porous medium and the elastic material, respectively, θ is the angle of incidence and α (complex) is the angle associated with the refracted wave. It should be noted that wave number in the context of wave propagation is the spatial analog of frequency, and defines the phase change per unit distance traveled by the wave. $\cos(\alpha)^*$ can be taken equal to 1.0, when the acoustic impedance of the elastic material is larger than the acoustic impedance of the other material [Alig et al. 1997].

The reflection coefficient, $r^*(f)$ is a complex number written as

$$r^*(f) = r(f)e^{j\Phi} \quad (5\text{-}2)$$

where r(f) and Φ represent changes in the amplitude and phase of the SH wave following reflection at the cement paste/fused quartz interface, respectively. The decrease in the amplitude of an incident wave following reflection at the interface depends upon the properties of the porous material in contact with the elastic material. Therefore, changes in the amplitude of the reflected waves with time can be related to changes in the microstructure of the poroelastic material.

5.3 Experimental program

The test program consisted of the following measurements: (a) ultrasonic SH wave reflection; (b) Thermogravimetric weight loss measurements; and (c) vibration measurements. All three measurements were performed on cement paste samples prepared from the same batch. Measurements were primarily performed within the first 24 hours after casting. Cement paste samples with different water-to-cement ratios were prepared and tested. The composition of the Type I/II cement used is shown in Table 5-1. The Blaine fineness of the cement was 390 m^2/kg and the average particle size was 15 μm.

Table 5-1Composition of the Type I/II Cement

SiO_2	Al_2O_3	Fe_2O_3	CaO	MgO	SO_3
20.55	4.57	3.03	63.21	3.02	2.79

5.3.1 Sample Preparation

Cement paste samples were mixed using a paddle mixer following a procedure suggested by Williams et al. [1999], which is similar to ASTM C-305. Cement and water were initially mixed at 140 rpm for 30 seconds, followed by a pause for 1 minute before mixing for another 2.5 minutes at 285 rpm. Cement paste adhering to the sides of the mixing bowl was scraped and the entire mixture was mixed for another 2.5 minutes at 285 rpm. Cement paste samples with three different water-to-cement ratios equal to 0.35, 0.45 and 0.5, were evaluated in the test program.

5.3.2 Ultrasonic SH Wave Reflection Method

The ultrasonic wave reflection experimental system was developed to monitor the SH wave reflection at the interface between a buffer plate and cement paste, at 0, 50 and 60 degree angles of incidence. The choice of the angles for reflection measurements is explained in a previous Chapter [Subramaniam and Wang 2010]. While the 50 and 60 degree measurements provide higher sensitivity, measurements at normal incidence provided a convenient reference for evaluating changes in the reflected waves. A buffer plate made of fused quartz with precisely machined faces at matched angles with respect to the vertical was used. Ultrasonic shear-wave transducer(s), with a nominal center frequency of 1 MHz, were attached to the buffer plate using a solid couplant. Normal incidence (0 degree angle) measurements were performed in the pulse-echo mode, where a single transducer attached on the bottom surface functions as the transmitter as well as the receiver. At each oblique angle of incidence, a matched pair of direct contact transducers mounted on the

oppositely-angled surfaces of the fused quartz plate, functioned as the transmitter and receiver. The transducers were attached precisely at the center of the angled surfaces. While attaching the transducers, the axes of the transducers were aligned to generate a horizontally polarized shear (SH) wave in the fused quartz.

The experimental system comprised equipment for generating, capturing and digitizing ultrasonic waves and included three pulse receivers, a function generator, an oscilloscope, and a computer. A schematic sketch of the test setup is shown in Figure 5-1. Signal generation at each angle of incidence was controlled by one of three separate pulser-receivers and was individually triggered using a timer system at discrete time intervals to ensure that only signals from one angle of incidence were incident at the interface at any given time. The reflected signal detected by the corresponding receiver was digitized by the oscilloscope. The data acquisition and transfer were controlled by the computer over a GPIB interface. The oscilloscope had a digitization rate of 500 MS/s which provides a temporal resolution of 2 ns. The influence of random noise in the signal was minimized by taking an average of 100 waveforms in each acquisition. At each angle of incidence, an averaged waveform was acquired every 30 minutes. Data collection was switched between the different angles every 10 minutes allowing sufficient time to take the average and minimize the volume of data collected over a typical monitoring period. The entire system was placed inside an environmental chamber, which was maintained at 24 ^{o}C throughout the duration of the test.

A cylindrical sample holder (diameter = 75 mm and height = 100 mm) was attached to the top surface of the fused-quartz plate using silicone. The data collection procedure consisted of collecting reflected ultrasonic waves with an empty sample holder for each angle of incidence. The waves collected from the fused-quartz/air interface were collected and recorded before commencing mixing of cement paste. Immediately after mixing, the cement paste was placed in the sample holder up to approximately half the height. The entire assembly of the fused quartz and sample holder was gently vibrated to remove any entrapped air. The weight of the fused-quartz plate and sample holder with the cement paste was recorded before initiating the readings. The top surface of the cement paste sample was covered with a moist sponge which filled the remaining space within the sample holder. The top surface of the sample holder was sealed using Aluminum tape. The transducers were then connected to the pulser-receivers and the data collection was initiated at the hour mark after mixing. At the end of the test, the instrumentation was disconnected and the weight of the fused quartz plate with sample holder and cement paste sample was recorded. The hardened cement paste was demolded, dried with paper towels and its density was determined using a balance with an accuracy of 0.01 g.

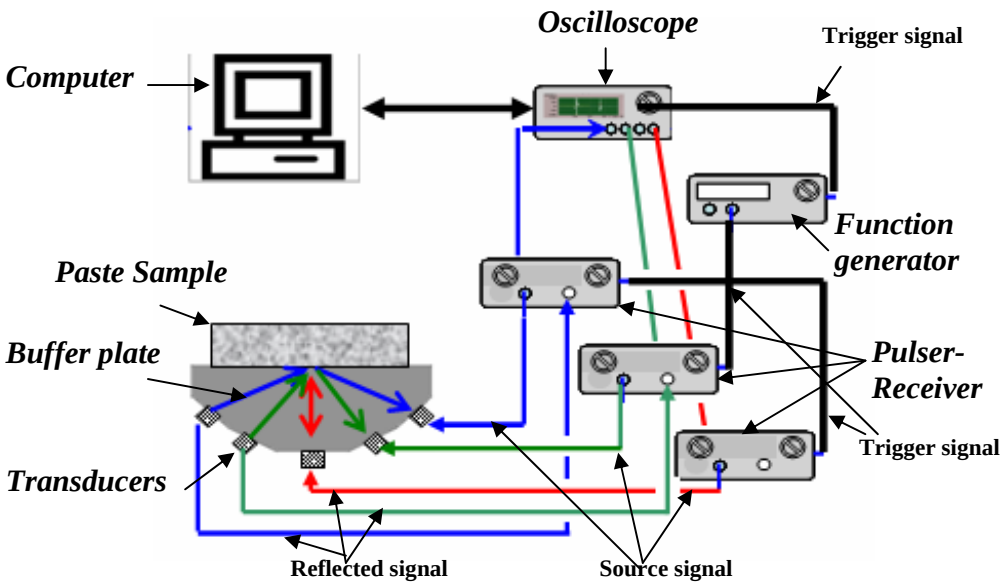

Figure 5-1 Schematic of ultrasonic experimental system

Data processing consisted of determining the change in the amplitude of the incident wave upon reflection at the fused-quart/cement paste interface. The reflection factor, which is the ratio of the reflected wave amplitude to the incident wave amplitude, r(f), was obtained using the self-compensating technique [Achenbach et al. 1992]. Using the reflected signal from the fused-quartz/air interface as the reference, r(f) at the cement paste/quartz interface was determined by normalizing the reflected magnitude off the fused quartz/cement paste interface with the reflected amplitude off the fused-quartz/air interface [Achenbach et al. 1992; Akkaya et al.2003; Subramaniam et al. 2002; Subramaniam 2005]. The time domain signals were transformed to frequency domain using the FFT algorithm and the amplitude reflection factor at 1 MHz, r(1), was determined as the ratio of the respective magnitudes of the FFT of the ultrasonic signals from the quartz/cement

paste to the quartz/air interface at that frequency. The r(1) obtained using this procedure corresponds to the change in the amplitude of a wave of 1 MHz frequency upon reflection at the interface between fused-quartz and cement paste.

5.3.3 Thermogravimetric Weight Loss Measurements

Thermogravimetric weight loss measurements were performed to determine the evaporable and the non-evaporable water contents within the hydrating cement paste at different ages. Cement paste samples for weight loss measurements, were cast inside sealed flexible plastic tubes. At a specified time, the cement paste sample was crushed inside the tube and then extracted by cutting the tube. The extracted sample was then ground using a mortar and pestle and the material passing through a No. 40 sieve was flushed with ethanol is a thistle tube. The sample was then divided into three replicates, approximately 150 mg each and introduced into crucibles of pre-measured weights. A slightly different procedure was followed for the measurements within the first few hours after casting while the cement had not set completely. The paste was extracted from the tube by cutting the tube, spread over the inside surface of the crucible using a spatula, immediately flushed with ethanol, weighed and introduced into a furnace. Weights of the samples were measured with an accuracy of 0.1 mg. The sample preparation was performed under flowing nitrogen gas. The temperature was ramped up to 105 ^{o}C in 2 hours and held constant. Weights of the samples were recorded after drying the sample at 105 ^{o}C before ramping the temperature to 1000 ^{o}C at 10 ^{o}C/minute. During the heating, the furnace was purged with nitrogen gas. The evaporable (w_e) and non-evaporable (w_n) water contents for

each crucible were determined. The non-evaporable water content was corrected for the loss on ignition of unhydrated cement powder, which was determined separately [Taylor 1985]. It should be noted that the weight loss measurements at 105 ^{o}C do contain contributions from the dehydration of ettringite. The contribution from dehydration of ettringite can be considered to be small considering the sulfate content of cement is low. The degree of hydration, $\alpha_h(t)$ was determined as follows

$$\alpha_h(t) = \frac{w_n(t)/w_c}{w_{n\infty}/w_c} \tag{5-3}$$

where $w_{n\infty}$ is the non-evaporable water content for the complete hydration [Hansen 1986; Powers and Brownyard 1947], w_c is the weight of cement powder. An approximation for the non-evaporable water for complete hydration, $w_{n\infty}/w_c \cong 0.23$, obtained by Powers was used. The porosity at certain degree of hydration then was calculated using the relations presented by Hansen [1986] as

$$\beta(t) = \frac{\rho_c(w/c) - (1.15 + 0.06\rho_c)\alpha_h(t)}{1 + (\rho_c)(w/c)} \tag{5-4}$$

where ρ_c is the specific gravity of cement and w/c is the water to cement ratio.

5.3.4 Vibration-based Measurement of Elastic Properties

A vibration-based technique was used to measure the dynamic elastic material constants (Young's modulus and Poisson's ratio) from the longitudinal modes of vibration of cylindrical specimens with length-to-diameter ratio equal to 2.0 [Subramaniam et al. 2000]. The test setup used for the vibration measurement is shown in Figure 5-2. In a typical measurement, the longitudinal vibrations are

initiated by the impact of a steel sphere at the center of one end of the cylindrical specimen. The resulting vibrations are monitored using a miniature accelerometer that is mounted at the center of the other end from the impact point. In the experimental setup used in this study, the signal from the accelerometer is acquired by the oscilloscope that is then transferred to a personal computer. The first two longitudinal resonance frequencies of the cylindrical specimen are then picked up from the frequency domain signal obtained from a Fourier transform of the time domain signal. The elastic constants of the cement paste sample are obtained using analytical formulas proposed by Subramaniam et al. [2000]. The Poisson's ratio, υ is determined as a function of measured first f_1 and second f_2 longitudinal resonance frequencies as

$$\upsilon = A_1\left(\frac{f_2}{f_1}\right)^2 + B_1\left(\frac{f_2}{f_1}\right) + C_1 \tag{5-5}$$

where, A_1, B_1 and C_1 are functions of the length, L and the diameter, D of the cylinder, given as

$$A_1 = -8.6457(L/D)^2 + 24.4431(L/D) - 12.4778,$$

$$B_1 = 34.5986(L/D)^2 - 101.7207(L/D) + 56.172$$

and $C_1 = -34.6807(L/D)^2 + 105.979(L/D) - 62.731$

Similarly, the shear modulus G is determined as

$$\boldsymbol{G} = \rho\left(\frac{2\pi \boldsymbol{f}_1 \boldsymbol{R}_o}{\boldsymbol{f}_n^1}\right)^2 \tag{5-6}$$

where ρ is the density of sample, R_o is the radius of cylinder,

$$f_n^1 = A_2(\upsilon)^2 + B_2(\upsilon) + C_2 \qquad (5\text{-}7)$$

A_2, B_2 and C_2 are functions of L/D, given as

$$A_2 = -0.2792(L/D)^2 + 1.4585(L/D) - 2.1093,$$

$$B_2 = 0.0846(L/D)^2 - 0.5868(L/D) + 1.3791$$

and $C_2 = 0.285(L/D)^2 - 1.7026(L/D) + 3.3769$

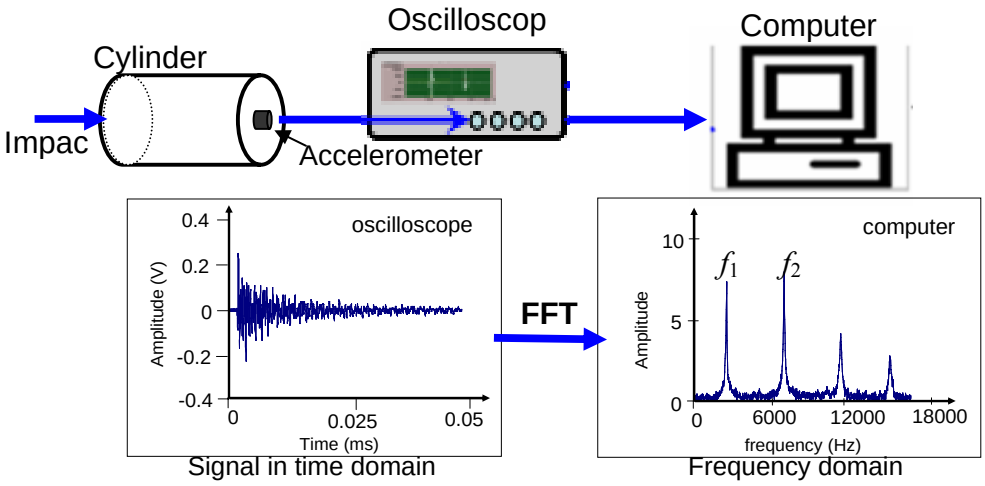

Figure 5-2 Schematic of vibration test setup and spectrum

Cement paste specimens with diameter and length equal to 2 in and 4 in, respectively were cast from the same batch of cement used for ultrasonic and thermogravimetric measurements. The specimens were cast in cylindrical molds and vibrated to remove any entrapped air. The specimens were demolded after 8 hours and wrapped in two layers of aluminum tape. Small portions of the circular faces approximately 5 mm x5 mm in size, centered on the longitudinal axis of the cylinder,

were left uncovered by the aluminum tape. These areas were covered using Teflon tape, which could be removed easily. During a measurement these areas, not covered by the aluminum tape, were used for attaching the accelerometer and for the impact point.

5.4 Experimental Results

5.4.1 Results from Ultrasonic Measurements

A typical result of the changes in *r(1)* at three different angles of incidence for cement paste with w/c ratio of 0.45 is shown in Figure 5-3. It can be seen that while the general trends from all three angles of incidence are nominally similar, measurements from larger angles of incidence register a larger magnitude of change at any given time. Immediately after mixing, the measured *r(1)* for the three angles of incidence are close to 1.0, suggesting that a significant portion of the incident wave energy is reflected at the quartz/cement paste interface. With time, initially, there is a gradual decrease, which is then followed by a more rapid change in *r(1)*. After approximately 12 hours, there is a distinctive change in the rate of decrease in *r(1)*. The changes in temperature recorded from the same sample are also shown in the plot for comparison. The different stages in the hydration reaction can clearly be identified from the temperature profile. The changes in measured *r(1)* at all three angles of incidence correspond well with the changes in temperature. There is a very rapid decrease in *r(1)* during the acceleration stage indicated by temperature measurements. There is a distinctive change in the rate of decrease of *r(1)* associated with the end of

the acceleration stage. The measured responses from the other w/c ratios were nominally similar.

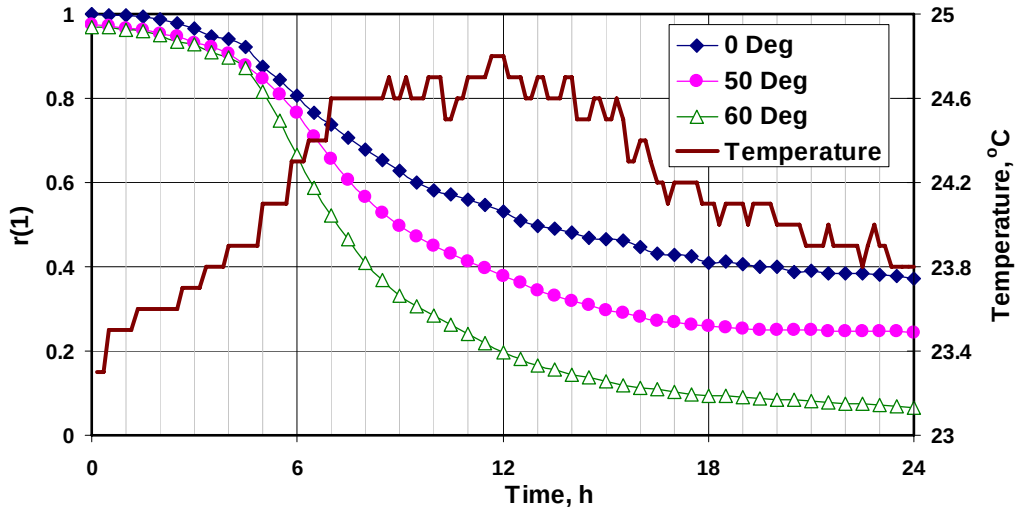

Figure 5-3 Evolution of amplitude reflection coefficient for different incident angles.

5.4.2 Results from Vibration Measurements

The values of Young's modulus ($E=2G(1+\upsilon)$) determined from the vibration measurements as a function of time are shown in Figure 5-4. For cement paste with w/c = 0.5, while readings were initiated for samples after 8 hours, it was not possible to obtain consistent readings until 10 hours. The trends in elastic modulus indicate a very rapid increase in E in the first 24 hours, while there an overall decrease in Poisson's ratio with some variation. The results from the different w/c ratios consistently indicate a higher magnitude of E for lower w/c ratio at any given time. It is however interesting to note that there is a larger relative increase in the magnitude of E for the cement paste with a larger w/c ratio.

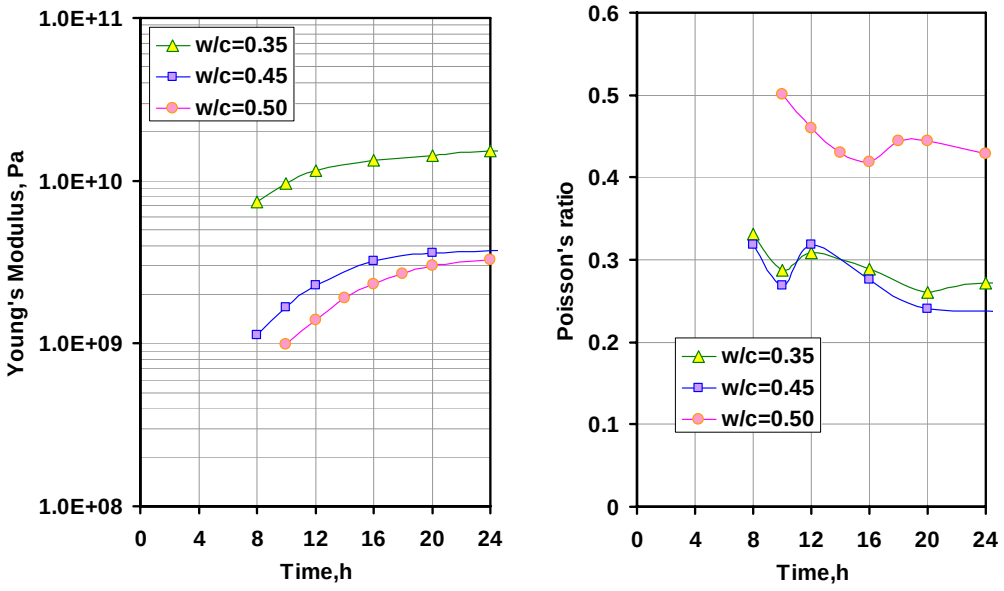

(a) (b)

Figure 5-4 Vibration measurements as a function of time: (a) Young's modulus; and (b) Poisson's ratio.

5.4.3 Results from Thermogravimetric Measurements

The degree of hydration and the changes in porosity of the hydrating cement pastes determined from the thermogravimetric weight loss measurements are shown in Figure 5-5. It can be seen that there is a steady decrease in the capillary porosity with an increase in the degree of hydration. The trends in the degree of hydration and changes in porosity are consistent with the rates of changes indicated by the temperature measurements.

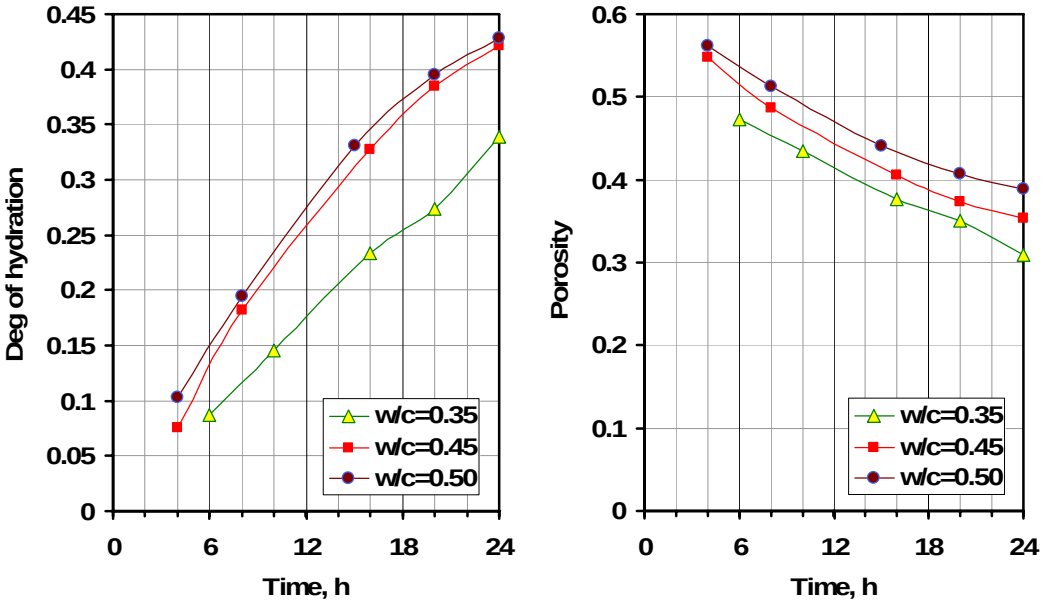

(a) (b)

Figure 5-5 Thermogravimetric weight loss measurements: (a) degree of hydration; (b) capillary porosity

5.5 Analysis of Results

5.5.1 Poroelasticity Inversion Procedure

The measured changes in the *r(1)* at the fused-quartz/cement paste interface can now be interpreted in terms of the expected result from the reflection of an SH wave at the interface between an elastic and a poro-elastic material. The reflection coefficient at the interface, *r(f)* depends upon the material properties of both media in contact. The functional form of *r(f)* given in Equation (5-8a), can be expressed as

$$r(f) = \left| \frac{\mu_b^* k_{sh}^* \cos(\alpha)^* - \mu_1 k_1 \cos(\theta)}{\mu_b^* k_{sh}^* \cos(\alpha)^* + \mu_1 k_1 \cos(\theta)} \right| \qquad (5\text{-}8a)$$

where $\boldsymbol{k}_{sh}^{*} = \left[\left(\rho_b\omega^2 - \frac{(\rho_f\omega^2)^2}{\boldsymbol{m}'\omega^2 - \boldsymbol{j}\omega(\boldsymbol{F}_v\eta/\kappa)}\right)/\mu_b^{*}\right]^{1/2}$ (5-8b)

$$\boldsymbol{F}_v(\omega,\boldsymbol{a}_p,\eta) = (1+\tfrac{1}{2}\boldsymbol{j}\omega\tfrac{\rho_f\kappa\boldsymbol{a}_p}{\eta\beta})^{1/2} \quad (5\text{-}8c)$$

$$\boldsymbol{m}' = \boldsymbol{c}_T\rho_f/\beta \quad (5\text{-}8d)$$

$$\rho_b = (1-\beta)\rho_s + \beta\rho_f \quad (5\text{-}8e)$$

$$\mu_b^{*} = \mu_b(1+\delta_\mu\boldsymbol{j}) \quad (5\text{-}8f)$$

$$\mu_1 = \frac{\boldsymbol{E}_1}{2(1+\upsilon_1)} \quad \text{and} \quad \boldsymbol{k}_1 = \frac{\omega}{\sqrt{\mu_1/\rho_1}} \quad (5\text{-}8g)$$

ρ_1, E_1, and υ_1 are the density, the Young's modulus and the Poisson's ratio, respectively of the fused quartz, μ_b and δ_μ are the drained shear modulus of the skeleton and the loss factor, respectively, a is the pore size parameter, κ is the permeability of the porous medium, c_T is the tortuosity of the pore space, η is the viscosity of the fluid, β is the porosity of the poroelastic medium, ρ_f is the density of the fluid, ρ_s is the density of the skeleton material and ρ_b is the bulk density of the poroelastic material. A better description of the variables involved is provided in Appendix A. It can be seen that the expression for *r(f)* does not allow for identifying the explicit functional relationships between the variables and *r(f)*. The function *r(f)* can however be symbolically expressed as a function R_s, given as

$$\boldsymbol{r}(\boldsymbol{f}) = \boldsymbol{R}_s\left(\rho_e,\boldsymbol{E}_e,\upsilon_e,\rho_s,\rho_f,\boldsymbol{K}_f,\mu_b^{*},\beta,\eta,\boldsymbol{a}_p,\boldsymbol{c}_T,\kappa\right) \quad (5\text{-}8h)$$

When applied to the case of hydrating cement paste, which is assumed to be a water-filled porous skeleton composed of cement grains and products of hydration,

the bulk properties of water are readily available as K_f =2.2x10^9 Pa, ρ_f=1x10^3 Kg/m^3 and the viscosity η = 0.9x10^{-3} Kg/ms.

The analysis can be simplified by considering inter-relations between some of the material parameters, which were introduced by Berryman [1980]. The tortuosity, *c* can be calculated as a function of porosity (β) as

$$\boldsymbol{c_T} = 1 - \boldsymbol{s_e}(1 - 1/\beta) \tag{5-9}$$

where s_e is a factor, which must be calculated from a microscopic model of the frame moving in the fluid. The value of s_e equals to ½, which is the exact value for the case of spheres in a fluid medium, was found to provide a reasonable estimate for shear waves in a porous medium [Berryman 1980]. The relationship between permeability, pore size and porosity, given by the Kozeny-Carman relation, was found to be suitable for porous media and is given as

$$\kappa(1-\beta)^2/\beta^3 = \kappa_o(1-\beta_o)^2/\beta_o^3 = \boldsymbol{const}. \tag{5-10}$$

and similarly

$$\boldsymbol{a_p}^2/\kappa = \boldsymbol{a_{po}}^2/\kappa_o = \boldsymbol{const}. \tag{5-11}$$

where $\boldsymbol{a_p}$ is the pore diameter, β_o,κ_o , a_{po} are the initial porosity, permeability and pore diameter, respectively. The pore size parameter, $\boldsymbol{a_p}$, cannot be measured directly but is estimated to be (1/6 – 1/7) of the grain size [Berryman 1980]. These inter-relations between some of the parameters of the porous material that were found to provide an accurate description of elastic wave propagation in fluid-saturated porous media such as fine grained sands and sintered porous glass [Plona 1980; Johnson and Plona 1982]. The results were also found to be insensitive to the exact

relationships between porosity of the solid and properties which influence bulk flow of the fluid, such as permeability and tortuosity.

Considering the hydrating cement material to be composed of two components, the porous skeleton (made up of cement grains and products of hydration) and water, a simple relation can be obtained considering the relationship for a sealed poro-elastic system given in Equation (5-8e). When applied to hydrating cement paste, ρ_s represents the effective density of the solid material composed of the unhydrated cement and the products of hydration, ρ_f is the bulk density of water, and ρ_b is the bulk density of the cement paste. In a sealed system, any changes in ρ_b can only be attributed to changes in volume due to contraction of the bulk. Changes in ρ_b of the hydrating cement paste with age (on account of any volumetric changes due to autogenous shrinkage) can be calculated using Powers' model for each degree of hydration and this effect, if significant, can be included in the bulk density evaluation. The ρ_b of cement paste samples were measured at three days of age and were found to be 2.06, 1.87 and 1.85 g/cm^3, respectively for w/c equal to 0.35, 0.45 and 0.5. These values compare very well with the calculated values of density obtained from the weight proportions of cement paste for a fixed w/c ratio

$$\rho_b = \frac{1 + w/c}{\frac{1}{\rho_c} + \frac{w}{c}} \tag{5-12}$$

Assuming ρ_c is equal to 3.2, the values of ρ_b are obtained to be 2.055, 1.907 and 1.855g/cm^3 for w/c equal to 0.35, 0.45 and 0.5, respectively. Thus, for the cement pastes evaluated in this program, ρ_b can be considered to be constant, equal to ρ_b,

during the period of observation. The ρ_s, can therefore be obtained using Equation (5-8e), further reducing the number of internal variables in the function R_s for r(f).

The material properties of fused quartz are readily available, further reducing the number of internal variables in the expression in R_s., The reflection at the fused quartz/cement paste interface can be expressed in terms of the porosity and shear modulus of the skeleton, as

$$\boldsymbol{r}(\boldsymbol{f}) = \boldsymbol{R}_s\left(\mu_b, \beta, \delta_\mu\right) \tag{5-13}$$

In the simplified form, changes in the amplitude of the incident SH wave depend upon three key internal variables of the poro-elastic medium, which are functions of age (time after mixing). Since obtaining analytical expressions for the inversion of the internal variables from the expression for R_s is intractable, numerical inversion was performed to optimize the material constants such that the theoretical prediction is close to the experimental response. The experimental data used in the optimization consists of the r(1) at three different angles of incidence. The generalized reduced gradient nonlinear optimization scheme was used to minimize an objective function given as

$$\mathrm{Fun}(c_i) = \sqrt{\frac{\sum_{n=1}^{3}\left(\left|r(1)\right|_{\theta_n} - \left|R_s(\theta_n, c_i)\right|\right)^2}{3}} \tag{5-14}$$

where θ_n is the discrete incident angle at which experimental values are obtained, and c_i are the internal system variables of the poroelastic solid.

For the numerical inversion, the starting guess of porosity for the first measurement after mixing was obtained using the relation

$$\beta_o = \frac{\rho_c \left(w/c \right)}{1 + \rho_c \left(w/c \right)} \tag{5-15}$$

where ρ_c, the specific gravity of cement, was assumed to be 3.2. The pore size parameter, a_{po} was taken to be 1/6 of the average cement grain size, which is equal to 2.5 μm. The initial value of permeability, κ_o was estimated using an expression obtained from the application of the general effective medium theory [Cui and Cahyadi 2001]

$$\kappa_o = \frac{l_c^2 (1.8)(\beta_o - \beta_c)^2}{226} \tag{5-16}$$

where β_c is a constant equal to 0.18 and l_c, the critical pore diameter was assumed to be equal to a_{po}. The starting guess for μ_b was taken as 10^5 Pa. The range for δ_μ was initially prescribed to be within 0.01 – 0.3. It was found that within the prescribed range, there was an insignificant influence of δ_μ on the final values of μ_b and β. The solution obtained at a given time was used as the starting guess for the next time.

5.5.2 Evolution of Porosity and Shear Modulus in Hydrating Cement Pastes

The shear modulus and porosity of the cement pastes of three water-cement ratios obtained from the numerical inversion of the test data are shown in Figure 5-6. Similar trends in the changes in modulus and porosity for the three mixtures can be observed. It is interesting to note that there is a continuous increase in the shear modulus after casting, which is almost exponential within the first few hours

following which there is a decrease in the rate. The change in the rate of increase of shear modulus corresponds in time with the end of the acceleration period indicated by the temperature measurements. The end of the acceleration period has been associated with a change in the rate controlling mechanism [Mindess and Young 1981]. The change in the rate of modulus increase is therefore indicative of a change to a chemical and diffusion controlled reaction. The porosity obtained from the ultrasonic data corresponds to relative proportion of the water filled space within a solid skeleton. The measured decrease in porosity is therefore equal to the increase in the solid fraction within the cement paste. Comparing the relative changes in the shear modulus and porosity obtained from the ultrasonic data, it is interesting to note that there is a three order of magnitude increase in the shear modulus corresponding to relatively small change in the porosity. Further there is no significant change in the rate of porosity decrease while the shear modulus exhibits a distinctive change in the rate of increase. There is hence a very non-linear relationship between the decrease in porosity and increase in modulus. Further, there appears to be a larger relative increase in the shear modulus for a given change in the porosity for lower w/c ratio. For a lower w/c ratio, because of the initial closer spacing of cement grains a smaller volume of hydration products produce a higher change in the shear modulus [Subramaniam and Wang 2010].

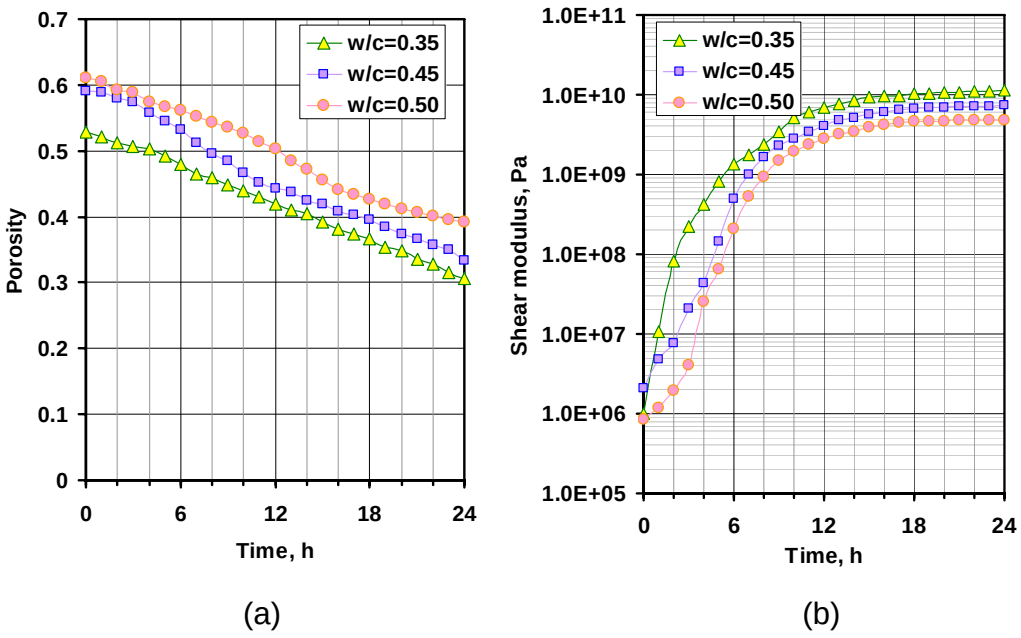

Figure 5-6 Evolution of (a) porosity and (b) shear modulus of solid skeleton

The measurements on porosity of cement paste obtained from the ultrasonic measurements are compared with the values obtained from the thermogravimetric weight loss measurements in Figure 5-7. The porosities obtained from weight loss measurements agree well with the porosities from poro-elasticity based inversion of ultrasonic data. The relationship between porosity and the degree of hydration, given in Equation (5-4), was given by Powers and provides an estimate of the capillary porosity in the system. In addition, the values of porosity determined from TGA measurements for cement paste with w/c equal to 0.5 by Voigt and Shah [2004] are also plotted in the Figure. The close agreement between the values of porosity obtained from the poro-elastic equivalent derived from wave reflection measurements and the capillary porosity calculated by applying Power's model to weight loss measurements provides a validation of the measured porosity. Further, it can be

inferred that on the scale of the observation indicated by the ultrasonic waves, the porosity of the equivalent water filled poro-elastic material corresponds with the capillary porosity within the hydrating cement paste.

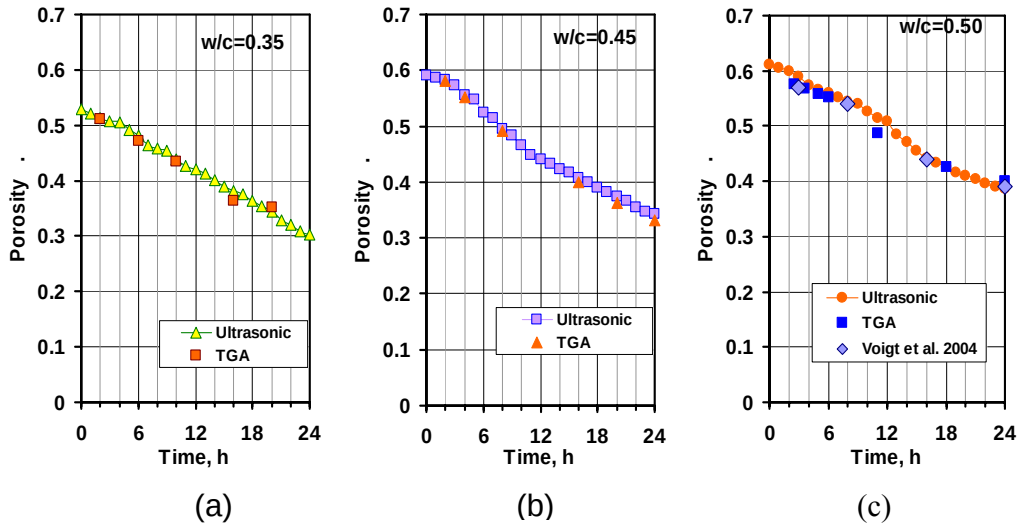

Figure 5-7 Comparison between the porosity determined from the ultrasonic measurements and the thermogravimetric weight loss measurements: (a) w/c = 0.35; (b) w/c =0.45; and (c) w/c = 0.5.

The shear modulus of solid skeleton from ultrasonic data is compared with the shear modulus obtained from the vibration test as shown in the Figure 5-8. It should be noted that while there is a good agreement between the trends and the values of shear moduli derived from the two measurements, the shear modulus of the equivalent poro-elastic skeleton, which is derived from the ultrasonic inversion is generally higher than the value obtained from low amplitude vibratory measurement. This is expected considering the dynamic modulus obtained from a poroelastic material exhibits an increase with frequency, which is influenced by the frequency dependence of the loss factor [Park 2005].

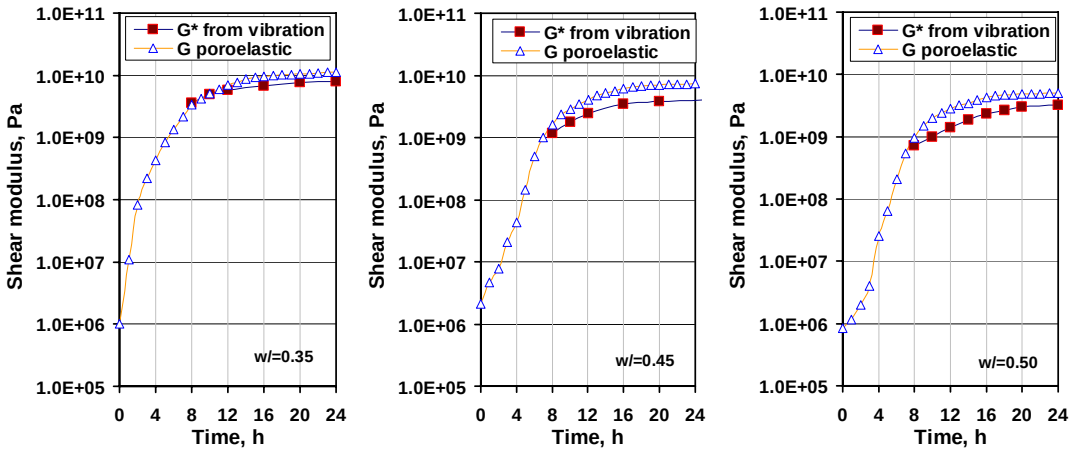

(a) (b) (c)

Figure 5-8 Comparisons of shear moduli from poroelastic inversion and vibration measurements for different w/c ratios: (a) w/c = 0.35; (b) w/c = 0.45; and (c) w/c = 0.5.

5.6 Discussion

The resolution of the information (also referred to as sensitivity) on the length scale accessed by the ultrasonic waves of the measurement is closely related to the wavelength of the wave (it is usually a fraction of the wavelength). A rough estimate of the influence of the measuring frequency on the length scales assessed by the waves is determined by the characteristic frequency, f_c derived by Biot [1956a] and given as

$$f_c = \frac{\pi\mu}{4\rho_f a_p^{\,2}} \tag{5-17}$$

For frequencies above the characteristic frequencies, the Pouisville flow breaks down within the pores. For 1 MHz measuring frequency, the value of the pore size

parameter can be estimated to be 0.8 μm. On this scale of observation, changes within the pore structure on length scales significantly smaller than the wavelength would be assigned to the skeleton. Thus changes in the gel porosity with time, which are typically associated with a length scale on the range of nano-meters, can only be indirectly inferred through changes in the skeleton properties. The water filled space which allows continuous bulk flow of water on the scale of capillary pores can however be clearly delineated in the early age.

The influence of shrinkage on the measured parameters obtained from the inversion of the ultrasonic data requires careful consideration. Autogenous shrinkage would result in a change in the macroscopic volume while chemical shrinkage produces changes within the structure of the paste. The potential influence of the shrinkage should be evaluated within the time frame of significance for changes in the capillary pore structure and the elastic modulus of the material. The shear modulus of hydrating cement pastes is known to evolve most rapidly (several orders of magnitude) in the first day of hydration [Boumiz et al. 2000]. There is a decrease in the rate with time and it is known to reach an asymptotic value after few days (7-10 days). Similarly significant changes in the capillary pore system have been shown to occur within the first few days of hydration [Consolati and Quasso 2003]. Therefore, the significant period of interest is the first few days of hydration.

For a sealed system, since the total mass of the system remains constant, the change in volume results in a change in the bulk density. Considering the typical

magnitude of autogenous shrinkage, which is typically on the order of 1000 με, changes in volume of the hydrating cement paste with age can be considered to produce insignificant changes in the bulk density of the material. In this early period, changes in the porosity and the elastic modulus of the hydrating cement paste occur on a significantly faster time scale than the corresponding change in density. The influence of changes in bulk density can therefore be treated as a second-order effect when compared to the corresponding change in the porosity of the system. This was verified by varying the bulk density used in the inversion within bounds associated with volume change due to autogenous shrinkage. There was an insignificant change in the values of the poro-elastic parameters obtained from the inversion when compared with the values predicted considering no change in the bulk modulus.

Chemical shrinkage is assessed from the decrease in volume of the products for a given volume of the reactants. Chemical shrinkage, may create air voids [Tazawa et al. 1995], which may influence the makeup of the hydration product. For low w/c ratio cement pastes, chemical shrinkage may also produce partial saturation in pores. In a saturated system, the additional water entering the unit volume may increase the density. Typical values of chemical shrinkage for completely hydrated cement paste are in the range of 5-7 ml/100 g of paste, which would result in a 7-8% internal reduction in volume [Geiker and Knudsen 1981]. For the lowest w/c ratio used in this study, w/c=0.35, following the methodology presented by Hansen (1986), the chemical shrinkage at 40% degree of hydration can be estimated to be approximately 5%. Considering some part of this 5% would manifest itself in the form of

disconnected porosity, the effect of partial saturation is insignificant. This effect may be come significant at later ages (with progressing hydration) or for w/c lower than 0.35 and would require careful consideration. Biot's model was primarily derived for fluid saturated porous medium and with some modification can be adopted for a partially saturated medium.

The ultrasonic measurements provide a measure of porosity where relative movement is possible between the water and the solid skeleton. The water transport within cement is dominated by capillary pores when the capillary pore network is connected [Ye et al. 2005]. Therefore capillary pore structure would play a significant role in determining the ultrasonic wave propagation in cement paste. Depercolated pores, if present, do not influence the movement of bulk water and would not influence the porosity determined from the ultrasonic measurements. Further, considering the length scales of resolution provided by the ultrasonic measurement, the depercolated pores within the solid matrix would be indirectly detected through their influence on the effective elastic property of the skeleton. It should be noted that very low w/c systems desaturate rapidly. In such systems, in addition to depercolation of pores, the influence of partial saturation should be considered in the poroelastic representation.

The measurement of elastic properties obtained from the ultrasonic and vibration-based procedures correspond with the undrained condition, where the rate of stress application is significantly faster than the time scale associated with pressure

decrease due to draining of the porous solid [Sanahuja et al. 2007]. The quasi-static measurements on specimens with no confining pressure, on the other hand, approach the drained conditions. Measurements under undrained conditions include the effect from inertial and viscous interaction associated with relative fluid flow. The elastic moduli obtained from dynamic measurements (both ultrasonic and vibration) therefore exhibit frequency dependence and provide higher values than those obtained from the quasi-static measurements. It should be noted that any disconnected porosity within the solid matrix would influence the skeleton properties under both drained and undrained conditions identically.

It has been previously shown that the application of established relations such as the Kozeny-Carmen relations, which are suitable for use in rocks and other porous materials are not suitable for hardened cement paste. The reason is attributed to the very fine scale porosity in the form of gel pores, which do not contribute strongly to transport [Christensen et al. 1996]. Early results by Powers et al. [1959] indicated that when the capillary porosity decreases below a critical value, the permeability drops rapidly as the gel pores control the permeability. In this range it is reasonable to expect the Kozeny-Carmen relations not to work. However, in the early ages when capillary pores control the permeability, direct application of a proven relations in rocks have been found to provide reasonable estimates [Christensen et al. 1996; Cui and Cahyadi 2001]. Extension of the proposed method as the capillary porosity decreases with progressing hydration requires careful consideration.

The results from the ultrasonic measurement can now be compiled to develop an understanding of the changes in the microstructure which produce setting and early strength gain in cement pastes. There are significant changes in shear modulus in the first few hours. Starting from a small value, there is an exponential increase in the shear modulus up to the end of the acceleration period, following which there is a noticeable change in the rate of increase. During the corresponding period there is a continuous decrease in the porosity and the trend indicates a slowing down in the rate with time. Changes in porosity are produced when the water is replaced with products of hydration. The formation of hydration products produces a larger relative increase in elastic modulus initially in the acceleration stage than later after setting. The sharp rise in the shear modulus, has previously been shown to indicate the emergence of a fully connected solid network of hydration products within the cement paste. This observation was first reported by Sayers and Grenfell [1993] using through thickness ultrasonic propagation and later confirmed by Subramaniam and Wang [2010] with rheological and ultrasonic reflection measurements. Following this, there is a very non-linear relationship between the pore structure densification (decrease in porosity) and shear modulus of the skeleton. The information on the evolution of porosity and the shear modulus can now be combined to directly understand the influence of structure formation and hydration on property development as show in Figure 9. The non-linear relationship between the porosity and shear modulus clearly depends upon the w/c ratio. This indicates the elastic modulus depends upon the initial porosity in addition to the porosity in the hydrating material. There is a larger relative increase in the shear modulus associated with a unit change of porosity for lower w/c ratios. This

suggests that for a lower w/c ratio, because of the initial closer spacing of cement grains a smaller volume of hydration products produce a higher change in the shear modulus.

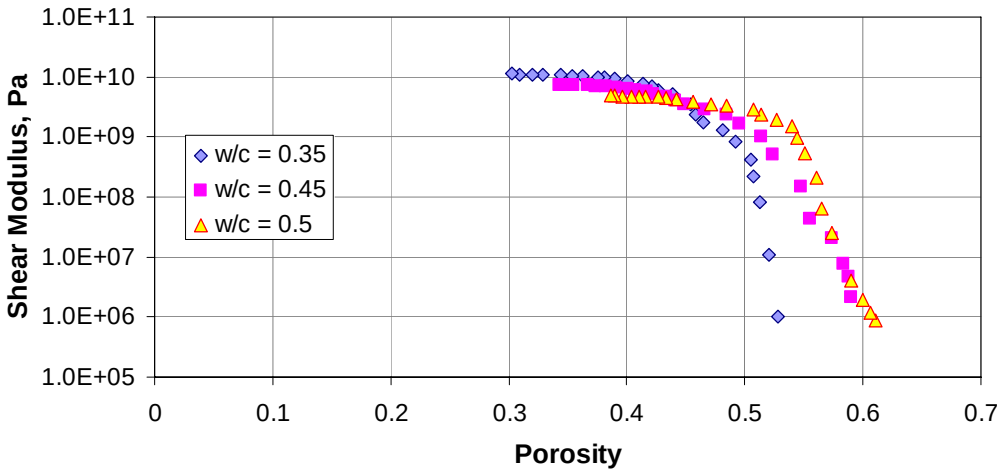

Figure 5-9 Relationship between shear modulus and porosity for cement pastes with different w/c ratios.

The information on the evolution of porosity and degree of hydration can now be combined to estimate changes in the effective density of the solid matrix. Considering the cement paste to be comprised of a water-filled solid skeleton, the density of the solid phase can be obtained as

$$\rho_s(t) = \frac{\rho_b(t) - \rho_f \beta(t)}{(1 - \beta(t))} \tag{5-18}$$

where ρ_b of cement paste applied in the porous inversion procedure, were measured at three days ages as 2.06, 1.87, and 1.85 g/cm^3 for w/c ratio equal to 0.35, 0.45 and 0.50, respectively. (The values estimated from densities of cement and water are 2.055, 1.907 and 1.855 respectively). The ρ_s in Equation (5-18) represents the

effective density of the solid comprised of unhydrated cement and the different products of hydration (comprised of CH, CSH and AFm). Since the degree of hydration represents the mass of cement which has hydrated, the combined density of the products of hydration (ρ_{hydr}) can be estimated as

$$\rho_{hydr}(t) = \frac{\rho_s(1-\beta(t)) - \rho_c(1-\beta_0)(1-\alpha_h(t))}{1-\beta(t)-(1-\beta_0)(1-\alpha_h(t))} \qquad (5\text{-}19)$$

where ρ_c is the density of cement (taken as 3.2 gm/cm^3) and β_o is the initial porosity of the cement paste obtained from Equation (5-15). The combined density of the hydration products for the three w/c ratios tested are plotted in Figure 5-10. As seen in the Figure, the final value for all the w/c ratios is a constant around 2.047 g/cm^3. The value of ρ_{hydr} obtained here is comparable to the results obtained from chemical shrinkage measurements [Fernandez 2008].

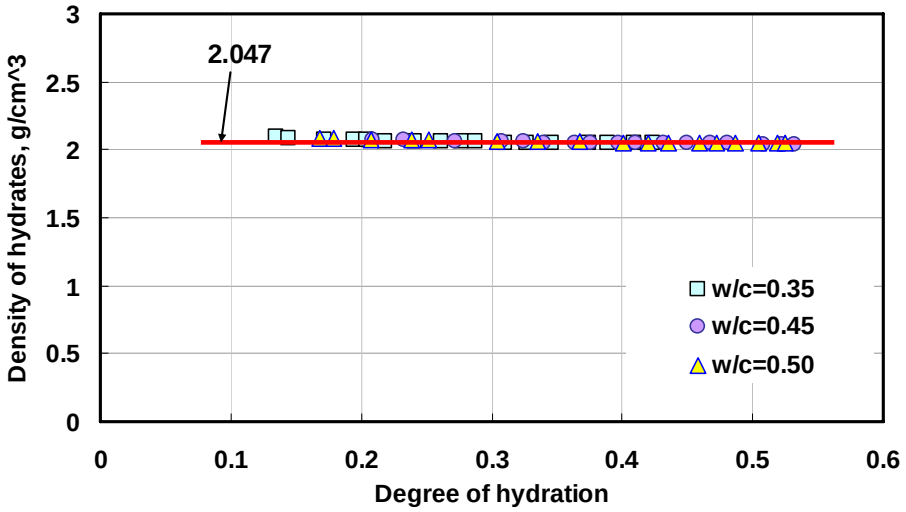

Figure 5-10 Evolution of densities of hydrates for cement pastes

The influence of porosity on the compressive strength of cement paste is shown in Figure 5-11. It can be seen that the relationship between the capillary porosity and the compressive strength is independent of the w/c ratio. This suggests that in hydrating cement paste the strength gain is controlled by the decrease in capillary porosity. While the relationship between the direct measured variable, the reflection factor (r) and the compressive strength is not unique for the different w/c ratios, there is a unique relationship between the microstructural variable derived from the reflection measurement and the compressive strength. It should be noted that the exact relationship between the capillary porosity and compressive strength will depend upon the exact composition of the cementitious material. However, the results presented in Figure 5-11 suggest that for a given type of cementitious material, if the relationship between capillary porosity is established, then microstructure based tools for predicting strength gain in hydrating cement based materials can be developed.

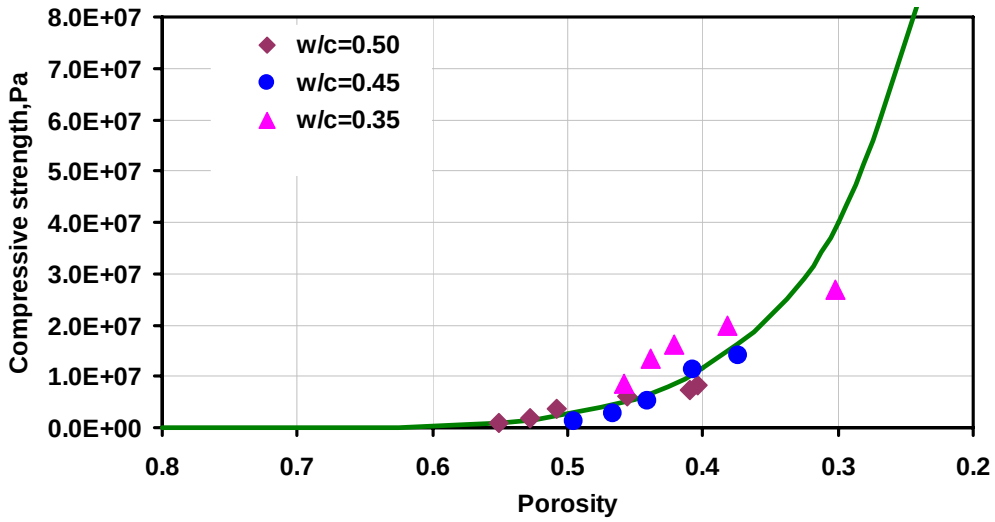

Figure 5-11 Relation between porosity and compressive strength

5.7 Conclusions

An ultrasonic method which measures the change in amplitude of horizontally polarized (SH) shear waves at the interface between fused-quartz and hydrating cement paste is presented. From the measured changes in the amplitude of the SH upon reflection, an equivalent poro-elastic material is derived. The shear modulus of the equivalent poro-elastic material is shown to compare favorably with the shear modulus of the cement paste obtained from vibration measurements. The porosity of the poro-elastic material obtained from the ultrasonic measurements is shown to match the capillary porosity in cement paste obtained from the weight loss measurements using Power's model. Considering the results from the measurements, the following specific conclusions can be made:

1. The ultrasonic method provides for continuous, simultaneous measurement of capillary porosity and shear modulus of the material, with time. It can be used to track the development of microstructure and the mechanical properties of the skeleton composed of hydration products with time.
2. There are significant changes in shear modulus in the first few hours. There is an exponential increase in the shear modulus up to the end of the acceleration period, following which there is a noticeable change in the rate of increase. During the corresponding period there is a continuous decrease in the porosity, while the trend indicates a slowing in the rate of decrease.
3. There is a very non-linear relationship between the porosity and the increase in shear modulus in the first 24 hours.
4. There is a unique relationship between he decrease in porosity and the

increase in compressive strength, which does not depend on the w/c ratio of the paste.

Chapter 6 Ultrasonic Assessment of Microstructure of Hydrating Mortar

6.1 Introduction

Concrete is a complex multi-scale heterogeneous material with microstructure ranging from the nanometers scale to the tens of centimeters. The microstructure of concrete varies depending on the scale of observation and can broadly be broken into levels as shown in Figure 6-1. Procedures for linking the scales have been established for mature concrete [Bernard et.al.2003; Ulm et.al. 2004; Garboczi and Bentz 1995]. Using the principles of micromechanics the properties at a larger length scale can be derived from the properties of the components at the smaller length scale. Recently, it has been shown that the poroelastic parameters derived from the nano scale are consistent across the different length scales of relevance in concrete [Ulm et. al. 2004]. At any scale, properties relevant for analysis are derived from a basic representative element volume (rev) through procedures of homogenization from the properties of the distinct phases which can be identified. At each scale, the properties of each phase are treated as statistically uniform and are in turn derived from a lower scale. In concrete, the distinct phases can broadly be identified as the coarse aggregate and mortar. Therefore, developing a homogenized representation for the mortar phase in concrete is important for relating the information obtained from cement hydration to the scale of rev in concrete.

Concrete gains strength with time due to a chemical reaction that involves hydration of cement. Hydration is a very complex multi-scale phenomenon involving changes in state and in the internal structure with time (see Mindess and Young [1981] and Taylor [1985] for comprehensive reviews). The change in the state is associated with the transformation of concrete from a fluid (workable) to a solid that is capable of resisting applied forces. After concrete sets, the products of hydration form within the fluid filled spaces of cement paste, which results in a network of pores and a pore structure [Powers et.al.1959]. The microstructure (internal structure) of hardening cementitious matrix continuously evolves with time due to progressing hydration. Progressing hydration and changing microstructure result in a continuous development of strength, mechanical and physical properties of concrete with time. In concrete, the changes in the microstructure are directly influenced by the cement hydration. The evolution of microstructure as a result of hydration comprises of a change in the density and elastic properties of products of hydration and a decrease in the porosity with time. This change is very rapid initially and asymptotically reaches a steady value after a very long time.

The current understanding of the hydration process has been assimilated by studying the different aspects of hydration reaction. For example, the rate and degree of hydration is assessed using calorimetry measurements [Odler and Dorr 1979; Brown 1989]; electron microscopy is used to study the microstructure and morphology of products [Copeland and Shulz 1962; Diamond and Bonen 1993; Daimon et al. 1971]; the change in porosity and pore structure of hardening cement paste are determined

using surface measuring techniques such as mercury intrusion porosimetry, nitrogen sorption, small angle neutron scattering etc.[Allen et.al 1982; Allen et.al. 1997; Cook and Hover 1993; Midgley and Illston 1983]; and the evolution of elastic material properties and compressive due to progressing hydration are measured using mechanical tests on control specimens [Day and Haque 1993; Bartlett and MacGregor 1999]. The fundamental understanding and modeling of the relationship between the internal structure and strength, elastic moduli, shrinkage, creep and transport properties of concrete is still evolving. Several theoretical complex material models for shrinkage [Bazant 1988], ionic transport [Bazant 1988; Bazant and Baweia 1995; Samson et.al. 1999; Garboczi and Bentz 1996; Halamickova et.al 1995], and strength gain [Ulm et.al. 2004] of concrete have been developed in terms of microstructural variables. Research is primarily hampered by the lack of proper tools which allow for continuous assessment of microstructure in concrete. Technology to directly infer the microstructure of hardening cement is needed to extend the fundamental understanding of development of material properties in early age concrete.

At each scale, a two phase representation of the material as a porous medium consisting of a solid matrix with a fluid filled porosity can be developed. The solid phase within an rev element at any scale, can be treated as homogeneous with average constant material properties. In hydrating cement paste the solid matrix was previously shown to be composed of unhydrated cement, products of cement hydration and gel pores with the pore space consisting of connected water filled capillary pores. The porosity at this scale of observation was found to be identical to the capillary porosity.

Application of the two-phase representation at higher scales during early hydration can also be explored. For instance, in hydrating mortar, the solid matrix would consist of sand in addition to the solid matrix for the hydrating cement. It is however not clear if the porosity derived by a direct application of the two-phase model at a higher scale would be consistent with the porosity obtained from hydrating cement paste. Understanding the link between the microstructural variables such as porosity on the scale of mortar and at level of cement paste is important for developing microstructure-based tools for predicting the development of properties in concrete.

In this chapter the porosity and shear modulus are directly obtained from ultrasonic reflection measurements by applying the two-phase idealization to mortar. The theoretical framework necessary to interpret the results of the ultrasonic technique and provide information about the microstructure of the hydrating cement paste in terms of physically-based variables developed in the previous chapters is extended to mortar. The application of Biot's poroelastic theory to the two-phase idealization of mortar is validated. The porosity obtained by applying poroelastic idealization to early age mortar is shown to be match the porosity derived from cement paste.

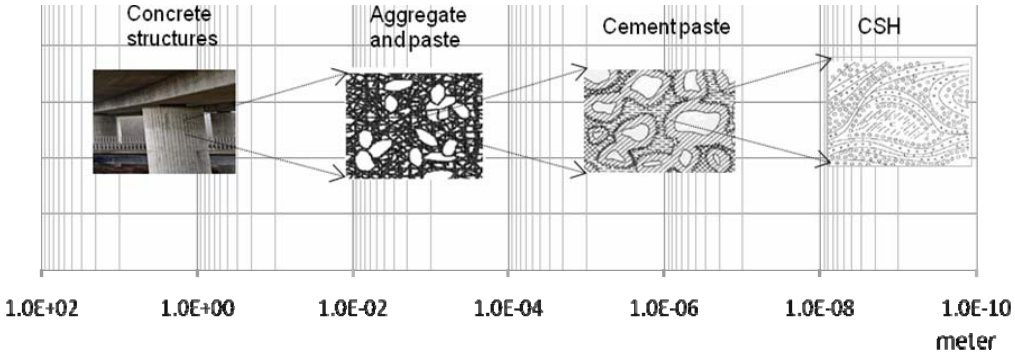

Figure 6-1 Schematic representation of the different length scales in concrete.

6.2 Materials and Test Procedure

An experimental program was conducted using mortars with different compositions shown in Table 6-1. Mortars with water to cement ratio by weight (w/c ratio) equal to 0.45 are prepared for three different sand to cement ratios by weight (s/c ratio) equal to 1, 1.5 and 2. Mortar with w/c ratio of 0.4 is prepared with sand/cement ratio equal to 2. River sand passing through a number 18 sieve (0.853 mm opening) was used for preparing the mortar. The cement composition is presented in Table 5-1 of Chapter 5 and is identical to the composition used previously for cement paste samples. The mortar compositions were chosen to introduce varying amount of sand in cement paste with w/c ratios, which were evaluated in Chapters 4 and 5. The cement paste with identical w/c ratio serves as the control and can be used to evaluate the influence of adding sand into cement paste.

Table 6-1 Proportion of the composition in test samples

Mixtures	Water/cement ratio	Sand/cement ratio
Mortar I	0.45	1
Mortar II	0.45	1.5
Mortar III	0.45	2
Mortar IV	0.4	2

A paddle mixer was used for mixing the mortar and the mixing procedure previously used for cement paste was followed. Cement, sand and water were initially mixed for three minutes and halted for three minutes while the walls of the mixing bowl were scraped with a plastic spatula. The mortar mixture was then mixed for another three minutes, before casting. In addition to preparing the sample for ultrasonic reflection measurements, 20 cylindrical samples were also prepared for strength and vibration tests. The nominal length and diameter of the specimens were equal to 102 mm and 51 mm, respectively. All the samples were filled in 3 layers and vibrated on a shaker table for 10 seconds.

Ultrasonic reflection measurements were performed using the setup presented in Chapter 4. The mortar sample was placed inside a cylindrical mold attached to the top of the buffer plate immediately after mixing. The reflected signals for all three incidence angles then were collected at half-hour intervals up to 48 hours. Vibration tests were conducted using cylinders cast with the same batch of mortar used in the ultrasonic measurements. The cylinders were demolded at 6 hours and wrapped in two layers of aluminum tape. The procedure for vibration measurement was identical to the procedure used for cement samples (presented in chapter 4). Additionally, the

compressive strength of the mortar mixtures was determined at 4 hour intervals staring at 6 hours up to 48 hours.

6.3 Experimental Results

6.3.1 Wave Reflection Coefficients

Typical ultrasonic waveforms recorded in time-domain after one reflection at the buffer plate-mortar interface are shown in the Figure 6-2. The waveforms recorded at the 60 degree angle of incidence are shown in the figure. It can be seen that there is a progressive change in the amplitude and shape of the reflected wave with time. Initially up to 15 hours there is a very rapid change in the amplitude. After 77 hours, the reflected wave form indicates that there is a significant phase change in the wave.

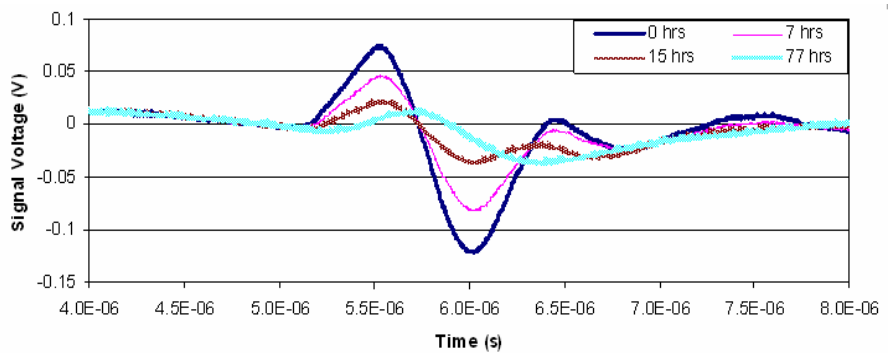

Figure 6-2 Typical reflected wave forms collected at different hydration ages.

The reflected signals in time domain were processed to obtain the amplitude reflection factor, r as a function of time. r was determined using the procedure

described in the Chapter 3. The reflection coefficient was determined at the resonant frequency of the transducer (1 MHz) for three different incidence angles and are plotted in Figures 6-3 (a), (b), (c) and (d) for Mortar mixtures I, II, III and IV, respectively. For a given mortar mixture, the actual variation in r at any age depends upon the angle of incidence used for reflection. The general trends indicate that a larger angle of incidence is associated with a more rapid initial decrease. This is in agreement with the previous measurements from cement paste, where it was shown a change in the material properties can be more sensitively detected at a larger angle of incidence. At the 60 degree angle of incidence, the r shows an increase following the initial decrease. A distinctive minimum value of r can be identified for each mortar mixture. In some mortar mixtures, the trend in the 50 degree angle of incidence measurement shows a gradual leveling followed by a slight increase above the minimum. The normal incidence shows a consistent decrease throughout the 48 hour period. The reversal in r was not previously observed in measurements with cement paste. Further, there is a faster decrease in r for mortar mixtures at all three angle of incidence than the corresponding change in r obtained from the respective control cement mixtures. This indicates that there is a faster increase in the acoustic impedance of mortar when compared to cement paste with identical w/c ratio.

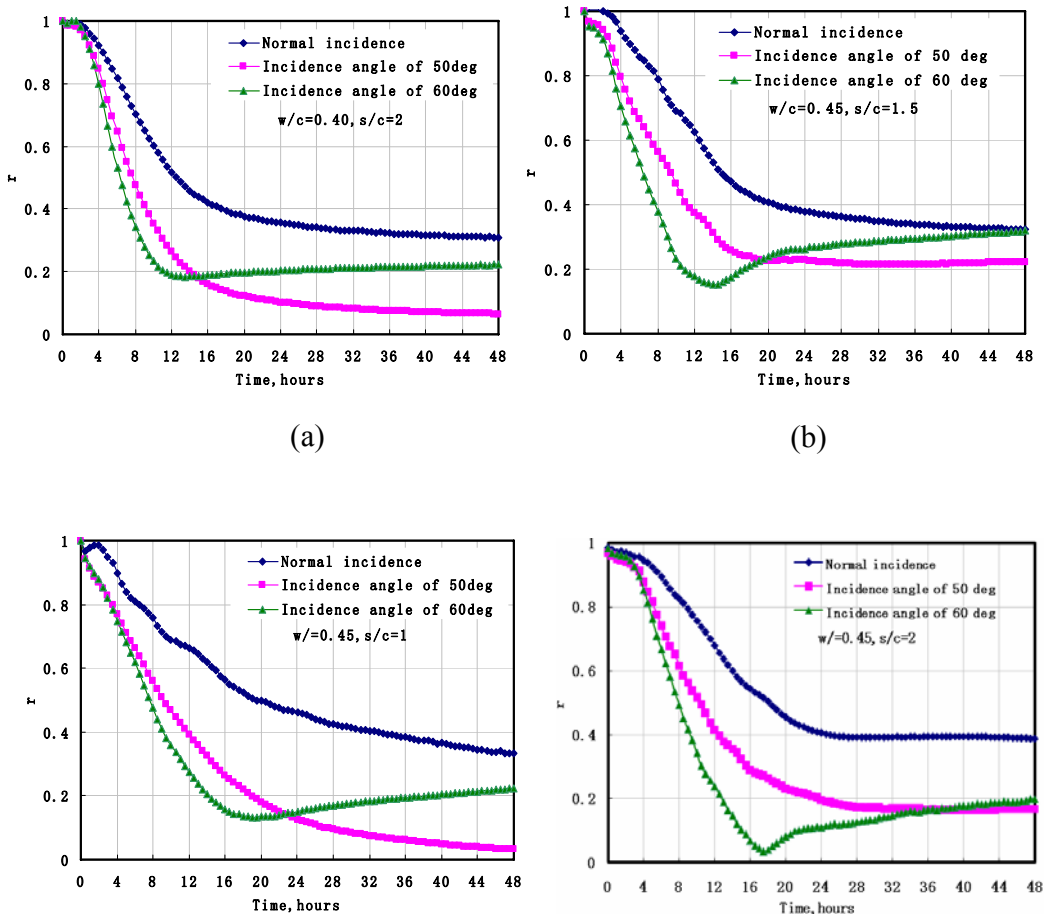

Figure 6-3 Measured amplitude reflection coefficients for mortar mixtures I(a), II(b), III(c) and IV(d)

6.3.2 Shear Modulus and Compressive Strength

The shear modulus obtained from the vibration tests and the compressive strength as function of time are plotted in Figures 6-4 and 6-5, respectively. The evolutions of elastic modulus and compressive strength follow the same trends for all the mixtures. However, there is a more rapid increase of the elastic modulus in the mortar mixtures than in cement paste samples with identical w/c ratios. The elastic modulus measured

from mortar mixtures are also higher than the values of elastic modulus obtained from cement paste mixture with identical w/c ratios. For a given w/c ratio, the measured elastic modulus and compressive strength of the mortar mixtures depend on the material composition of the mixture. For given w/c ratio, the mortar mixtures with larger sand content have higher elastic moduli. It should be noted that consistently all mortar mixtures exhibit a shear modulus larger than 10 GPa by 12 hours. In comparison, the shear modulus of the cement paste reaches 10 GPa at a later time.

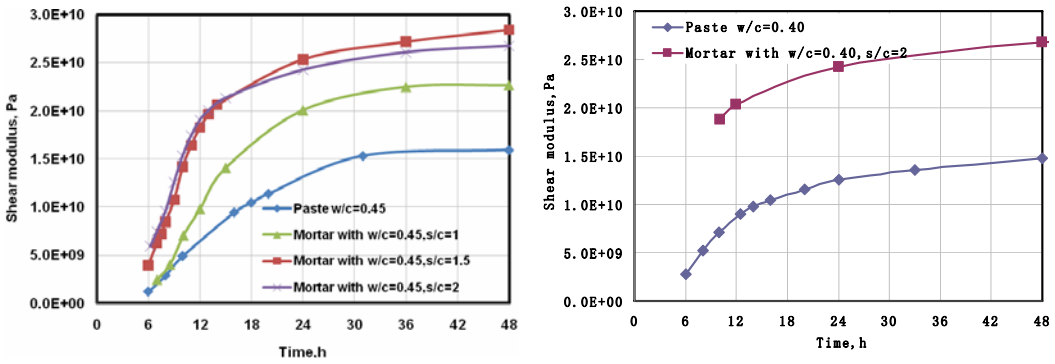

(a) (b)

Figure 6-4 Comparison of shear modulus obtained from vibration tests.

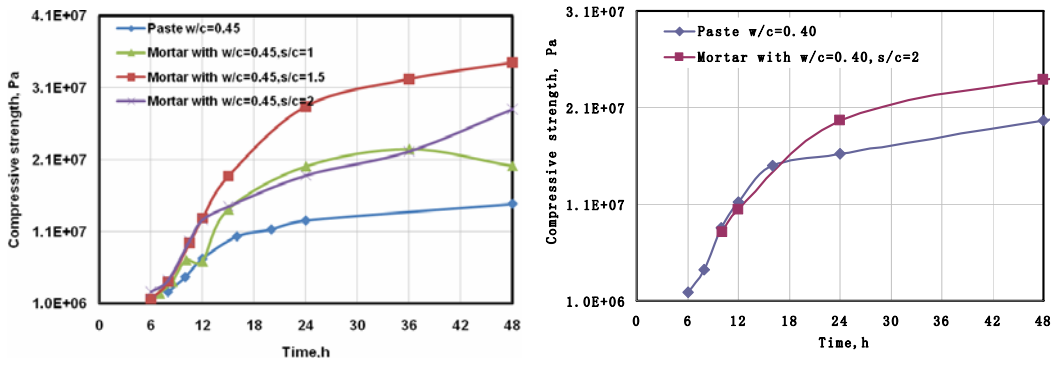

(a) (b)

Figure 6-5 Compressive strength as a function of hydration age.

6.4 Theoretical Interpretation of Results

An interpretation of the observed trends in the amplitude reflection factor, r for the mortar mixtures is now attempted through an analysis considering a simplistic representation of the cementitious materials (mortar and cement paste) as poro-elastic materials. The application of poroelasticity has been shown to be suitable for representing the microstructure of cement paste at the scale of capillary porosity [Subramaniam and Wang 2010]. This idealization is now extended to early-age mortar.

The poroelastic formulation for wave reflection coefficient $\boldsymbol{re}^{\boldsymbol{j}\Phi}$ at the interface between an elastic medium and porous medium has been derived in the previous chapter, and is given as

$$re^{j\Phi} = \frac{\frac{\mu_2^*}{\mu_1}\frac{k_{sh}^*}{k_1}\frac{\cos(\alpha)^*}{\cos(\theta)} - 1}{\frac{\mu_2^*}{\mu_1}\frac{k_{sh}^*}{k_1}\frac{\cos(\alpha)^*}{\cos(\theta)} + 1} \tag{6-1}$$

where, for the porous medium, the dynamic shear modulus μ_2^* of the skeletal frame is a complex number given as

$$\mu_2^* = \mu_2(1 + \delta_\mu \boldsymbol{j}) \tag{6-2}$$

δ_μ is the loss factor, which accounts for the effects of interaction between the solid skeleton and the fluid. μ_1 and $\boldsymbol{k}_1$ are the shear modulus and the shear wave number in elastic medium, respectively

$$\boldsymbol{k}_1 = \omega\sqrt{\rho_1 / \mu_1} \tag{6-3}$$

ω is the angular frequency of the wave, and ρ_1 is the density of the elastic medium. $\boldsymbol{k}_{sh}^{*}$ is the shear wave number in the porous medium and can be obtained from the following equation

$$\boldsymbol{k}_{sh}^{*2} = [\rho_2\omega^2 - \frac{(\rho_f\omega^2)^2}{\boldsymbol{m}'\omega^2 - \boldsymbol{j}\omega(\boldsymbol{F}_v\eta/\boldsymbol{k})}]/\mu_2^* \tag{6-4}$$

where $\rho_2 = (1-\beta)\rho_s + \beta\rho_f$, is the density of porous medium. ρ_s and ρ_f are the densities of solid and the fluid components in porous medium, respectively. β is the porosity of porous medium, κ is the coefficient of intrinsic permeability of the porous frame, $\boldsymbol{m}' = \boldsymbol{c}_T\rho_f/\beta$, $\boldsymbol{c}_T$ is the tortuosity coefficient (dimensionless parameter), which is experimentally determined, $F_v(\omega, a_p, \eta)$ is a correction function for the viscosity introduced by Biot which is considered as complex function of pore dimension, a_p, angular frequency ω and fluid viscosity η.

In Equation (6-1), θ is the angle of incidence and α is the refraction angle of the transmitted wave in the porous medium which is determined using Snell's law as

$$\cos(\alpha)^* = [1 - (\frac{\boldsymbol{k}_1}{\boldsymbol{k}_{sh}^*})^2(\sin\theta)^2]^{1/2} \tag{6-5}$$

The refraction angle from the interface between the elastic medium and porous medium is a complex number.

As presented in the previous chapter, considering the inter-relations between some of the material parameters, the reflection at the fused quartz/mortar interface can be

expressed in terms of three independent parameters, the porosity, the shear modulus of the skeleton and the loss factor, as

$$\boldsymbol{re}^{j\Phi} = \boldsymbol{R}_s\left(\mu_2, \beta, \delta_\mu\right) \tag{6-6}$$

Therefore, for given μ_1 and $\boldsymbol{k}_1$, varying μ_2, δ_μ and β would produce changes in both r and Φ. The results showing variations in r and Φ as functions of the non-dimensional ratio $\left|\mu_2^*\right|/\mu_1$ are plotted in Figures 6-6 through 6-14 for different values of β and δ_μ. In these figures, values of β expected in hydrating mortar samples are used. A range of δ_μ from 0.01 to 1.0 has been considered. The values of ρ_1, μ_1 and other parameters corresponding to fused quartz were used in generating the graphs and are given in Table 6-2.

Table 6-2 Properties of the elastic medium

	Density ρ_1 (Kg/m^3)	Shear Modulus $\boldsymbol{G}_1$ (GPa)	Shear impedance $\boldsymbol{Z}_1$ (Kg/ms)	Shear velocity $\boldsymbol{V}_1$ (m/s)
Fused quartz	2.2x10^3	31.0	8.26x10^6	3.75x10^3

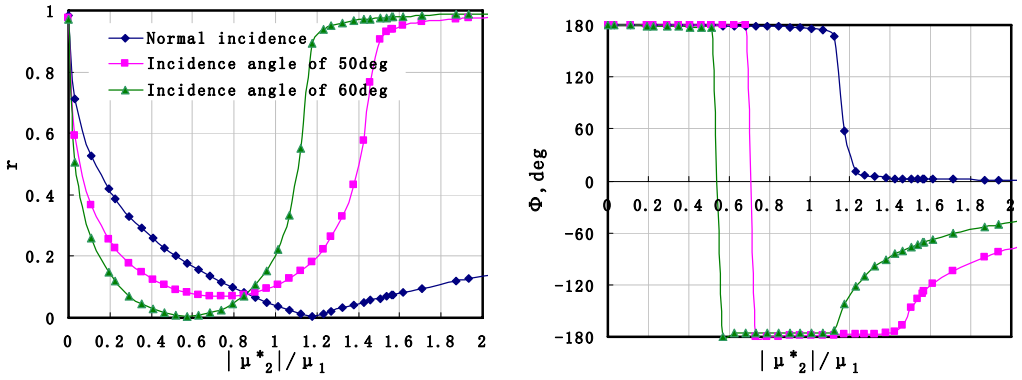

(a) (b)

Figure 6-6 Change of reflection coefficients as a function of $\left|\mu_2^*\right|/\mu_1$ for the case: β=0.4 and δ_μ=0.01

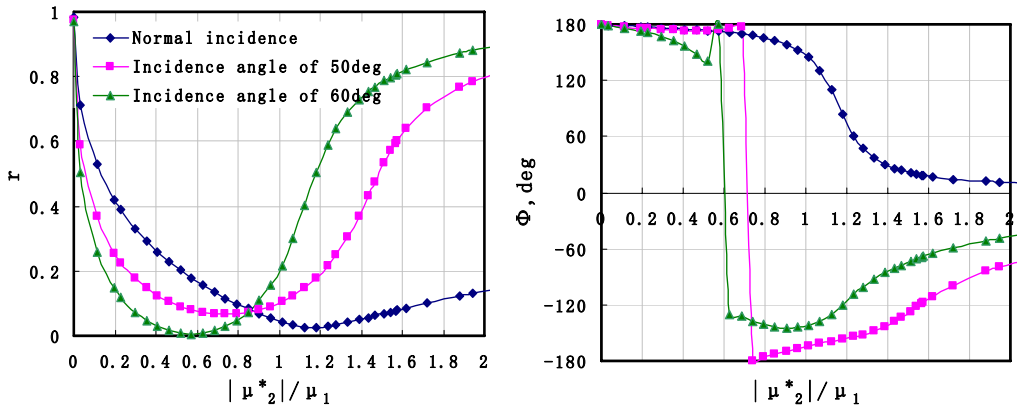

Figure 6-7 Change of reflection coefficients as a function of $\left|\mu_2^*\right|/\mu_1$ for the case: β=0.4 and δ_μ=0.1

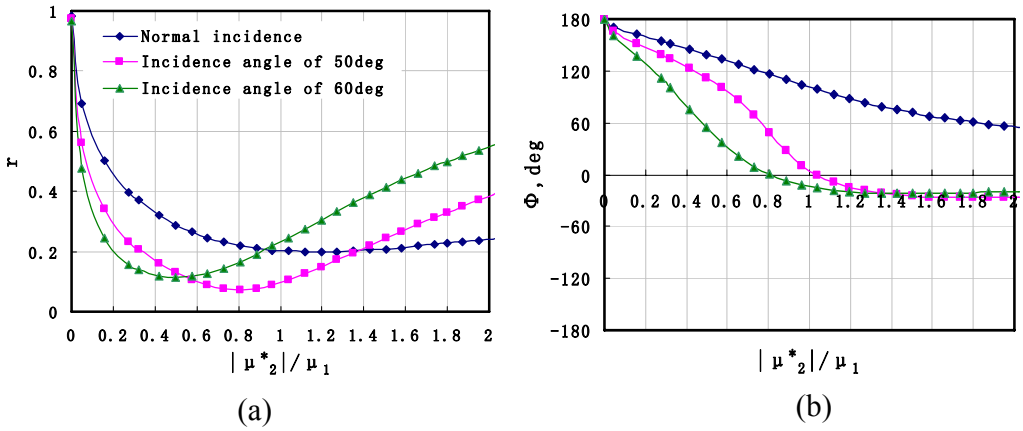

Figure 6-8 Change of reflection coefficients as a function of $\left|\mu_2^*\right|/\mu_1$ for the case: β=0.4 and δ_μ=1.0

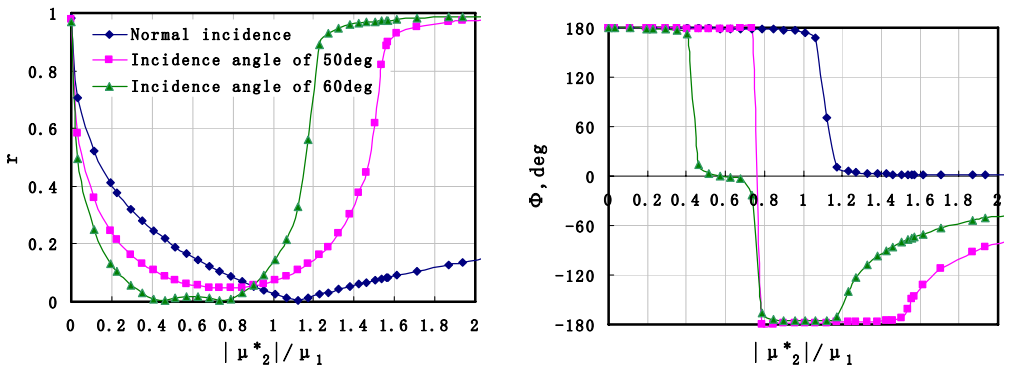

(a) (b)

Figure 6-9 Change of reflection coefficient as a function of $\left|\mu_2^*\right|/\mu_1$ for the case: β=0.3 and δ_μ=0.01

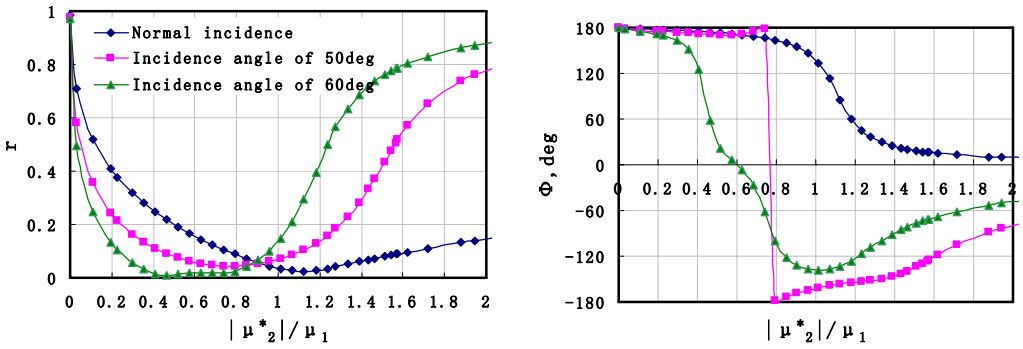

(a) (b)

Figure 6-10 Change of reflection coefficient as a function of $\left|\mu_2^*\right|/\mu_1$ for the case: β=0.3 and δ_μ=0.1

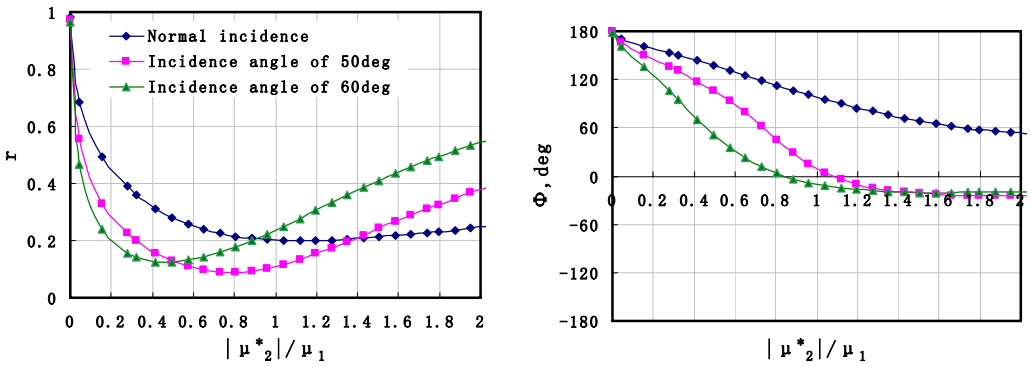

(a) (b)

Figure 6-11 Change of reflection coefficient as a function of $\left|\mu_2^*\right|/\mu_1$ for the case: β=0.3 and δ_μ=1.0

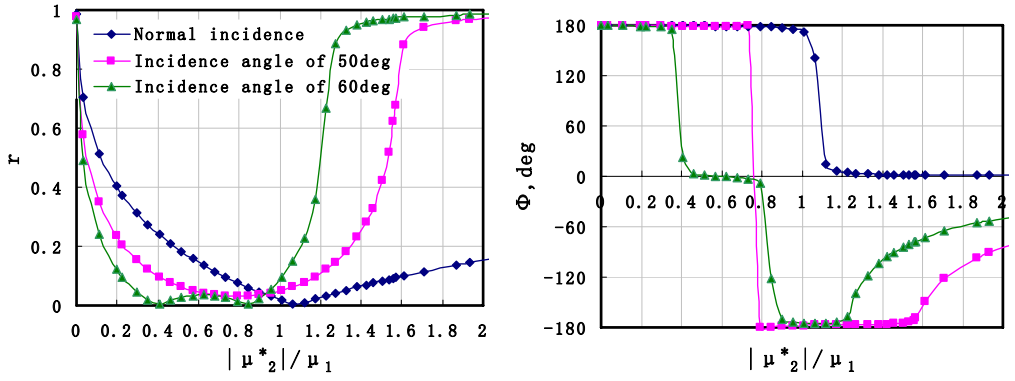

(a) (b)

Figure 6-12 Change of reflection coefficient as a function of $\left|\mu_2^*\right|/\mu_1$ for the case: β=0.2 and δ_μ=0.01

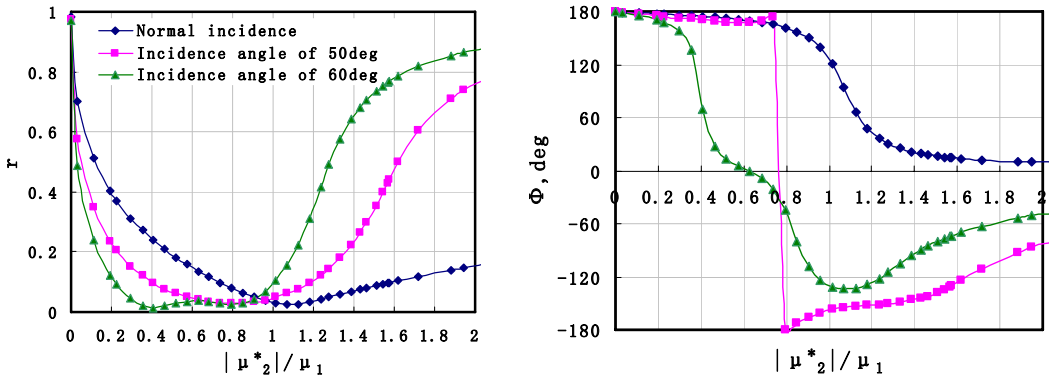

(a) (b)

Figure 6-13 Change of reflection coefficient as a function of $\left|\mu_2^*\right|/\mu_1$ for the case: β=0.2 and δ_μ=0.1

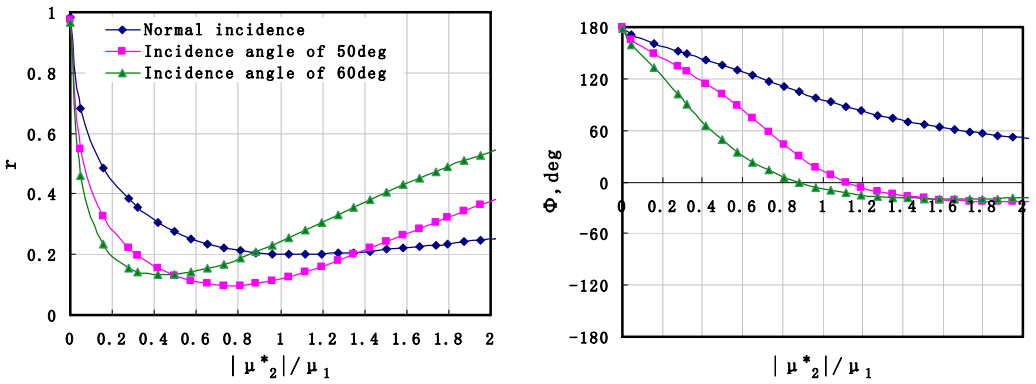

(a) (b)

Figure 6-14 Change of reflection coefficient as a function of $\left|\mu_2^*\right|/\mu_1$ for the case: β=0.2 and δ_μ=1.0

It can be seen that on increasing $\left|\mu_2^*\right|$, there is initially a decrease in r, which reaches a minimum and then starts increasing. For given β and δ_μ, minimum value of r occurs at a smaller value of $\left|\mu_2^*\right|$ for a larger angle of incidence. The minimum value

or r is attained when there is a distinctive change in the phase, Φ of the reflected wave. The minimum value of r is associated with a 90 degree change in phase for normal incidence. At 50 and 60 degree angles of incidence, the minimum value corresponds with a change in the phase angle from the second quadrant (ranging from π/2 to π) to the third quadrant (ranging from π to 3/4π).

The minimum value of r is not zero and the exact value depends upon both β and δ_μ. This is illustrated in Figure 6-15, where r is plotted as a function of $\left|\mu_2^*\right|/\mu_1$ for a value of β equals to 0.4 at three different angles of incidence. The minimum value of r is more strongly influenced by δ_μ than β and it approaches zero as the δ_μ decreases. This is illustrated in Figure 6-16, where the minimum value of r for the 60 degree angle of incidence is plotted as a function of β for different values of δ_μ. Larger the value of δ_μ, the larger the minimum value of r on increasing $\left|\mu_2^*\right|$.

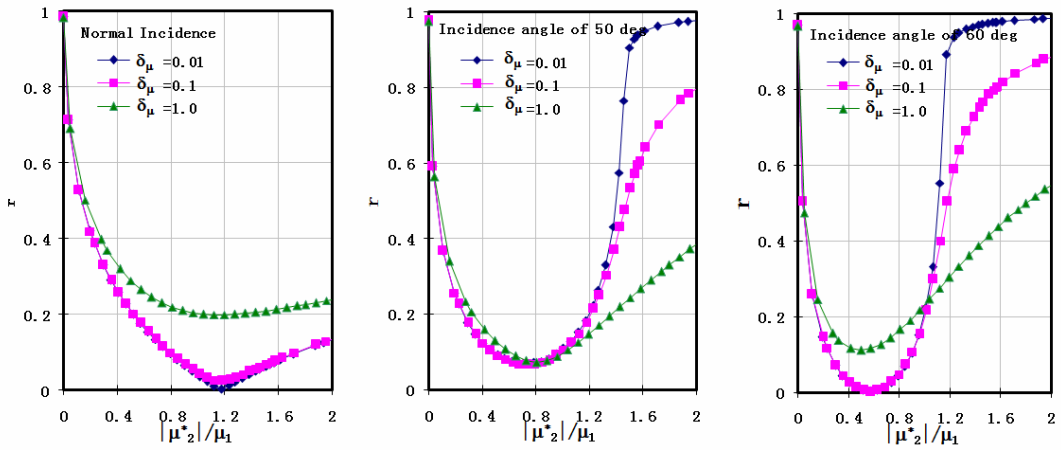

(a) (b) (c)

Figure 6-15 Change of amplitude reflection coefficient with the change of ratio of shear moduli: (a) Normal incidence;(b) 50 degree angle of incidence;(c) 60 degree angle of incidence

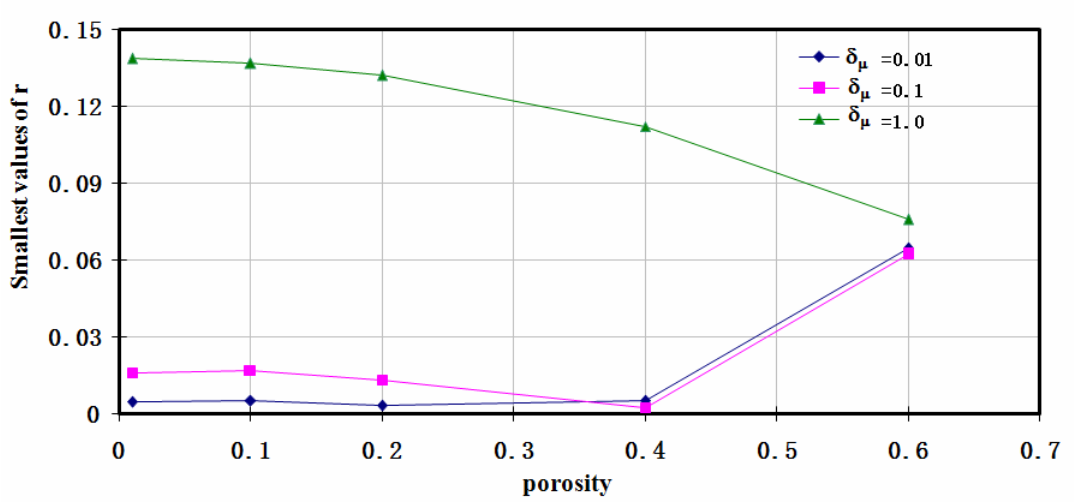

Figure 6-16 Change of smallest amplitude reflection coefficient with a change in porosity for 60 degree angle of incidence

The expression for $\cos(\boldsymbol{a})^*$ given in Equation (6-5) is a function of incidence angle and shear moduli of the interfacial media. On substituting for $\cos(\boldsymbol{a})^*$ from Equation (6-5) in Equation (6-1), the equation for the reflection co-efficient is of a form which cannot be readily inverted to determine the properties (β, μ_2 and δ_μ) of the cementitious material. To overcome this problem, approximate expressions where the $\cos(\boldsymbol{a})^*$ was set equal to 1.0 in the expression for reflection coefficient used in previous chapters.

The refraction angle is plotted as a function of $\left|\mu_2^*\right|/\mu_1$ for different values of in Figure 6-17. $|\cos(\boldsymbol{a})^*|$ is close to 1.0 for small values of $\left|\mu_2^*\right|/\mu_1$. However, on increasing $\left|\mu_2^*\right|/\mu_1$, there is a change in $|\cos(\boldsymbol{a})^*|$ and it must therefore be included in the expression for $\boldsymbol{re}^{j\Phi}$. Referring to the measurements from the vibration test, the modulus of the hydrating mortar can produce changes in $\left|\mu_2^*\right|/\mu_1$,which approach and

exceed 1.0. Therefore, for mortar, it will be no longer be valid to consider $|\cos(\boldsymbol{a})^*|$ equal to 1.0 in the expression for $\boldsymbol{re}^{j\Phi}$. The inversion procedure to access the microstructural evolution based on the poroelasticity, as discussed in the previous chapter, therefore has to consider the effects from the refraction angle.

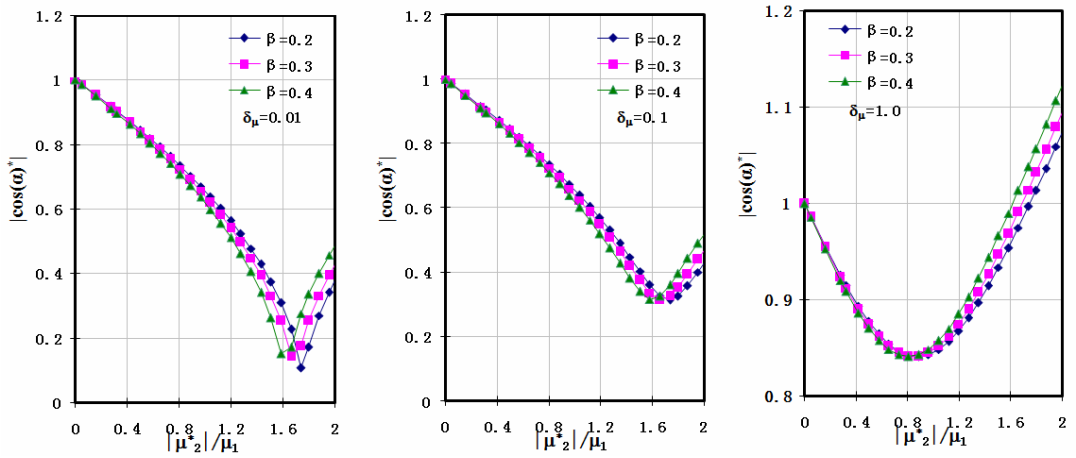

(a) (b) (c)

Figure 6-17 Variation of $|\cos(\boldsymbol{a})^*|$ with a change in the ratio of shear moduli, $\left|\mu_2^*\right|/\mu_1$ for 60 degree angle of incidence

6.5 Analysis of Results

The results presented in Figures 6-6 to 6-14 provide a basis for interpreting the experimental results. With increasing shear modulus of hydrating mortar, the r is expected to show an initial decrease, reach a minimum, and then start to increase. The exact variation in r with time in the cementitious mixtures would depend upon the variations in μ_2, δ_μ and β with time. The experimental trends are in agreement with the theoretical predictions, where the minimum values of r are attained earlier for larger angles of incidence. The fact that the reversal in r after an initial decrease was only

observed in mortar can also be explained considering that at any age the shear modulus of mortar is significantly higher than the shear modulus of cement paste. The shear modulus of cement paste is smaller than 10 GPa at one day. The ratio $\left|\mu_2^*\right|/\mu_1$, therefore, is smaller than the range 0.4, where the increase of the reflection is expected. Thus, the reversal in r for cement paste would occur at a later time than for mortar. The change in the shape of the wave observed in the time domain can also be explained by the change in phase of the wave expected at the minimum value of r.

Considering mortar to be a two-phase porous material, the poroelastic parameters can now be obtained from the measured reflection coefficients by the application of Biot's theory. In the 2-phase idealization, mortar is composed of a solid matrix with water filled, connected porosity. Any porosity at a scale smaller than the characteristic frequency is attributed to the solid skeleton. While the solid matrix is composed of sand, unhydrated cement and products of hydration, it is treated as homogeneous. With age, while the volume of sand inside the solid is fixed, the composition of the cementitious part of the matrix varies with hydration. Any disconnected porosity produced by hydration is included in the solid matrix and does not influence the measured porosity.

The general inversion procedure was similar to the procedure used previously for cement paste mixture. Changes in the amplitude of the incident SH wave depend upon three key internal variables of the poro-elastic medium (Equation (6-6)), which are functions of age (time after mixing). Since obtaining analytical expressions for the inversion of the internal variables from the expression for R_s is intractable, numerical

inversion was performed to optimize the material constants such that the theoretical prediction is close to the experimental response. The experimental data used in the optimization consists of the *r(1)* at three different angles of incidence. The generalized reduced gradient nonlinear optimization scheme was used to minimize an objective function given as

$$\mathrm{Fun}(c_i) = \sqrt{\frac{\sum_{n=1}^{3}\left(\left|r(1)\right|_{\theta_n} - \left|R_s(\theta_n, c_i)\right|\right)^2}{3}} \tag{6-7}$$

where θ_n is the discrete incident angle at which experimental values are obtained, and c_i are the internal system variables of the poroelastic solid.

At any given age, the values of the poroelastic parameters were obtained using an iterative procedure since $\cos(\boldsymbol{a})^*$ depends on the values of the parameters extracted from the optimization process. At each age, $\cos(\boldsymbol{a})^*$ was initially evaluated using the values of the poroelastic parameters obtained at the previous age. The poroelastic parameters were obtained by minimizing the objective function. $\cos(\boldsymbol{a})^*$ was then recalculated using the new values of the parameters and used for determining a new set of poroelastic parameters. This iteration procedure was performed until the $\cos(\boldsymbol{a})^*$ obtained from the values converged.

The starting guess of porosity for the first measurement after mixing was obtained using the relation

$$\beta_o = \frac{\rho_c\left(w/c\right)}{1 + \rho_c\left(w/c\right) + \rho_c/\rho_{sand}\left(s/c\right)} \tag{6-8}$$

where $\left(s/c\right)$ is the sand to cement weight ratio, ρ_c, the specific gravity of cement, was assumed to be 3.2 and ρ_{sand} the specific gravity of sand was taken equal to 2.6. The density of the mortar was assumed to be constant during hydration. The value ρ_2 was taken equal to the density of the mortar mixture, which was estimated as

$$\rho_2 = \frac{\rho_c(1 + w/c + s/c)}{1 + \rho_c(w/c) + (\rho_c / \rho_{sand})(s/c)} \tag{6-9}$$

The pore size parameter, a_p was taken to be 1/6 of the average cement grain size, which is equal to 2.5 μm. The initial value of permeability, κ_o was estimated using an expression obtained from the application of the general effective medium theory [Cui and Cahyadi 2001]

$$\kappa_o = \frac{l_c^2(1.8)(\beta_o - \beta_c)^2}{226} \tag{6-10}$$

where β_c is a constant equal to 0.18 and l_c, the critical pore diameter was assumed to be equal to a_p. The starting guess for μ_2 was taken as 10^6 Pa. The range for δ_μ was initially prescribed to be within 0.01 – 0.4. It was found that within the prescribed range, there was an insignificant influence of δ_μ on the final values of δ_μ and β. The solution obtained at a given time was used as the starting guess for the next time.

The shear modulus and porosity of the mortar samples obtained from the poroelastic inversion are shown in Figure 6-18 (a) and (b), respectively. μ_2 is the drain shear modulus of solid skeleton. Similar trends in the changes in modulus and porosity for all the mixtures can be observed. The evolution of shear modulus exhibits a very rapid increase of up to 3 orders of magnitude in the first 18 - 24 hours. This is followed

by a more gradual rate of increase. The values of μ_2 obtained from mortar are higher than the corresponding values obtained from cement paste with identical w/c ratios. The mortar samples exhibit a faster rate of increase and therefore higher values of μ_2 after the initial period of rapid increase. These results are in agreement with the results obtained from the vibration measurements. From Figure 6-19, the changes in porosity are clearly distinct for all the mortars and cement paste. Both mortar and cement paste exhibit a continuous decrease in porosity with age, the trends are nominally similar. At any age, the porosity of mortar samples is however significantly smaller than the porosity of cement paste with the same w/c ratio. Further, the porosities obtained for the mortar mixtures also exhibit a dependence on the s/c ratio; higher s/c ratio gives a smaller porosity at any age.

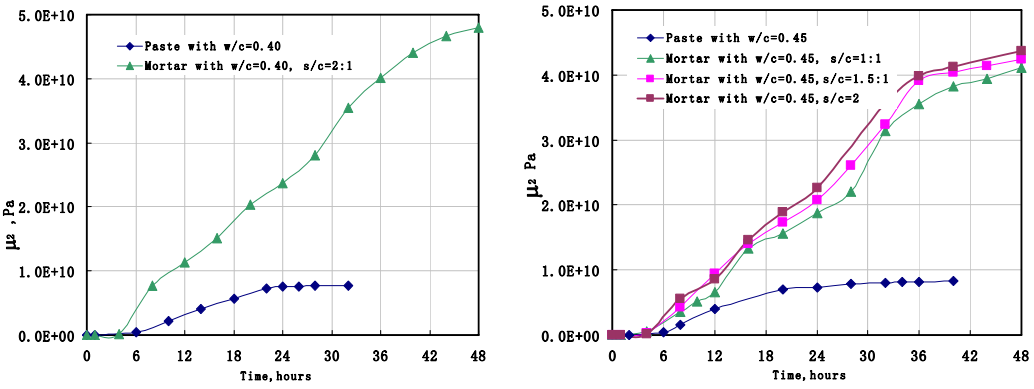

(a) (b)

Figure 6-18 Shear modulus evolution in mortar mixtures I, II, III and IV and in control cement paste mixtures.

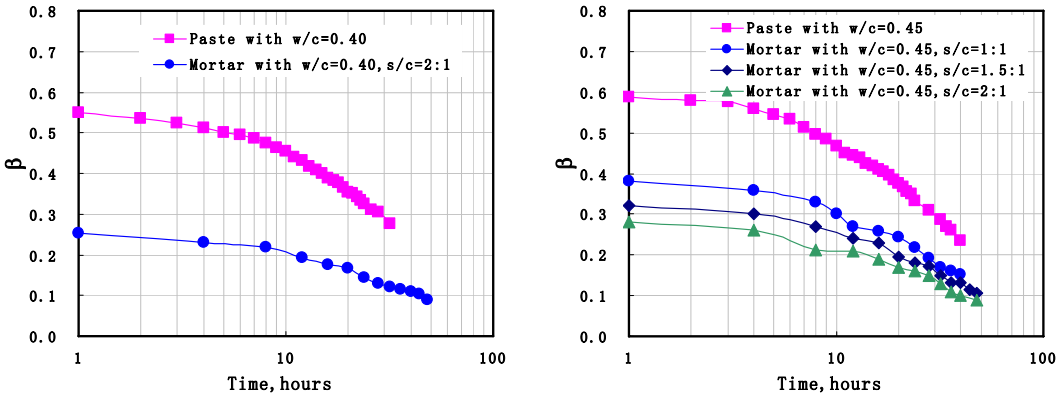

(a) (b)

Figure 6-19 Porosity evolution in mortar mixtures I,II,III and IV and in control cement paste mixtures.

6.6 Discussion

The porosity obtained from the poro-elastic inversion refers to the volume occupied by connected water-filled pore space inside a unit volume of mortar. This is different from the porosity in cement paste, where the porosity is the water-filled connected capillary pore space within a matrix of cement gel and unhydrated cement. For a given w/c ratio, a comparison between mortar and cement paste can be made if the volume of cement paste (cement paste content) in the two materials is considered to be the same. This is illustrated in Figure 6-20, which shows the initial volumetric proportions of cement paste and mortar with the same w/c ratio. The total volume used for volumetric calculations in mortar, then, is larger than 1. With this representation, the volumetric proportions obtained by Powers derived in Hansen [Hansen 1986] can be used for changes in mortar with hydration referred to a unit volume of cement paste.

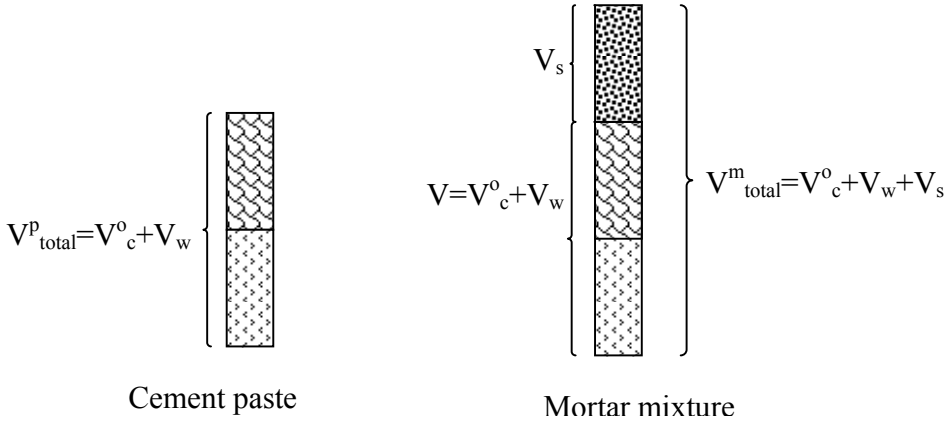

Figure 6-20 Schematic of initial volumes of individual components in cement paste and mortar

Considering the initial volumetric proportions, for paste containing c grams of unhydrated cement, the total volume is given as

$$\boldsymbol{V}^{\boldsymbol{p}}_{\boldsymbol{total}} = \boldsymbol{V}^{0}_{\boldsymbol{c}} + \boldsymbol{V}_{\boldsymbol{w}} = 1.0 \tag{6-11}$$

where $\boldsymbol{V}^{0}_{\boldsymbol{c}}$ = initial volume of c grams of cement, in cm^3

$\boldsymbol{V}_{\boldsymbol{w}}$ = initial of water in a given w/c paste, in cm^3

For a given w/c ratio, the original volume of mortar containing c grams of unhydrated cement is given as

$$\boldsymbol{V}^{\boldsymbol{m}}_{\boldsymbol{total}} = \boldsymbol{V}^{0}_{\boldsymbol{c}} + \boldsymbol{V}_{\boldsymbol{w}} + \boldsymbol{V}_{\boldsymbol{s}} > 1.0 \tag{6-12}$$

where V_s is the volume of sand

$$V_s = V_c^0(\rho_c / \rho_{sand})(s/c) \tag{6-13}$$

The total volume of hydrating cement paste can be expressed as a sum of the volumes of the individual components as shown:

$$\boldsymbol{V}^{\boldsymbol{p}}_{\boldsymbol{total}} = \boldsymbol{V}_{\boldsymbol{c}} + \boldsymbol{V}_{\boldsymbol{gs}} + \boldsymbol{V}_{\boldsymbol{gw}} + \boldsymbol{V}_{\boldsymbol{cw}} + \boldsymbol{V}_{\boldsymbol{cs}} \tag{6-14}$$

where

V_c = Volume of unhydrated cement in a hydrating paste, in cm^3

V_{gs} = Volume of gel solid in a hydrating paste, in cm^3

V_{gw} = Volume of gel water in a hydrating paste, in cm^3

V_{cw} = Volume of capillary water in a hydrating paste, in cm^3

V_{cs} = Volume introduced by chemical shrinkage, in cm^3

In hydrating cement paste, the volumetric proportions of unhydrated cement, gel solids and capillary pore space change as a function of the degree of hydration (m). The volumetric relations in hydrating cement paste were presented by Hansen (1986) based on the initial work of Powers and are shown in Appendix B. The capillary porosity, and gel porosity which are defined as the volume of capillary and gel water, respectively in a unit volume of cement paste can be obtained as functions of the degree of hydration as

$$\frac{V_{cs}}{V_{total}^{p}} = \frac{(1-m)V_c^0 + V_w}{V_c^0 + V_w} - \frac{V_{gw}}{V_{total}} - \frac{V_{cw}}{V_{total}} - \frac{V_{gs}}{V_{total}} = \beta_p \tag{6-15}$$

$$\frac{V_{gw}}{V_{total}^{p}} = \frac{\lambda_e k_e \frac{w_{nw}}{\rho_{gw}}}{\frac{c}{\rho_c} + \frac{w}{\rho_w}} = \frac{\lambda_e k_e m \frac{w_{nw}^{\infty}}{c}}{\frac{w}{c} + \frac{\rho_w}{\rho_c}} \tag{6-16}$$

Similarly the volume fraction of the gel solids as a function of the degree of hydration is given as

$$\frac{V_{gs}}{V_{total}^{p}} = \frac{m\dfrac{c}{\rho_c} + \dfrac{w_{nw}}{\rho_{nw}}}{V_c^0 + V_w} = \frac{m[1 + \dfrac{\rho_c}{\rho_{nw}} \cdot \dfrac{w_{nw}^{\infty}}{c}]}{1 + \dfrac{w}{m} \cdot \dfrac{\rho_c}{\rho_w}} \tag{6-17}$$

The degree of hydration in hydrating cement paste determined as

$$m = \frac{c_h}{c} = \frac{w_{nw}}{w_{nw}^{\infty}} \tag{6-18}$$

where

$\boldsymbol{w_{nw}}$ = Weight of non-evaporable water, in g.

$\boldsymbol{w_{nw}^{\infty}}$ = Weight of non-evaporable water in a completely hydrated cement paste, in g.

The volumetric proportions in hydrating cement paste as a function of degree of hydration is illustrated in Figure 6-21 for cement paste with w/c = 0.45. In generating the figure values of ρ_c , ρ_{sand}, $\boldsymbol{w_{nw}}$, λ, κ and $\boldsymbol{w_{nw}^{\infty}/c}$ were taken equal to 3.2, 2.6 , 1.33, 3.3, 0.25 and 0.23 respectively [Hansen 1986].

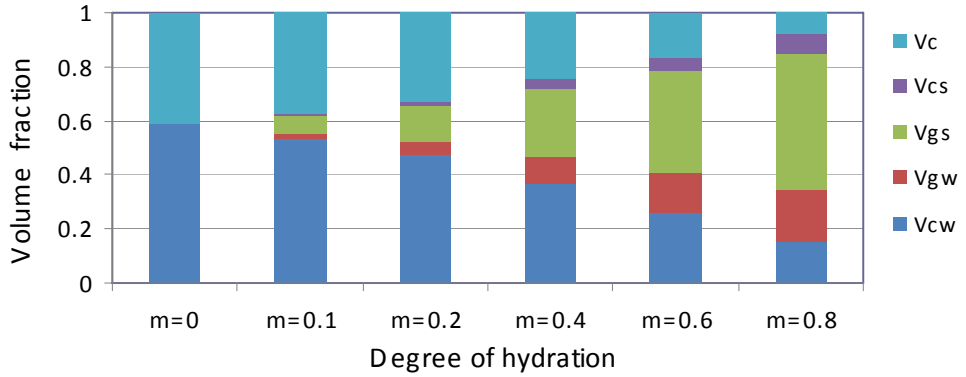

Figure 6-21 Illustration of Powers' model for cement hydration for cement paste with w/c=0.45 at the indicated degrees of hydration

The volume proportions of the individual components derived based on Power's law for cement hydration can be applied to a unit volume of cement paste within mortar and the volumetric proportions relative to the total volume of mortar can now be derived. If for a given w/c ratio, the initial paste content in cement paste and mortar is kept the same, then changes within hydrating cement in both can be related to the degree of hydration of cement. Since sand contributes to the total volume, the volumetric proportions relative to the total volume of mortar would however be different. The volume fraction of capillary pores in mortar is the ratio of capillary water volume to the total volume of mortar. The porosity of mortar then can be identified with the volume fraction of capillary pores and obtained from the capillary porosity of cement paste as

$$\beta_m = \beta_p (\boldsymbol{V}_{total}^{p} / \boldsymbol{V}_{total}^{m}) \tag{6-19}$$

where β_m represents the porosity of mortar mixture and β_p represents the porosity of cement paste.

The volumetric proportions in mortar derived from an application of Power's model is illustrated in Figure 6-22 for the case of mortar with w/c=0.45 and s/c=1. In Figure 6-23, the changes in the volumetric proportions with the degree of hydration are identical to the volumetric proportions shown in Figure 6-21. The volume fractions of the different components normalized to a unit volume of mortar are plotted in Figure 6-23. It can be seen that, relative to the total volume of mortar the volumetric fractions for a given degree of hydration are different from those of cement paste with identical w/c ratio. For a given degree of hydration, the volume

fractions relative to the total volume of mortar would depend upon the volume of sand in the mixture.

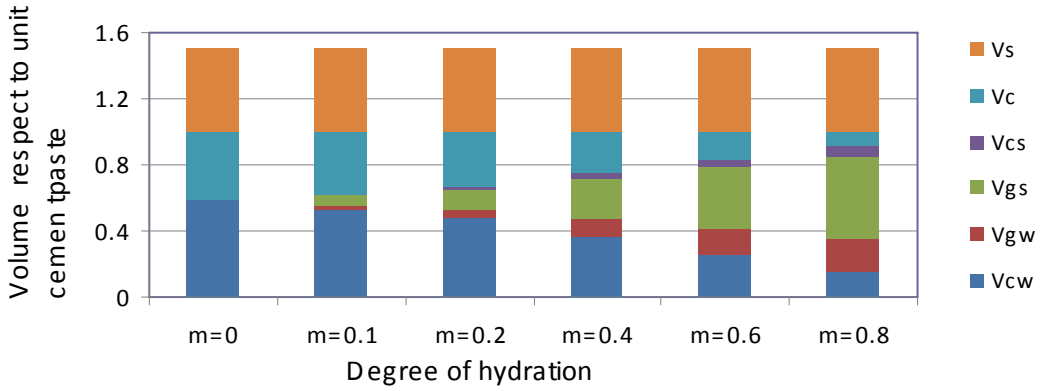

Figure 6-22 Illustration of Powers' model for cement hydration in mortar with w/c=0.45 and s/c=1:1 at the indicated degrees of hydration

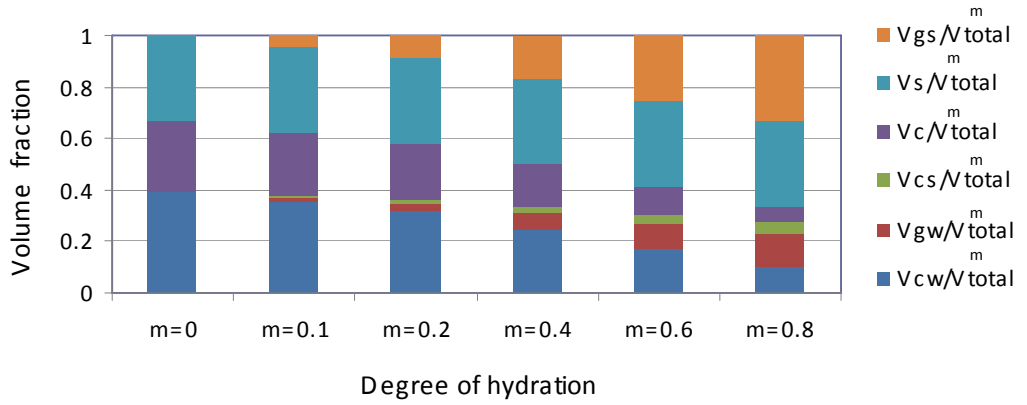

Figure 6-23 Volume fractions in mortar with w/c=0.45 and s/c=1:1 at the indicated degrees of hydration

Porosity is defined as the fraction of capillary water in the total volume of the mixture. Therefore for a mortar mixture (treated as a composite composed of sand and cement paste), the total porosity is obtained as the fraction of capillary water to total mortar volume. The content of capillary water in a unit volume of cement paste within mortar calculated using Equation (6-19) for the different mortar mixtures are

shown in Figure 6-23. The porosity of mortar was taken equal to the value obtained from the poroelastic inversion. It can be seen that the porosity derived as the fraction of capillary water within the cement paste fraction of a mortar is independent of the s/c ratio and only depends on the w/c ratio. Further, the close agreement between the capillary water content in mortar and cement paste validates the results of the poroinversion. The results indicate that the two-phase idealization applied to mortar results in porosity which is identical to the capillary water content in cement paste of a given w/c ratio.

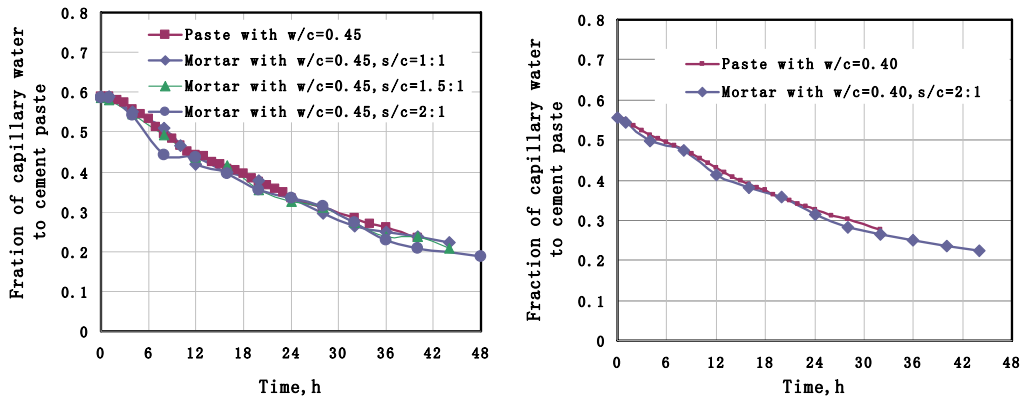

(a) (b)

Figure 6-24 Comparison of fraction of capillary water in cement paste and mortar mixtures

The influence of porosity on the compressive strength of mortar is shown in Figure 6-25. It can be seen that the relationship between the capillary porosity and the compressive strength is independent of the w/c and s/c ratios. This result is in agreement with the earlier finding from cement paste and it suggests that in hydrating mortar the strength gain is controlled by the decrease in capillary porosity within the cement paste part of the mortar. While the relationship between the direct measured

variable, the reflection factor (r) and the compressive strength is not unique for the different w/c ratios, there is a unique relationship between the microstructural variable, porosity derived from the reflection measurement and the compressive strength. It should be noted that the exact relationship between the capillary porosity and compressive strength will depend upon the exact composition of the cementitious material in the mix. However, the results presented in Figure 6-25 suggest that for a given type of cementitious material, if the relationship between capillary porosity is established, then microstructure based tools for predicting strength gain in hydrating cement based materials can be developed.

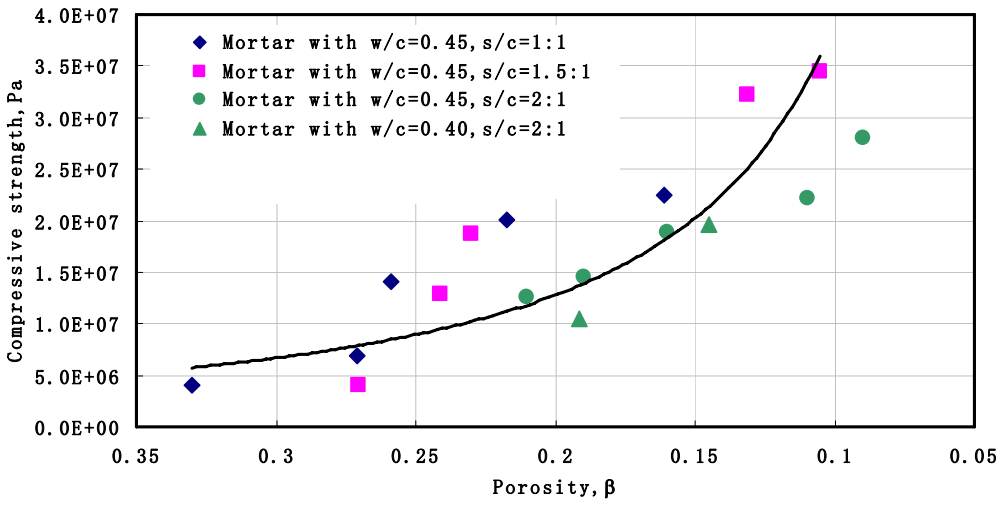

Figure 6-25 Relation between porosity and compressive strength of mortar mixtures

6.7 Conclusions

Based on the work presented in this chapter the following conclusions can be drawn

1）Poroelastic idealization for analyzing the microstructural evolution of cement paste mixture is suitable to analyze the microstructure evolution of mortar mixture. Mortar can be idealized as a two phase composite material consisting of a solid matrix with water filled porosity. The solid matrix is composed of sand, unhydrated cement and products of cement hydration. The sand is an inert filler and evolution of properties of mortar are only influenced by changes in the cement paste component of the mixture.

2) The trends in reflection coefficients for mortar measurements are significantly different from the changes in the reflection coefficient obtained from plain cement paste. There is a more rapid change in the reflection coefficient, which corresponds with a a more rapid increase in the modulus of mortar than the corresponding increase in the modulus of plain cement paste with identical w/c ratio.

3) Porosity of mortar obtained from the poroelastic inversion when referred to the volume of cement paste within mortar is comparable to the capillary obtained directly from plain cement paste with identical w/c ratio. The porosity of mortar obtained from the capillary water content within the cement paste part of mortar, which is obtained using Power's model, compares favorably with the porosity of the two-phase poroelastic material obtained from the ultrasonic reflection measurements.

Chapter 7 Conclusions and Future Work

7.1 Conclusions

A one-sided ultrasonic reflection technique which allows for sensitively detecting the distinct stages in the development of internal structure of hydrating cementitious matrix was developed. The application of the poroelastic theory proposed by Biot to develop a two-phase representation for was explored hydrating cement paste and mortar. The theoretical framework necessary to interpret the results of the ultrasonic technique and to provide information about the microstructure in terms of physically-based variables within the poroelastic theory was developed. The key findings of this study are:

1) The porosity obtained from an application of poro-elastic framework to interpret the ultrasonic wave information provides a measure of capillary porosity in the hydrating cementitious matrix. The ultrasonic reflection method therefore allows for a direct assessment of the early age development of microstructure in the cementitious materials.
2) The evolutions of shear modulus obtained from the application of poro-elastic framework are consistent to the development of shear modulus of hydrating cement paste and mortar composites respectively. The consistence indicates the macro-properties of hydrating cementitious materials relate to the microstructural properties in a significant way.

3) The relations between the porosity and compressive strength developed through experimental techniques and poro-elasticity framework provide a understanding of effects of evolution of porosity to the development of compressive strength for hydrating cement paste and mortar. The developed laboratory-based experimental system allows for a prediction of compressive strength in cementitious materials

7.2 Future work

The developed test system and theoretical framework can be extended in the future to understand the microstructure of cementitious material and the relations between the microstructure and mechanical properties of materials. Specifically

1) The effects of the additives on the microstructure and mechanical properties of cementitious materials can be investigated using the test technique and theoretical framework developed here.
2) The work can be extended for developing a test technique, which is suitable for investigation of concrete. The experimental setup and data acquisition system need to be improved to consider the wave propagation characteristic through large size scale of aggregates. The effective two phase poroelasicity idealization needs to be evaluated when applied to concrete, considering the effects of the aggregates which could have different size scales.
3) The relation between the microstructure and mechanical properties of early age concrete need to be developed. Explicit relations between the microstructure and mechanical properties of cementitious material need to be

established. Finally, an in situ test system, which allows predicting material property development in concrete structures, based on an assessment of physically-based internal variables can potentially be developed.

Appendix A

a. Wave Propagation in Poro-elastic medium

Wave propagation through the porous medium is predicted by a pair of coupled displacement equations of motion governing both rotational and dilatational motions, obtained by combining the Biot's constitutive relationship and Darcy's law for flow through a porous medium [Biot 1962]

$$\mu_b \nabla^2 \vec{\boldsymbol{u}} + (\boldsymbol{H} - 2\mu_b)\nabla(\nabla \cdot \vec{\boldsymbol{u}}) - \boldsymbol{C}\nabla(\nabla \cdot \vec{\boldsymbol{w}}) = \rho_b \ddot{\vec{\boldsymbol{u}}} - \rho_f \ddot{\vec{\boldsymbol{w}}} \tag{A1a}$$

$$\boldsymbol{C}\nabla(\nabla \cdot \vec{\boldsymbol{u}}) - \boldsymbol{M}\nabla(\nabla \cdot \vec{\boldsymbol{w}}) = \rho_f \ddot{\vec{\boldsymbol{u}}} - \boldsymbol{m}' \ddot{\vec{\boldsymbol{w}}} - \boldsymbol{F}_v \eta / \boldsymbol{\kappa}\, \dot{\boldsymbol{w}} \tag{A1b}$$

where $\vec{u} = \vec{u}(x,t)$ and $\vec{U} = \vec{U}(x,t)$ denote the average displacement of solid skeletal frame and the fluid, respectively, $\vec{\boldsymbol{w}}(\boldsymbol{x},\boldsymbol{t}) = \beta(\vec{\boldsymbol{u}} - \vec{\boldsymbol{U}})$ is the relative displacement of fluid and skeletal frame, ρ_b and ρ_f are bulk density of porous media and density of fluid respectively, κ is the coefficient of intrinsic permeability of the porous frame, $\boldsymbol{m}' = \boldsymbol{c}_T \rho_f / \beta$, $\boldsymbol{c}_T$ is the tortuosity coefficient (dimensionless parameter), which is a experimentally determined, β is the porosity of porous media, $\boldsymbol{F}_v(\omega, \boldsymbol{a}_p, \eta)$ is a frequency correction function for the viscosity introduced by Biot which is considered as a complex function of the pore diameter $\boldsymbol{a}_p$, angular frequency ω and fluid viscosity η [Biot 1956 a and b], to represent that the friction force of fluid resulting from out-of-phase, rate of flow relative to the solid. In Equation(s) (A1) μ_b is the bulk shear modulus of the solid frame, H , C and

M represent Biot's poro-elastic constants, which characterize the response of the composite [Stoll and Kan 1981] given as

$$\boldsymbol{H} = \frac{(\boldsymbol{K}_s - \boldsymbol{K}_b)^2}{\boldsymbol{D}_e - \boldsymbol{K}_b} + \boldsymbol{K}_b + \frac{4\mu_b}{3} \tag{A2a}$$

$$\boldsymbol{M} = \frac{\boldsymbol{K}_s^{\,2}}{\boldsymbol{D}_e - \boldsymbol{K}_b} \tag{A2b}$$

$$\boldsymbol{C} = \frac{\boldsymbol{K}_s(\boldsymbol{K}_s - \boldsymbol{K}_b)}{\boldsymbol{D}_e - \boldsymbol{K}_b} \tag{A2c}$$

where $\boldsymbol{K}_b$ is the bulk modulus of the skeletal frame (under drained conditions), $\boldsymbol{D}_e = \boldsymbol{K}_s(1+\beta\frac{\boldsymbol{K}_s}{\boldsymbol{K}_f - 1})$, $\mathrm{K_s}$ is the bulk modulus of the material of the skeletal frame and $\boldsymbol{K}_f$ is the bulk modulus of the pore fluid. When Equations (A1) transfer to the frequency domain, the poroelastic constants result in a complex constants $\boldsymbol{H}^*, \boldsymbol{M}^*, \boldsymbol{C}^*, \boldsymbol{K}_b^*, \mu_b^*$, and $\boldsymbol{K}_b^* = \boldsymbol{K}_b(1+\delta_k \boldsymbol{j})$, $\mu_b^* = \mu_b(1+\delta_\mu \boldsymbol{j})$. Here δ_k and δ_μ are the corresponding loss factors and $\boldsymbol{j} = \sqrt{-1}$.

To solve the Equations (A1), it is convenient to express the displacement vectors in terms of scalar and vector potentials

$$\vec{u} = \nabla\phi_s + \nabla\times\vec{\varphi}_s \quad \text{and} \quad \vec{w} = \nabla\phi_f + \nabla\times\vec{\varphi}_f \tag{A3a and b}$$

By substituting Equation(s) A3 in Equation(s) A1, two pairs of equations are obtained in terms of potentials

$$\begin{cases} \boldsymbol{H}\nabla^2\phi_s - \boldsymbol{C}\nabla^2\phi_f = \rho_b\ddot{\phi}_s - \rho_f\ddot{\phi}_f \\ \boldsymbol{C}\nabla^2\phi_s - \boldsymbol{M}\nabla^2\phi_f = \rho_f\ddot{\phi}_s - \boldsymbol{m}'\ddot{\phi}_f - (\eta/\kappa)\dot{\phi}_f \end{cases} \tag{A4}$$

and

$$\begin{cases} \mu_b \nabla^2 \vec{\varphi}_s = \rho_b \ddot{\vec{\varphi}}_s - \rho_f \ddot{\vec{\varphi}}_f \\ (\eta/\kappa)\dot{\vec{\varphi}}_f = \rho_f \ddot{\vec{\varphi}}_s - \boldsymbol{m}' \ddot{\vec{\varphi}}_f \end{cases} \tag{A5}$$

Both Equations (A4) and (A5) admit the solutions of harmonic form. Equations (A4) govern the compression wave propagation, while the Equations (A5) determine the shear waves propagation. The wave propagation solutions for the shear wave could be written as

$$\begin{cases} \vec{\varphi}_s = \boldsymbol{A}\exp[\boldsymbol{j}(\omega \boldsymbol{t} - \vec{\boldsymbol{k}} \cdot \vec{\boldsymbol{r}})] \\ \vec{\varphi}_f = \boldsymbol{B}\exp[\boldsymbol{j}(\omega \boldsymbol{t} - \vec{\boldsymbol{k}} \cdot \vec{\boldsymbol{r}})] \end{cases} \tag{A6}$$

where $\vec{k}$ is a complex vector (complex wave number), $\vec{r}$ is the position vector and ω is the frequency of waves. The real part of $\vec{k}$ determines the direction of the normal to planes of equal phase, the imaginary part determines the directions of the normal to planes of equal amplitudes. When the solutions of forms given by Equation (A6) are substituted into Equation (A5), equations for obtaining the shear wave number can be obtained in Equation (A7).

$$(\rho_b \omega^2 - \mu_b^* \boldsymbol{k}_{sh}^{*2})(\boldsymbol{m}'\omega^2 - \boldsymbol{j}\omega \boldsymbol{F}_v \eta/\kappa) - (\rho_f \omega^2)^2 = 0 \tag{A7}$$

$\boldsymbol{k}_{sh}^*$ is the complex shear wave number in the porous medium, and $\boldsymbol{F}_v$ was derived as a complex quantity by Biot, considering three dimensional flow in a circular duct and is given as

$$\boldsymbol{F}_v(\xi) = \frac{1}{4}\frac{\xi \boldsymbol{T}(\xi)}{(1 - 2\boldsymbol{T}(\xi)/\boldsymbol{j}\xi)} \tag{A8a}$$

where

$$\boldsymbol{T}(\xi) = \frac{\boldsymbol{ber}'(\xi) + \boldsymbol{jbei}'(\xi)}{\boldsymbol{ber}(\xi) + \boldsymbol{jbei}(\xi)}, \tag{A8b}$$

$$\xi = (\omega \boldsymbol{a}_p^2 / \eta)^{1/2} \tag{A8c}$$

The functions $\boldsymbol{ber}(\xi)$ and $\boldsymbol{bei}(\xi)$ are the real and imaginary parts of the Kelvin function. The factor $\boldsymbol{a}_p$ represents the pore size.

The complex shear wave number is obtained from Equation (A7) in the following form

$$\boldsymbol{k}_{sh}^{*} = \sqrt{[\rho_b \omega^2 - \frac{(\rho_f \omega^2)^2}{\boldsymbol{m}' \omega^2 - \boldsymbol{j}\omega(\boldsymbol{F}_v \eta / \kappa)}] / \mu_b^*} \tag{A9}$$

b. Oblique SH wave reflection

SH wave incidence at an interface between an elastic and a poro-elastic material is considered. Assuming an SH wave traveling in an elastic material is incident at an angle θ at the interface, shown in Figure A1, the potentials of the incident, reflected and refracted waves are given as

$$\varphi_i(x,z) = A_i \exp[j(\omega t - k_1 \cos(\theta) z - k_c x)] \tag{A10}$$

$$\varphi_r(x,z) = A_r \exp[j(\omega t + k_1 \cos(\theta) z - k_c x)] \tag{A11}$$

$$\varphi_{ts}(x,z) = A_{ts} \exp[j(\omega t - k_{sh}^{*} \cos(\alpha)^{*} z - k_c x)] \tag{A12}$$

$$\varphi_{tf}(x,z) = A_{tf} \exp[j(\omega t - k_{sh}^{*} \cos(\alpha)^{*} z - k_c x)] \tag{A13}$$

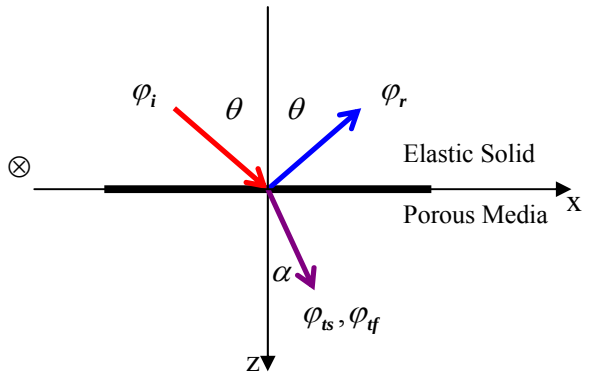

Figure A1 Reflection and refraction at the interface with oblique SH incidence

As the specified characteristics of plane SH wave, no modes conversion would occur at the interface.

In developing the equations for the potentials, Snell law has been implicitly applied such that all the potentials which are generated at the interface give the same projection of the propagation vector on the interface.

$$k_{sh}^{*} \sin(\alpha)^{*} = k_1 \sin(\theta) = k_c \tag{A14}$$

c. Boundary Conditions

The boundary conditions at the interface, z=0, are given as

(1) For the continuity of displacement

$$u_y\big|_{ealstic} = u_y\big|_{porous} \quad \text{or} \quad \frac{\partial \varphi_i}{\partial z} + \frac{\partial \varphi_r}{\partial z} = \frac{\partial \varphi_{ts}}{\partial z} \tag{A15}$$

(2) For the equilibrium of tangential stress.

$$\tau_{yz}\big|_{ealstic} = \tau_{yz}\big|_{porous} \quad \text{or} \quad \mu_1 \left(\frac{\partial^2 \varphi_i}{\partial z^2} + \frac{\partial^2 \varphi_r}{\partial z^2}\right) = \mu_b^{*} \frac{\partial^2 \varphi_{ts}}{\partial z^2} \tag{A16}$$

(3) Continuity of fluid movement. It has the same boundary conditions with the previous case, and this conditions is satisfied automatically because of the characteristics of the SH wave mode.

d. Reflection Coefficients

The ratios of the amplitudes of the potentials can be obtained as

$$\frac{\boldsymbol{A_r}}{\boldsymbol{A_i}} = \frac{\mu_b^* \boldsymbol{k}_{sh}^* \cos(\alpha)^* - \mu_1 \boldsymbol{k}_1 \cos(\theta)}{\mu_b^* \boldsymbol{k}_{sh}^* \cos(\alpha)^* + \mu_1 \boldsymbol{k}_1 \cos(\theta)}, \tag{A17}$$

$$\frac{\boldsymbol{A_{ts}}}{\boldsymbol{A_i}} = \left(\frac{2\mu_1 \boldsymbol{k}_1 \cos(\theta)}{\mu_b^* \boldsymbol{k}_{sh}^* \cos(\alpha)^* + \mu_1 \boldsymbol{k}_1 \cos(\theta)}\right) \frac{\boldsymbol{k}_1 \cos(\theta)}{\boldsymbol{k}_{sh}^* \cos(\alpha)^*} \tag{A18}$$

$$\frac{\boldsymbol{A_{tf}}}{\boldsymbol{A_i}} = \left(\frac{2\mu_1 \boldsymbol{k}_1 \cos(\theta)}{\mu_b^* \boldsymbol{k}_{sh}^* \cos(\alpha)^* + \mu_1 \boldsymbol{k}_1 \cos(\theta)}\right) / \left(\frac{\boldsymbol{k}_{sh}^* \cos(\alpha)^*}{\boldsymbol{k}_1 \cos(\theta)} \frac{\rho_f \omega^2}{\rho\omega^2 - \mu_b^* (\boldsymbol{k}_{sh}^*)^2}\right) \tag{A19}$$

Appendix B

a. Degree of Cement Hydration

The degree of cement hydration is donated as m, which is defined as the weight fraction of original cement which has become hydrated.

$$m = \frac{c_h}{c} \tag{B1}$$

Where c_h = Weight of hydrated cement, in g

c = Weight of original cement, in g

For all cements it has

$$m = \frac{c_h}{c} = \frac{w_{nw}}{w_{nw}^{\infty}} \tag{B2}$$

Where w_{nw} = weight of non-evaporable water, in g.

w_{nw}^{∞} = weight of non-evaporable water in a completely hydrated cement paste, in g.

b. Fractional Volume of Gel Solid

$$V_{gs} = mV_c^0 + V_{nw} \tag{B3}$$

Where V_{nw} = Volume of non-evaporable water, in cm^3.

By introducing the density of cement, ρ_c and the density of non-evaporable water, ρ_{nw}, so $V_c^0 = \frac{c}{\rho_c}$ and $V_{nw} = \frac{w_{nw}}{\rho_{nw}}$

Then

$$V_{gs} = m\frac{c}{\rho_c} + \frac{w_{nw}}{\rho_{nw}} \tag{B4}$$

The fraction of volume of gel solid

$$\frac{V_{gs}}{V_{total}^{p}} = \frac{m\frac{c}{\rho_c} + \frac{w_{nw}}{\rho_{nw}}}{V_c^0 + V_w} = \frac{m[1 + \frac{\rho_c}{\rho_{nw}} \cdot \frac{w_{nw}^{\infty}}{c}]}{1 + \frac{w}{m} \cdot \frac{\rho_c}{\rho_w}} \tag{B5}$$

Where ρ_w = density of water, in g/cm^3.

w = Weight of original water, in g.

c. Fractional Volume of Gel Water

$$\frac{V_{gw}}{V_{total}^{p}} = \frac{\frac{w_{gw}}{\rho_{gw}}}{V_c^0 + V_w} = \frac{\frac{w_{gw}}{\rho_{nw}}}{\frac{c}{\rho_c} + \frac{w}{\rho_w}} \tag{B6}$$

Here $\rho_w = \rho_{gw}$, density of gel water , in g/cm^3 , here the value is 1 g/cm^3

And also $w_{gw} = \lambda_e k_e w_{nw}$

Where λ_e and k_e are experimentally determined constants.

So Equation (B6) can be rewritten as

$$\frac{V_{gw}}{V_{total}^{p}} = \frac{\lambda_e k_e \frac{w_{nw}}{\rho_{gw}}}{\frac{c}{\rho_c} + \frac{w}{\rho_w}} = \frac{\lambda_e k_e m \frac{w_{nw}^{\infty}}{c}}{\frac{w}{c} + \frac{\rho_w}{\rho_c}} \tag{B7}$$

d. Fractional Volume of Capillary Water

$$\frac{V_{cw}}{V_{total}^{p}} = \frac{V_w - V_{gw} - V_{nw}}{V_c^0 + V_w} = \frac{\frac{w}{\rho_w} - \frac{w_{gw}}{\rho_w} - \frac{w_{nw}}{\rho_w}}{\frac{c}{\rho_c} + \frac{w}{\rho_w}} \tag{B8}$$

Combining $w_{gw} = \lambda_e k_e w_{nw}$

$$\frac{V_{cw}}{V_{total}^{p}} = \frac{\frac{w}{\rho_w} - \lambda_e k_e \frac{w_{nw}}{\rho_w} - \frac{w_{nw}}{\rho_w}}{\frac{c}{\rho_c} + \frac{w}{\rho_w}} = \frac{\frac{w}{c} - (\lambda_e k_e + \frac{\rho_w}{\rho_{nw}})\frac{w_{nw}}{c}}{\frac{w}{c} + \frac{\rho_w}{\rho_c}} \tag{B9}$$

Using Equation (B2)

$$\frac{V_{cw}}{V_{total}^{p}} = \frac{\frac{w}{c} - (\lambda_e k_e + \frac{\rho_w}{\rho_{nw}})m\frac{w_{nw}^{\infty}}{c}}{\frac{w}{c} + \frac{\rho_w}{\rho_c}} \tag{B10}$$

e. Chemical Shrinkage

From Equation 14 in Chapter 6

$$V_{cs} = V_{total}^{p} - V_c - V_{gs} - V_{gw} - V_{cw} \tag{B11}$$

Using (B5) (B7) (B10)

$$\frac{V_{cs}}{V_{total}^{p}} = \frac{(1-m)V_c^0 + V_w}{V_c^0 + V_w} - \frac{V_{gw}}{V_{total}} - \frac{V_{cw}}{V_{total}} - \frac{V_{gs}}{V_{total}} \tag{B12}$$

Bibliography

Achenbach, J.,(1973) *Wave Propagation in Elastic Solids*, North-Holland Publishing Company, Amsterdam; American Elsevier, New York.

Achenbach, J.D., Komsky, I.N., Lee, Y.C. and Angel, Y.C., (1992) *Self-calibrating ultrasonic technique for crack depth measurement*, Journal of Nondestructive Evaluation, 11: 103-108.

Allen, A.J., Windsor, C.G., Rainey, V., Pearson, D., Double, D.D., (1982) Phys. D: *Applied Physics*, Vol. 15, 1817-1833.

Allen, A.J., Oberthur, R.C., Pearson, D., Schoefield, P., Wilding, C.R., (1987), Phil. Mag. B, Vol. 56, 263-288

ASTM C 305 (2001) "*Annual book of ASTM Standards*," American Society for Testing Materials, West Conshohocken, PA

ASTM C 191, (2001) "*Annual book of ASTM Standards*," American Socienty for Testing Materials, West Conshohocken, PA

Akkaya, Y., Voigt, T., Subramaniam, K.V., Shah, S.P.,(2003) *Nondestructive Measurement of Concrete Strength by an Ultrasonic Wave Reflection Method*, Materials and Structures Journal, RILEM, Vol. 36, No.262

Albert, D.G.,(1993) *A Comparison between Wave-Propagation in Water-Saturated and Air-Saturated Porous Materials.* Journal of Applied Physics, **73**(1): pp. 28-36.

Alig, I., Lellinger, D.,Sulimma, J. and Tadjbakhsch, S. (1997). *Ultrasonic shear wave reflection method for measurements of the viscoelastic properties of polymer films*, Review of Scientific Instruments 68: 1536.

Bartlett, F. M.; MacGregor, J. G., (1999) Variation *of in-place concrete strength in structures*, ACI Materials Journal, v. 96 no2, pp. 261-70

Bazant, Z.P., ed., (1988) *Mathematical Modeling of Creep and Shrinkage of Concrete,* John Wiley and Sons, Chichester, NY.

Bazant, Z.P., and Baweja, S., (1995) *Creep and Shrinkage Prediction Model for Analysis and Design of Concrete Structures – Model B3*," Materials and Structures, Vol. 28, pp. 357-365.

Bentz DP, Garboczi EJ., (1991) *Percolation of Phases in a Three-Dimensional Cement Paste Microstructural Model*, Cement Concrete Res. v21: pp. 325-344.

Bentz, D.P., Garboczi, E.J., Haeckerb C.J., and Jensen O.M., (1999) *Effects of cement particle size distribution on performance properties of Portland cement-based materials*, Cement and Concrete Research, Volume 29, No.10, pp. 1663-1671.

Bentz D.P., and Stutzman, P.E., (2006) *Curing, Hydration, and Microstructure of Cement Paste*, ACI Materials Journal, **103**(5): pp. 348-356.

Bernard, O., Ulm, F.J., and Lemarchand, E., (2003) *A multiscale micromechanics-hydration model for the early-age elastic properties of cement-based materials.* Cement and Concrete Research, **33**(9): pp. 1293-1309.

Berryman, J. , (1980) *Confirmation of Biot theory*, Applied Physics Letters, Vol. 37, pp. 382.

Biot, M. ,(1956a) *Theory of Propagation of Elastic Waves in a Fluid-Saturated Porous Solid. I. Low-Frequency Range*, The Journal of the Acoustical Society of America, Vol. 28, pp. 168.

Biot, M. ,(1956b), *Theory of Propagation of Elastic Waves in a Fluid-Saturated Porous Solid. II. Higher Frequency Range*, The Journal of the Acoustical Society of America, Vol. 28, pp. 179.

Biot, M., (1962) *Mechanics of Deformation and Acoustic Propagation in Porous Media*, Journal of Applied Physics, Vol. 33, pp. 1482.

Boumiz A, Sorrentino D, Vernet C, Cohen Tenoudji F. ,(2000) *Modelling the Development of the Elastic Moduli as a Function of the Hydration Degree of Cement Pastes and Mortars*, In Nonat A, editor. Proceedings 2nd International RILEM Symposium, Hydration and Setting, RILEM, Cachan Cedex, France, pp. 295-316.

Bourbie, T., Coussy, O., Zinszer, B., (1987) *Acoustics of Porous Media*, Gulf Publishing Company, Houston, TX.

Brown, P.W., (1989) *Effects of Particle Size Distribution on the Kinetics of Hydration of Tricalcium Silicate*, Journal of American Ceramic Society, Vol. 72, No. 10.

Chotiros, N.P.,(2002) *An inversion for Biot parameters in water-saturated sand.* Journal of the Acoustical Society of America, **112**(5): pp. 1853-1868.

Chotiros, N.P.,(1995) *Biot model of sound propagation in water-saturated sand.* The Journal of the Acoustical Society of America, **97**: pp. 199.

Chotard, T.J., Boncoeur-Martel, M.P., Smith, A., Dupuy G.P. and Gault, C., (2003) *Application of X-ray computed tomography to characterise the early hydration of calcium aluminate cement,* Cement and Concrete Composites, **25**(1): pp. 145-152.

Christensen, B. J., Coverdale, T.,Olson, R. A.,Ford, S. J.,Garboczi, E. J.,Jennings, H. M. and Mason, T. O., (1994)*Impedance Spectroscopy of Hydrating Cement-Based Materials: Measurement, Interpretation, and Application*, Journal of the American Ceramic Society 77(11): pp.2789-2804.

Christensen BJ, Mason TO, Jennings HM,(1996) *Comparison of Measured and Calculated Permeabilities for Hardened Cement Paste*. Cement Concrete Res, 26(9): pp.1325-1334.

Copeland and Shulz, (1962) *Electron Optical Investigation of the Hydration Products of Calcium Silicates and Portland Cement*, Journal of PCA Research and Development Laboratories, Vol. 4, No. 1, pp. 2.

Cook, R. A., Hover, K. C., (1993) *Mercury porosimetry of cement-based materials and associated correction factors*, ACI Materials Journal, v. 90, pp. 152-161

Coussy O., (2004) Poromechanics, West Sussex, England: Wiley, 2004.

Cui L, Cahyadi JH.(2001) *Permeability and Pore Structure of OPC Paste,* Cement Concrete Res 2001; 31: pp.277-282.

Daimon, Ueda and Kondo, (1971) *Morphological Studies on Hydration of Tricalcium Silicate*, Cement and Concrete Research, Vol. 1, pp. 391.

D'Angelo, R., Plona, T, Schwartz, L., and Coveney, P., (1995), *Ultrasonic measurements on hydrating cement slurries: The onset of shear wave propagation*, Adv Cem-Based Materilas, Vol. 2, No. 1, pp. 8-14.

Day, R. L.; Haque, M. N., (1993) *Correlation between strength of small and standard concrete cylinders*, ACI Materials Journal, v. 90, pp. 452-462.

Deresiewicz, H.a.S., R., (1963) *On Uniqueness in Dynamic Poroelasticity.* Bull. Seismol. Soc. Am., **53**: pp. 783-789.

Diamond, S., Bonen, D., (1993) *Microstructure of hardened cement paste--a new interpretation*, Journal of the American Ceramic Society, v. 76, pp. 2993-2999/.

Domone, P.L., (2003), *Fresh Concrete*, Advanced Concrete Technology 2, Concrete Properties Vol. 2, Ed. Newman, J., and Choo, B.S., Elsevier Science & Technology, Burlington, MA, pp. 15.

Dixon, S. and B. , Lanyon, (2005) *Phase change measurement of ultrasonic shear waves on reflection from a curing epoxy system*, Journal of Physics, D Applied physics, 38(22): pp.4115.

Fernandez, M.M.C.,(2008) *Effect of Particle Size on the Hydration Kinetics and Microstructural Development of Tricalcium Silicate, Ph.D. Thesis, École Polytechnique Federale De Lausanne,* pp 234.

Garboczi, E. J.; Bentz, D. P., (1995) *Microstructure Property Relationships in Concrete: From Nanometers to Centimeters*, 2nd Canmet/ACI. Advances in Concrete Technology. International Symposium. Supplementary Papers, Las Vegas, NV, Malhotra, V. M., Editor, pp. 573-585.

Garboczi, E. J.; Bentz, D. P., (1996) *Modelling of the Microstructure and Transport Properties of Concrete, Construction and Building Materials*, Vol. 10, No. 5, pp. 293-300

Geiker M, Knudsen T.,(1982) *Chemical Shrinkage of Portland Cement Pastes*, Cement Concrete Res , 12(5): pp. 603-610.

Gu, P., Xie P., Xu, Z. and Beaudoin, J.J. ,(1993) *A rationalized AC impedance model for microstructural characterisation of hydrating cement systems*, Cem. Concr. Res., 23(2): pp. 359–367.

Gurevich, B. and M. Schoenberg,(1999) *Interface conditions for Blot's equations of poroelasticity.* Journal of the Acoustical Society of America, **105**(5): pp. 2585-2589.

Halamickova, P.; Detwiler, R. J.; Bentz, D. P.; Garboczi, E. J., (1995) *Water Permeability and Chloride Ion Diffusion in Portland Cement Mortars: Relationship to Sand Content and Critical Pore Diameter,* Cement and Concrete Research, Vol. 25, No. 4, pp. 790-802.

Hansen, T.C.,(1986) *Physical structure of hardened cement paste. A classical approach.* Materials and structures, **19**(6): pp. 423-436.

Jennings, H.M., Bullard, J.W., Thomas, J.J, Andrade,J.E., Chen, J.J., and Scherer G.W.,(2008) *Characterization and Modeling of Pores and Surfaces in Cement Paste:Correlations to Processing and Properties*, Journal of Advanced concrete technology, **6**(1): pp. 5-29.

Jennings, H.M., Thomas, J.J., Gevrenova, J.S., Georgios Constantinides, G. and Ulm, F.J.,(2007) *A multi-technique investigation of the nanoporosity of cement paste.* Cement and Concrete Research, **37**(3): pp. 329-336.

Johnson, D., and Plona, T., (1982) *Acoustic slow waves and the consolidation transition*, The Journal of the Acoustical Society of America, vol. 72, pp. 556.

Johnson, D. and Sen, P., (1981) *Multiple scattering of acoustic waves with application to the index of refraction of fourth sound*, Physical Review B, Vol. 24, No. 5, pp. 2486-2496.

Juenger, M.C.G., Lamour, V.H.R., Monteiro, P.J.M.,Gartner, E.M. and Denbeaux, G.P.D.,(2003) *Direct observation of cement hydration by soft X-ray transmission microscopy.* Journal of Materials Science Letters, **22**(19): pp. 1335-1337.

Kielczynski, P. and Pajewski W.,(1987) *Reflection of an Obliquely Incident Sh Plane-Wave at a Plane Interface between an Elastic Solid and a Viscoelastic Liquid.* Journal of the Acoustical Society of America, **81**(3): pp. 599-605.

Keating J., Hannant, D.J., Hibbert, A.P., (1989) *Comparison of Shear Modulus and Pulse Velocity Techniques to Measure Build-up Structure in Fresh Concrete*, Cement and Concrete Research, Vol. 19, pp. 554-566.

Lin, F. and Meyer, C., *Modeling Shrinkage of Portland Cement Paste.* ACI Materials Journal, 2008. 105(3): pp. 302.

Lura P. (2003) *Autogenous deformation and internal curing of concrete*, Ph.D. thesis, Delft University of Technology, Delft, The Netherlands.

Lura, P., Jensen, M.O., (2007) *Measuring techniques for autogenous strain of cement paste*, Materials and Structures, 40: pp.431–440.

McCarter, W. J., Chrisp, T. M., Starrs, G.., and Blewett, J. ,(2003) *Characterization and monitoring of cement-based systems using intrinsic electrical property measurements*, Cement and Concrete Research 33(2): pp 197-206.

Mezger, T., (2006) *The Rheology Handbook: For Users of Rotational and Oscillatory Rheometers, Vincent Verlag,* Hannover, Germany.

Midgley, H.G., Illston, J.M., (1983) *Some comments on the microstructure of hardened cement pastes*, Cement and Concrete Research, Vol. 13, pp. 197-206.

Mindess S, Young JF,(1981) *Concrete*, Englewood Cliffs, NJ., Prentice Hall

Nachbaur, L., Mutin, J.C., Nonat, A., Choplin, L., (2001) *Dynamic mode rheology of cement and tricalcium silicate pastes from mixing to setting*, Cement and Concrete Research, Vol. 31, No. 2, pp. 183-192.

Odler I., and Dorr, H., (1979) *Early Hydration of Tricalcium Silicate I. Kinetics of hydration and Stoichiometry of Hydration Products*, Cement and Concrete Research, Vol. 9, pp. 239-248.

Park, J., (2005) *Measurements of the frame acoustic properties of porous and granular materials*, J. Acoust. Soc. Am., 118 (6): pp: 3483–3490.

Phuaksuk, Pariya, (2000) *Plastic Shrinkage cracking in Fly-Ash Concrete*, Master thesis , Northwestern University

Parrott, L.J., (1983) *Thermogravimetric and sorption studies of methanol exchange in alite paste.* Cem Concr Res, **13**(1): pp. 18-27.

Pichler, C., R. Lackner, and H.A. Mang,(2007) *A multiscale micromechanics model for the autogenous-shrinkage deformation of early-age cement-based materials.* Engineering Fracture Mechanics, **74**(1-2): pp. 34-58.

Plona, T. (1980) *Observation of a second bulk compressional wave in a porous medium at ultrasonic frequencies*, Applied Physics Letters, Vol. 36, pp. 259.

Powers, T.C. and Brownyard, T.L., (1947) *Studies of the physical properties of hardened Portland cement paste*, ACI18(8):pp 972-990.

Powers, T.C.,(1958) *Structure and physical properties of hardened Portland cement paste.* Journal of the American Ceramic Society, **41**(1): pp. 1-6.

Powers TC, Copeland LE, Mann HM,(1959) *Capillary continuity or discontinuity in cement pastes*, J. Portland Cem. Assoc. Res. Dev. Lab., v10, pp 38- 48.

Pratt, P.L., and Jennings, H.M., (1981) *The Microchemistry and Microstructure of Portland Cement*, Ann. Rev. Mater. Sci., Vol. 11, pp.123-49.

Punurai, W., Jarzynski,J., Qu, J., Kim,J. Jacobs,L.J. and Kurtis,K.E.,(2007) *Characterization of multi-scale porosity in cement paste by advanced ultrasonic techniques*, Cement and Concrete Research, 37(1): pp. 38-46

Rapoport, J. R., Popovics, J. S., Kolluru, S. V. and Shah, S. P. (2000) *Using Ultrasound to Monitor Stiffening Process of Concrete with Admixtures*, ACI Materials Journal 97(6).

Saak, A. W., Jennings, H.M., and Shah, S.P., (2001) *The influence of wall slip on yield stress and viscoelastic measurements of cement paste*, Cement and Concrete Research, Vol. 31, No. 2, pp. 205-212.

Saak, A.W., (1999) *Characterization and Modeling of the Rheology of Cement Paste: With Applications Toward Self-Flowing Materials*, PhD thesis, Northwestern University, Evanston, IL.

Samson, E., Marchand, J., Robert, J.L., Bournazel, J.P., (1999) *Modeling the mechanisms of ion diffusion transport in porous media*, International Journal of Numerical Methods in Engineering, Vol. 46, pp. 2043-2060.

Sant, G, Rajabipour, F., Fishman, P., Lura, P. and Weiss,J.,(2006) *Electrical Conductivity Measurements in Cement Pastes at Early Ages: A Discussion of the Contribution of Pore Solution Conductivity, Volume, and Connectivity to the Overall Electrical Response*, in Advanced Testing of Fresh Cementitious Materials, Ed. H.W. Reinhardt, Stuttgart, Germany.

Sayers CM, Dahlin A,(1993) *Propagation of ultrasound through hydrating cement pastes at early times*. Adv Cem Based Mater, 1(1): pp 12-21.

Shah, V. V. and Balasubramanian, K. (2000), *Measuring Newtonian viscosity from the phase of reflected ultrasonic shear wave,* Ultrasonics ,38(9): pp 921-927.

Stoll, R. and T. Kan ,(1981) *Reflection of acoustic waves at a water Sediment interface*, The Journal of the Acoustical Society of America, Vol. 70, pp. 149.

Struble, L. J., Zhang, H., Sun, G. K. and Lei,W. G, (2000) *Oscillatory shear behavior of Portland cement paste during early hydration*, Concrete Science and Engineering, 2(7): pp 141-149.

Subramaniam K.V, J.S. Popovics, and S.P. Shah,(2000) *Determining elastic properties of concrete using vibrational resonance frequencies of standard test cylinders.* Cement Concrete and Aggregates, **22**(2): pp. 81-89.

Subramaniam, K. V., Mohsen, J.P., Shaw, C., and Shah, S.P., (2002) *Ultrasonic technique for monitoring concrete strength gain at early age*, ACI Materials Journal, Vol. 99, No. 5, pp. 458-462.

Subramaniam, K. V. and J. Lee, (2003) *Ultrasonic Measurement of Early Age Viscoelastic Properties of Cementitious Materials*, Proceedings of 16th ASCE-EMD conference, Seattle.

Subramaniam, K. V., Lee, J., and Christensen, B., (2005) *Monitoring the setting behavior of cementitious materials using one-sided ultrasonic measurements*, Cement and Concrete Research, Vol. 35, No. 5, pp. 850-857.

Subramaniam, K.V., and Lee, J., (2007) *Ultrasonic Assessment of Early-age changes in the Material Properties of Cementitious Materials*, Materials and Structures, RILEM, Vol. 40, No. 3, pp. 301-309.

Subramaniam KV, Wang X.(2010) *An Investigation of Microstructure Evolution in Hydrating Cement Paste through Setting using Ultrasonic and Rheological Measurements*. Cement Concrete Res , 40(1): pp. 33-44.

Sun, Z., Voigt, T., and Shah, S.P., (2006) *Rheometric and ultrasonic investigations of viscoelastic properties of fresh Portland cement pastes,* Cement and Concrete Research 36(2): pp. 278-287.

Taylor, H. F. W. ,(1985) *Portland Cement: Hydration Products*, a publication of Materials Education Council, Materials Research Laboratory, University Park, PA.

Tazawa E, Miyazawa S, Kasai T.(1995) *Chemical Shrinkage and Autogenous Shrinkage of Hydrating Cement Paste*. Cement Concrete Res., 25(2): pp. 288-292.

Thomas, J.J., Jennings, H.M., and Allen, A.J., (1999) *The Surface Area of Hardened Cement Paste as Measured by Various Techniques*, Concrete Science and Engineering, Vol. 1, pp. 45-64.

Thomas, J.J., Jennings, H.M., Gevrenov, J.S., Constantinides, G., and Ulm, F-J, (2007) *A multi-technique investigation of the nanoporosity of cement paste*, Cement and Concrete Research, Vol. 37, pp. 329-336.

Ulm, F.J., Constantinides, G., and Heukamp,F.H.,(2004) *Is concrete a poromechanics material? - A multiscale investigation of poroelastic properties.* Materials and Structures, **37**(265): pp. 43-58.

Valič, M. I., Stepišnik, J.S., (1996) *A Study of Hydration of Cement Pastes by Reflection of Ultrasonic Shear Waves. Part I: Apparatus, Experimental Method and Application Examples*, Kov. Zlit. Tech., 32(6): pp 551-600.

Valič, M. I., (2000) *Hydration of cementitious materials by pulse echo USWR: Method, apparatus and application examples*, Cem Concr Res., (30), pp. 1633-1640.

Voigt, T. and S.P. Shah,(2004) *Properties of early-age portland cement mortar monitored with shear wave reflection method.* Aci Materials Journal, **101**(6): pp. 473-482.

Voigt, T.,(2004) *The Application of an Ultrasonic Shear Wave Reflection Method for Nondestructive Testing of Cement-Based Materials at Early Age,* Univerisity of Leipzig: Germany. pp. 224.

Voigt, T., Akkaya, Y., Subramaniam, K.V., and Shah, S.P., (2003) *Determination of early age mortar and concrete strength by ultrasonic wave reflections*, Journal of Materials in Civil Engineering, Vol. 15, No. 3, pp. 247-254.

Wang X, Subramaniam KV, Lin F,(2010) *Ultrasonic Measurement of Viscoelastic Shear Modulus Development in Hydrating Cement Paste*. Ultrasonics, 50(7): pp 726-738.

Williams, D., Saak, A., and Jennings, H.M., (1999) *The influence of mixing on the rheology of fresh cement paste*, Cement and Concrete Research, Vol. 29, No. 9, pp. 1491-1496.

Yamamoto,T., and Turgut, A., (1988) *Acoustic Wave Propagation through Porous Media with arbitrary pore size distribution*, Journal of Acoustical society of America, Vol. 83, pp. 1744-1751.

Ye, G., K. van Breugel, et al. (2003) *Experimental study and numerical simulation on the formation of microstructure in cementitious materials at early age*, Cement and Concrete Research, Vol. 33, No. 2, pp. 233-239.

Ye G.,(2005) *Percolation of Capillary Pores in Hardening Cement Pastes*, Cement Concrete Res., 35 **:** pp. 167– 176.

Zimmerman, C. and M. Stern ,(1994) *Analytical Solutions for Harmonic Wave Propagation in Poroelastic Media*, Journal of Engineering Mechanics, ASCE, Vol. 120, pp. 2154-2154.